

Report No. POL-005

**Executive Summary
Final Report: TU154M
101 Accident
Reconstruction**

2020-12-18

Prepared by:

Gerardo Olivares Ph.D.

NIAR AVET Laboratories



National Institute for Aviation Research
1845 Fairmount • Wichita, Kansas 67260-0093
800.642.7078 • <http://www.niar.wichita.edu/>



Table of Contents

Table of Contents	iii
Table of Tables	v
Table of Figures	vi
Nomenclature	xi
1 Introduction.....	1
1.1 Accident Reconstruction Process	1
1.1.1 Definitions.....	1
1.1.2 Accident Reconstruction Working Packages	2
1.2 Accident Reconstruction Models and Documentation	4
1.3 Accident Reconstruction Deliverables	10
1.4 Summary of Factual Information Based on Official Accident Investigation Report	12
1.4.1 Flight History	12
1.4.2 Aircraft Information	13
1.4.3 Injuries to Persons	14
1.4.4 Damage to Aircraft.....	14
1.4.5 Accident Site Information	20
1.4.6 Impact Conditions	21
2 Trajectory Analysis.....	22
2.1 Summary of Reconstruction Methodology.....	22
2.2 Case: Low Trajectory	24
2.3 Impact Conditions	33
2.3.1 Bodin Birch Tree Impact Condition	34
2.3.2 Ground Impact Condition.....	35
2.4 MAK Report Discrepancies	38
3 Bodin Birch Tree Accident Reconstruction	42
3.1.1 Aircraft Orientation and Velocities	42
3.1.2 Engine Thrust Loads	44
3.1.3 Aerodynamic Forces	44
3.2 Bodin Birch Tree FEA Model Definition.....	44
3.2.1 Tree Geometry	45
3.2.2 Tree Material Definition.....	46
3.2.3 Tree FEA Model.....	46
3.3 Bodin Birch Tree Impact Analysis Setup	48
3.4 Bodin Birch Tree Impact Analysis Results	50
3.4.1 Left Wing to Bodin Birch Tree Impact Kinematics Analysis.	50
3.4.2 Wing Damage Evaluation	59
3.4.3 Tree Top Trunk Trajectory – Simulation	76
3.5 Comparison to MAK Report	80
4 Ground Collision Accident Reconstruction	84



4.1	Ground Impact Reconstruction Evaluation Criteria	84
4.1.1	Survivability Evaluation Criteria and Supporting Documentation	84
4.1.2	Debris Field Evaluation Criteria and Supporting Documentation	93
4.2	Ground Collision Reconstruction	114
4.2.1	Overall Aircraft Kinematics and Damage Evaluation	114
4.2.2	Ground Marks Analysis – Comparison with MAK Report	137
4.3	Door 823 Analysis.....	144
4.4	Survivability evaluation summary.....	148
4.5	Conclusion of the ground collision reconstruction	152
5	References.....	158



Table of Tables

Table 1.1 Information of aircraft involved in crash [1]	13
Table 2.1 Enforced conditions in the Case Low trajectory	24
Table 2.2 Case Low: Summary of checks on aircraft heights and positions passing through corresponding heights and positions of TAWS/FMS2 and major accident landmarks	33
Table 2.3 Case Low: Aircraft velocities and orientations at impact with the Bodin birch	34
Table 2.4 Case Low: Aircraft control surface deflections at impact with the Bodin birch	34
Table 2.5 Case Low: Aircraft engine low and high compressor speeds, and thrust at impact with the Bodin birch ...	34
Table 2.6 Case Low: Aircraft aerodynamic loads at impact with the Bodin birch	35
Table 2.7 Case Low: Aircraft velocities and orientations at impact with the ground	36
Table 2.8 Case Low: Aircraft control surface deflections at impact with the ground	36
Table 2.9 Case Low: Aircraft engine low and high compressor speeds, and thrust at impact with the ground	36
Table 2.10 Case Low: Aircraft aerodynamic loads at impact with the ground	36
Table 2.11 Case High: Aircraft velocities and orientations at impact with the ground	37
Table 2.12 Case High: Aircraft control surface deflections at impact with the ground	37
Table 2.13 Case High: Aircraft engine low and high compressor, speeds and thrust at impact with the ground	38
Table 2.14 Summary of checks on aircraft heights and positions passing through corresponding heights and positions of major accident landmarks for the low trajectory	41
Table 2.15 Distance of the major accident site landmarks from Runway 26 threshold/reference	41
Table 3.1 Case Low: Aircraft velocities and orientations at impact with the Bodin birch.	43
Table 3.2 Case Low: Aircraft control surface deflections at impact with the Bodin birch.	43
Table 3.3 Engine rpm and thrust for Bodin birch impact condition	44
Table 3.4 Case Low: Aircraft aerodynamic loads at impact with the Bodin birch.	44
Table 3.5 Margin of safety on remaining attached parts of wing – Time: 138ms	59
Table 4.1 List of documented injured bones [7]	87
Table 4.2 Bone structure damage level criterion [7]	88
Table 4.3 List of documented internal organs [7]	89
Table 4.4 Internal organs damage level criterion [7]	89
Table 4.5 Ground mark analysis results.....	137
Table 4.6 Section 1 survivability analysis summary.....	149
Table 4.7 Section 2 survivability analysis summary.....	149
Table 4.8 Section 3 survivability analysis summary.....	150
Table 4.9 Section 4 survivability analysis summary.....	150
Table 4.10 Section 5 survivability analysis summary.....	151



Table of Figures

Figure 1.1 Accident reconstruction process.....	3
Figure 1.2 Tu-154M NIAR aircraft reverse engineering process	5
Figure 1.3 Tu-154M 3D CAD Model.....	6
Figure 1.4 Tu-154M FEA model and Building Block approach for full aircraft FEA model verification	7
Figure 1.5 Tu-154M CFD Model	8
Figure 1.6 Birch Tree Material Model Definition – Building block approach	9
Figure 1.7 Bodin Birch Tree FEA Model and Geometry	9
Figure 1.8 Tu-154M Aircraft dimensions – top view	13
Figure 1.9 Tu-154M Aircraft dimensions – side view.....	14
Figure 1.10 Damage layout [1].....	15
Figure 1.11 Aircraft first impact on a tree top [1].....	16
Figure 1.12 Birch tree impacted by left wing [1].....	16
Figure 1.13 Detached part of left wing [1]	17
Figure 1.14 Traces of impact on ground [1]	17
Figure 1.15 Detached right stabilizer panel [1]	18
Figure 1.16 Multiple fragments of aircraft systems and airframe [1]	19
Figure 1.17 Damaged engine mount [1]	19
Figure 1.18 Nose landing gear [1]	20
Figure 1.19 Wreckage plot [1].....	21
Figure 2.1 Case Low: Aircraft CG positions on the satellite image and CG heights.....	25
Figure 2.2 Case Low: Aircraft horizontal trajectory with respect to distance from Runway 26 threshold	27
Figure 2.3 Case Low: Aircraft vertical trajectory with respect to distance from Runway 26 threshold	28
Figure 2.4 Case Low: Aircraft vertical trajectory with respect to time elapsed from the TAWS 34 event	29
Figure 2.5 Case Low: Isometric view of aircraft 3D trajectory with respect to distance from Runway 26 threshold .	30
Figure 2.6 Case Low: Top view of aircraft 3D trajectory with respect to distance from Runway 26 threshold.....	31
Figure 2.7 Case Low: Side view of aircraft 3D trajectory with respect to distance from Runway 26 threshold	32
Figure 2.8 Case Low: Aircraft orientation at impact with the Bodin birch tree (a) Front view (b) Side view (c) Top view	35
Figure 2.9 Case Low: Aircraft orientation at initial impact with the ground (a) Front view (b) Side view (c) Top view	37
Figure 2.10 Case High: Aircraft orientation at initial impact with the ground (a) Front view (b) Side view (c) Top view	38
Figure 3.1 Aircraft coordinate system	43



Figure 3.2 Case Low: Aircraft orientation at impact with the Bodin birch tree (a) Front view (b) Side view (c) Top view.....	43
Figure 3.3 Tree geometry provided by the PSC [17].....	45
Figure 3.4 Tree angle and orientation provided by the PSC [17]	46
Figure 3.5 Tree FEM discretization.....	47
Figure 3.6 Tree FEM element length.....	47
Figure 3.7 Tree impact location definition for analysis by the PSC [17].....	48
Figure 3.8 Tree impact analysis setup – front view	49
Figure 3.9 Tree impact analysis setup – side view	49
Figure 3.10 Tree impact analysis setup – control surface orientations	50
Figure 3.11 Tree impact analysis kinematics – top view	52
Figure 3.12 Tree impact analysis kinematics – section view (9 and 20 ms).....	53
Figure 3.13 Tree impact analysis kinematics – section view (26 and 31 ms).....	54
Figure 3.14 Tree impact analysis kinematics – section view (46 and 51 ms).....	55
Figure 3.15 Tree impact analysis kinematics – section view (83 and 91 ms).....	56
Figure 3.16 Tree impact analysis kinematics – section view (109 and 138 ms).....	57
Figure 3.17 Tree impact analysis kinematics – tree kinematics from side view.....	58
Figure 3.18 Separated wing damage – Top View (138 ms).....	63
Figure 3.19 Separated wing damage comparison (138 ms) with debris image by the PSC [19]	64
Figure 3.20 Separated wing damage – Side View (138 ms).....	65
Figure 3.21 Separated wing damage – Upper and Lower Left Side View (138 ms)	66
Figure 3.22 Separated wing damage – Upper and Lower Right Side View (138 ms)	67
Figure 3.23 Separated wing damage comparison with debris image by the PSC [19]	68
Figure 3.24 Separated wing damage comparison with debris image by the PSC [19]	69
Figure 3.25 Separated wing damage comparison with debris image by the PSC [20]	70
Figure 3.26 Separated wing damage comparison with debris image by the PSC [20]	71
Figure 3.27 Separated wing damage comparison with debris image by the PSC [20]	72
Figure 3.28 Separated wing damage comparison with debris image from the PSC [20].....	73
Figure 3.29 Fragments embedded in birch tree identified by the PSC [21].....	74
Figure 3.30 Top fragment analysis in tree impact simulation.....	74
Figure 3.31 Bottom fragment analysis in tree impact simulation	74
Figure 3.32 Von Mises stresses on Spar 1 - MPa	75
Figure 3.33 Von Mises stresses on Spar 2 - MPa	75
Figure 3.34 Tree impact analysis – tree damage view 1	76
Figure 3.35 Tree impact analysis – tree damage view 2.....	76



Figure 3.36 Tree impact analysis – tree damage view	77
Figure 3.37 Crash site satellite image close-up view of the Bodin birch tree [19]	78
Figure 3.38 Broken simulation tree top piece trajectory analysis – time: 0 (Tree Broken in two pieces, Upper and Lower Trunk)	79
Figure 3.39 Broken simulation tree top piece trajectory analysis – time: 0.25 s	79
Figure 3.40 Broken simulation tree top piece trajectory analysis – time: 0.5 s	80
Figure 3.41 NIAR trajectory analysis showing birch tree impact at 5 m height as per MAK report	81
Figure 3.42 Photograph of Bodin hut provided by the PSC [19]	81
Figure 3.43 Tree dimensions drawing in Prosecutor report [11]	82
Figure 4.1 Local accelerometer output coordinate system	85
Figure 4.2 Example of evaluation criteria of a survivable event	86
Figure 4.3 Bone structure damage – Passenger #71 [7]	88
Figure 4.4 Internal organs damage – Passenger #71 [7]	90
Figure 4.5 Injury values – Passenger #71 [7]	90
Figure 4.6 Injury values per body area – Passenger #71	91
Figure 4.7 Injury assessment – Passenger #71	91
Figure 4.8 Injury report – Passenger #71	92
Figure 4.9 MAK report wreckage site [1]	93
Figure 4.10 MAK large debris [1]	94
Figure 4.11 MAK identified fragments – 1 through 49 [1]	95
Figure 4.12 MAK identified fragments – 50 through 71 [1]	96
Figure 4.13 MAK report main debris field image [1]	97
Figure 4.14 PSC satellite image [6]	99
Figure 4.15 Bodin birch debris region [6]	100
Figure 4.16 PSC large debris images – left wing tip [6]	100
Figure 4.17 Pre-ground impact debris region [6]	101
Figure 4.18 PSC large debris images – left horizontal stabilizer [6]	102
Figure 4.19 Post-ground impact debris region [6]	103
Figure 4.20 PSC ground marks images [6]	104
Figure 4.21 PSC large debris images – Section 1-2-3 [6]	105
Figure 4.22 PSC large debris images – Section 5-6 [6]	106
Figure 4.23 PSC large debris images – Stabilizers [6]	106
Figure 4.24 PSC large debris images – Left wing [6]	107
Figure 4.25 PSC large debris images – Right wing [6]	107
Figure 4.26 PSC aircraft debris fragmentation sketch [25]	108

Figure 4.27 MAK debris documentation table – Fragment #57 [1]	109
Figure 4.28 Left outer-wing lower skin panel	110
Figure 4.29 Northeast debris field images overlay. MAK [1] (color) and PSC [6] (gray scale)	111
Figure 4.30 Left stabilizer debris alteration	112
Figure 4.31 Southwest debris field images overlay. MAK [1] (color) and PSC [6] (gray scale)	113
Figure 4.32 Tu154 numerical model kinematics – Top view (time: 165 ms and 335 ms)	115
Figure 4.33 Tu154 numerical model kinematics – Top view (time: 505 ms and 675 ms)	116
Figure 4.34 Tu154 numerical model kinematics – Top view (time: 845 ms and 1035 ms)	117
Figure 4.35 Tu154 numerical model kinematics – Bottom view (time: 165 ms and 335 ms)	118
Figure 4.36 Tu154 numerical model kinematics – Bottom view (time: 505 ms and 675 ms)	119
Figure 4.37 Tu154 numerical model kinematics – Bottom view (time: 845 ms and 1035 ms)	120
Figure 4.38 Tu154 numerical model kinematics – Right side view (time: 165 ms and 335 ms)	121
Figure 4.39 Tu154 numerical model kinematics – Right side view (time: 505 ms and 675 ms)	122
Figure 4.40 Tu154 numerical model kinematics – Right side view (time: 845 ms and 1035 ms)	123
Figure 4.41 Tu154 numerical model kinematics – top view overlaid with corpses and body fragments (time: 0 ms and 100 ms)	124
Figure 4.42 Tu154 numerical model kinematics – top view overlaid with corpses and body fragments (time: 200 ms and 300 ms)	125
Figure 4.43 Tu154 numerical model kinematics – top view overlaid with corpses and body fragments (time: 400 ms and 500 ms)	126
Figure 4.44 Tu154 numerical model kinematics – top view overlaid with corpses and body fragments (time: 600 ms and 700 ms)	127
Figure 4.45 Tu154 numerical model kinematics – top view overlaid with corpses and body fragments (time: 800 ms and 900 ms)	128
Figure 4.46 Tu154 numerical model kinematics – top view overlaid with corpses and body fragments (time: 1000 ms and 1035 ms)	129
Figure 4.47 Tu154 numerical model damage at t = 1035 ms – Top view (top) and bottom view (bottom)	130
Figure 4.48 Tu154 numerical model damage at t = 1035 ms – Left side view (left) and right side view (right)	131
Figure 4.49 Left side Tu154 numerical model damage at t = 1035 ms – Comparison with PSC debris sketch [25]	132
Figure 4.50 Right side Tu154 numerical model damage at t = 1035 ms – Comparison with PSC debris sketch [25]	133
Figure 4.51 Top side Tu154 numerical model damage at t = 1035 ms	134
Figure 4.52 Top side Tu154 numerical model damage (Von-Mises Stress) at t = 1035 ms	135
Figure 4.53 Tu154 numerical model damage (Von-Mises Stress) at t = 1035 ms	136
Figure 4.54 Stabilizer (left) and left wing (right) furrows in the accident site	137
Figure 4.55 Stabilizer (left) and left wing (right) furrows in the accident site and the numerical model	138



Figure 4.56 Comparison of the stabilizer furrow in the numerical model and the accident site	139
Figure 4.57 Comparison of the left wing furrow in the numerical model and the accident site	139
Figure 4.58 Depth of the ground marks in the numerical model	140
Figure 4.59 Von Mises stress of the ground marks in the numerical model – Time = 350 ms.....	141
Figure 4.60 Overlay of the depth of the ground marks in the numerical model – Time = 350 ms	142
Figure 4.61 Overlay of the Von Mises stress ground marks in the numerical model – Time = 350 ms.....	143
Figure 4.62 Section 3 (Simulation Time: 90 ms) – Door 823 initial impact versus door debris GPS location	145
Figure 4.63 Section 3 (Simulation Time: 180 ms) – Door 823 release.....	145
Figure 4.64 Section 3 door 823 top view kinematics overlaid with door debris GPS location.....	146
Figure 4.65 Section 3 door 823 (Simulation Time: 180ms) compared to door debris image by PSC [6]	146
Figure 4.66 Section 3 door 823 kinematics (time: 160 – 200 ms) and total velocity and Z displacement and velocity of door 823 and fuselage section 4	147
Figure 4.67 Case C1 – pushing door into soil [30]	147
Figure 4.62 Aircraft sections survivable volume cross sections at 300 ms.....	148
Figure 4.63 Seat analysis results with row 10 right outboard accelerations compared to various seat debris images provided by the PSC [6]	154
Figure 4.64 Left side Tu154 numerical model damage at t = 1035 ms – Comparison with PSC debris sketch [25]	155
Figure 4.65 Right side Tu154 numerical model damage at t = 1035 ms – Comparison with PSC debris sketch [25]	156
Figure 4.66 Overall passenger injury assessment [7] (left) and floor peak resultant accelerations (right)	157



Nomenclature

ADC	Air Data Computer
ATM-QAR	Quick Access recorder manufactured by ATM company
CG	Center of Gravity
FAA	Federal Aviation Administration
FDR	Flight Data Recorder
FMS	Flight Management System
ICAO	International Civil Aviation Organization
KBN	Russian name for the QAR recorder
MAC	Mean Aerodynamic Chord
MAK	Russian name for Interstate Aviation Committee
MLP	Russian name for the tape-based flight recorder
MSL	Mean Sea Level
MSRP	Russian name for the FDR system
NTSB	National Transportation Safety Board
PIC	Pilot-in-Command
PSC	Polish Sub-Committee
QAR	Quick Access Recorder
QFE	Atmospheric pressure at runway threshold
QNH	Atmospheric pressure at sea level
SRTM	Shutter Radar Topography Model
TAWS	Terrain Awareness and Warning System
UTC	Universal Coordinated Time



1 Introduction

The work presented in this report will provide the data required by the Polish Sub-Committee (PSC) to determine whether or not the April 10, 2010, Polish Air Force Tupolev Tu-154M Registration 101 plane crash was an accident as described in the MAK report [1]. Any investigation that is politically, financially, or emotionally charged can produce findings that are inherently bias to find fault or innocence no matter how unsubstantiated. NIAR's accident reconstruction findings summarized in this report are held to quality accident reconstruction standards and methodologies:

- We evaluate hypotheses or theories based on the most accurate, reliable, consistent, and non-arbitrary representation of the investigative findings.
- When gathering all the available information, we do not favor selected facts to form a conclusion when one or more pertinent findings contradict the applicable event or what caused the failure or crash, unless supporting evidence outweighs the compared circumstances.
- The hierarchy of prioritizing investigative findings are physical evidence, recorded data, empirical knowledge and/or personal experience, and witnessed events, respectively.
- We maintain [i] objectivity of analysis (managing potential bias); [ii] openness to discussion and challenge (accepting constructive criticism); and [iii] self-insight (evaluating our weaknesses and strengths in expertise).

1.1 Accident Reconstruction Process

1.1.1 Definitions

When the following terms are used in this accident reconstruction report, they have the following meaning:

- 1) **Accident:** An occurrence associated with the operation of an aircraft which takes place between the time any person boards the aircraft with the intention of flight until such time as all such persons have disembarked [2], in which:
 - a) a person is fatally or seriously injured as a result of:
 - i) being in the aircraft, or
 - ii) direct contact with any part of the aircraft, including parts which have become detached from the aircraft, except when the injuries are from natural causes, self-inflicted or inflicted by other persons, or when the injuries are to stowaways hiding outside the areas normally available to the passengers and crew; or



- b) the aircraft sustains damage or structural failure which:
- i) adversely affects the structural strength, performance or flight characteristics of the aircraft, and
 - ii) would normally require major repair or replacement of the affected component
- 2) **Accident Reconstruction:** is the scientific process of investigating, analyzing, and drawing conclusions about the causes and events during a collision. Accident reconstruction analysis includes processing data collecting, evaluating possible hypotheses, creating models, recreating accidents, testing, and utilizing software simulations.
- 3) **Incident:** An occurrence, other than an accident or purposeful act of sabotage, associated with the operation of an aircraft, which affects or could affect the safety of operation [3].

1.1.2 Accident Reconstruction Working Packages

The accident reconstruction process was divided into six working packages as shown in Figure 1.1:

- **Working Package I - Data Collection:** Collect and revise the data provided by the PSC, Polish Prosecutor Office [4], and the official accident investigation reports (MAK [1] and Miller Reports [5]).
 - **Working Package II – Tupolev 154M Reverse Engineering:** Reverse engineering process to create an accurate 3D CAD model of the aircraft using laser scanning, precision hand measurements, 2D and 3D spherical photography. Data for the aircraft systems specifications (mass, location, interface) was collected from aircraft and maintenance manuals in this working package. Material coupon level samples were extracted from the aircraft primary structure in order to characterize the mechanical properties of the materials used for the construction of the TU-154M. Once the reverse engineering data was collected, a detail Finite Element Model of the aircraft was developed using the Building Block approach. All the data collected and models created in this working package will be part of the final deliverables of the project. It may be used by the PSC to evaluate future accident reconstruction scenarios.
 - **Working Package III- Trajectory Analysis Methods:** Collection and analysis of the flight data from MLP-14-5 tape recorder, the quick access recorder (QAR) or KBN tape recorder, the ATM-QAR memory chip, and the K3-63 three-component recorder. Development and validation of CFD models and analytical methods to support the reconstruction efforts of the Tu-154M P101 trajectory prior to ground impact.
 - **Working Package IV- Debris Field and Passenger Survivability Analysis:** Collection and analysis of data from the following sources: MAK Report [1], and PSC Debris Field [6] and Passenger Survivability data [7].
-

- **Working Package V- Tu-154M Fleet Accident Data Review:** Review past Tupolev Tu-154 accidents and survivability data in the Aviation Safety Network Database [8].
- **Working Package VI- Tu-154M 101 Accident Reconstruction Analysis:** The numerical models developed in WP II and III are used to conduct the three accident reconstruction phases:
 - **Phase I:** Trajectory analysis pre and post Birch Tree impact to define the Birch Tree and Ground impact Simulation initial conditions and comparison with MAK report [1] and PSC accident site data [4] collected in WP IV.
 - **Phase II:** Birch Tree impact accident reconstruction and comparison with MAK report [1] and PSC accident site data [4] collected in WP IV.
 - **Phase III:** Ground impact accident reconstruction and comparison with MAK report [1] and PSC accident debris [6] and passenger injury data [7] collected in WP IV.

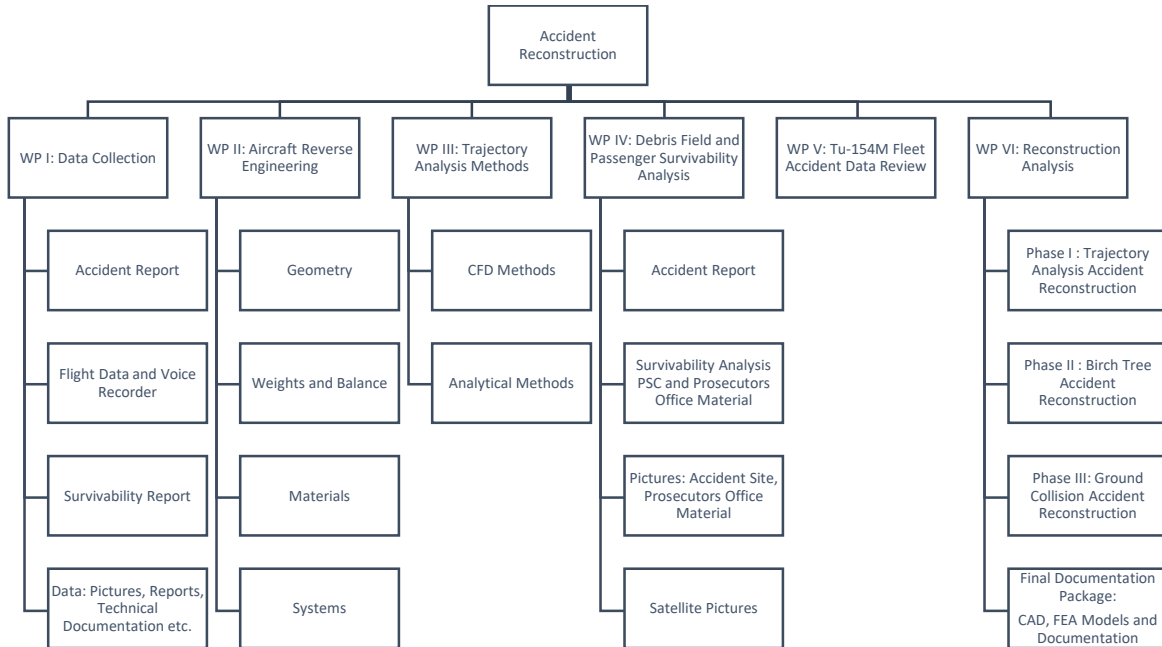


Figure 1.1 Accident reconstruction process



1.2 Accident Reconstruction Models and Documentation

The final report consists of the following documents and models:

- A. Executive Summary Extended Report: This documents summarizes the accident reconstruction results (Trajectory, Bodin Birch Tree Impact, and Ground Impact), and provides a summary of comparisons with the MAK report [1].
 - B. Annex Reports:
 - a. Annex I Report: TU154M 101 Accident Reconstruction – Reverse Engineering Process (See Figure 1.2), CAD (see Figure 1.3), FEA (See Figure 1.4), and CFD (See Figure 1.5) Models. This reports contains a description and documentation of all the numerical models used for the accident reconstruction and their validation using the Building Block approach. [31]
 - b. Annex II Report: TU-154M 101 Accident Reconstruction - Trajectory Analysis. This report contains a description of the Tu-154m trajectory before the ground impact. The available data from the MAK report and FDR logs are evaluated to recreate the trajectory of the Tu154m aircraft using a 6 DOF model. [10]
 - c. Annex III Report: TU-154M 101 Accident Reconstruction – Bodin Birch Tree Impact Reconstruction. This reports contains the description and evaluation of the Bodin birch impact (see Figure 1.7), the wood material modeling methodology, and the validation of the wood material card (see Figure 1.6). The results from the trajectory analysis are used as boundary conditions to perform a finite element analysis of the left wing impact with the Birch tree. [32]
 - d. Annex IV Report: TU-154M 101 Accident Reconstruction – Ground Collision. This report contains the accident site modeling methodology, structural evaluation and occupant injury analysis results from the accident reconstruction investigation. The trajectory analysis results are used as boundary conditions to perform a finite element analysis of the Tu-154M impact with the ground. [33]
-

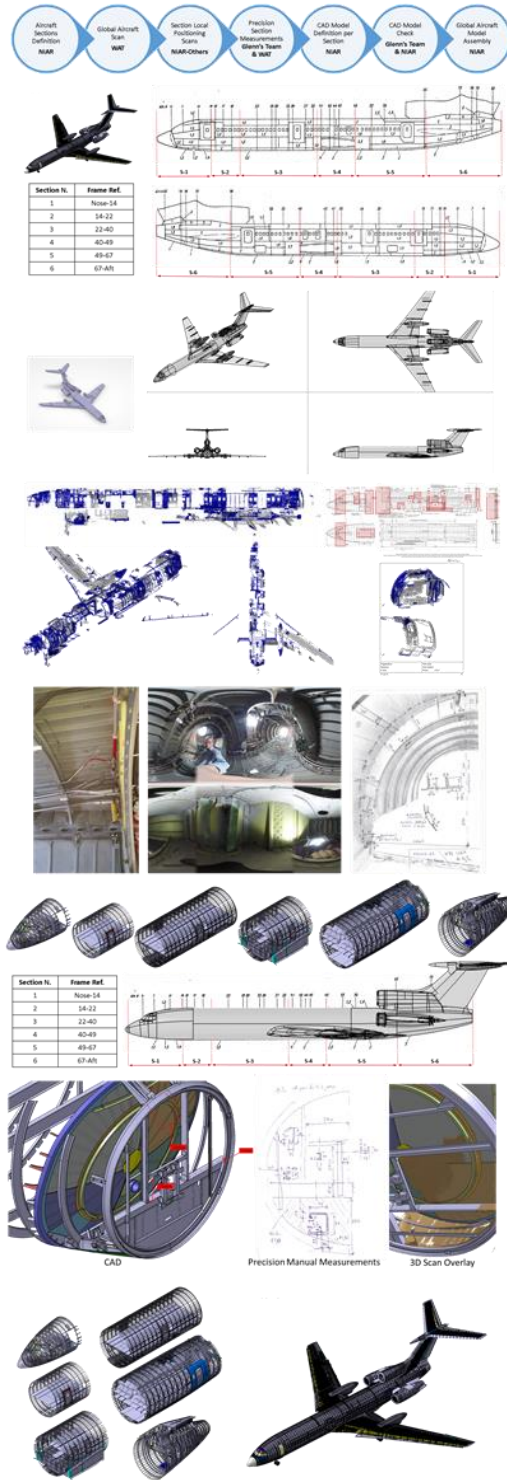


Figure 1.2 Tu-154M NIAR aircraft reverse engineering process

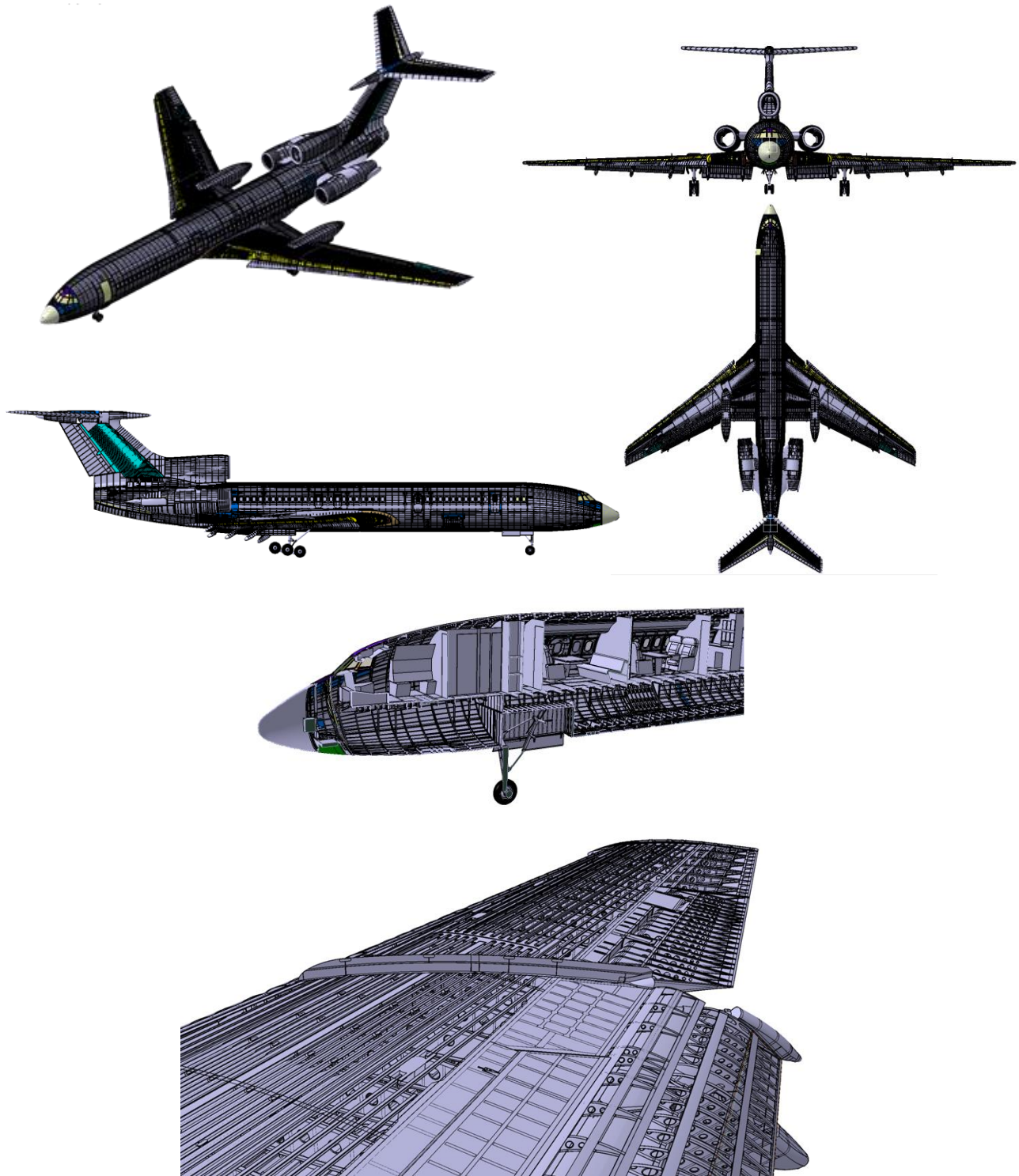


Figure 1.3 Tu-154M 3D CAD Model

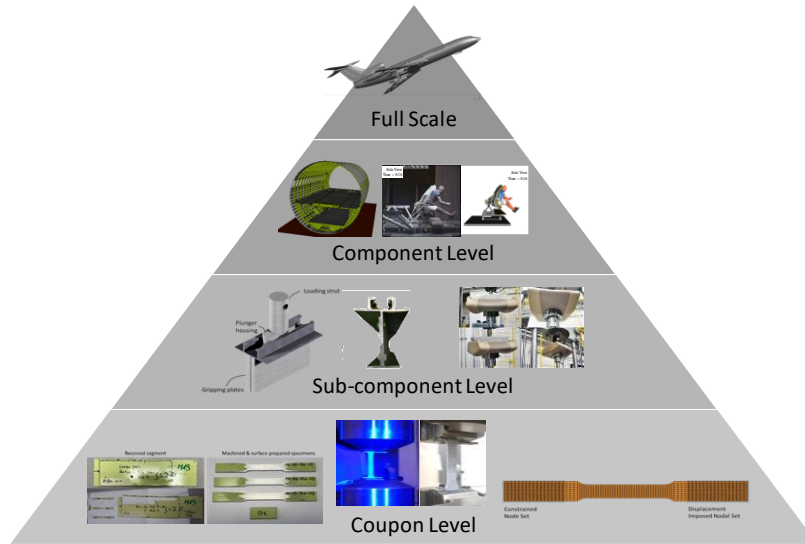


Figure 1.4 Tu-154M FEA model and Building Block approach for full aircraft FEA model verification

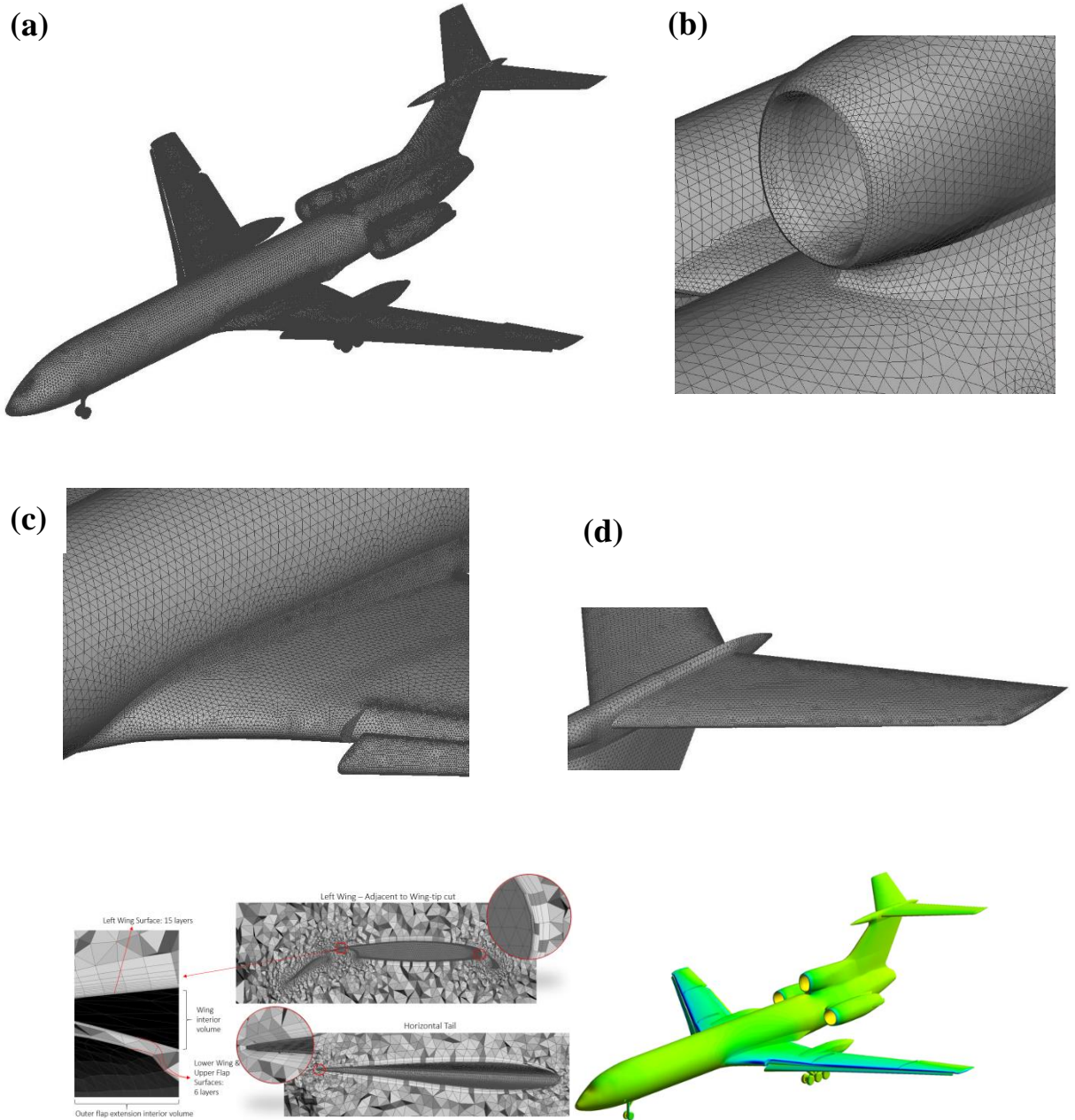


Figure 1.5 Tu-154M CFD Model

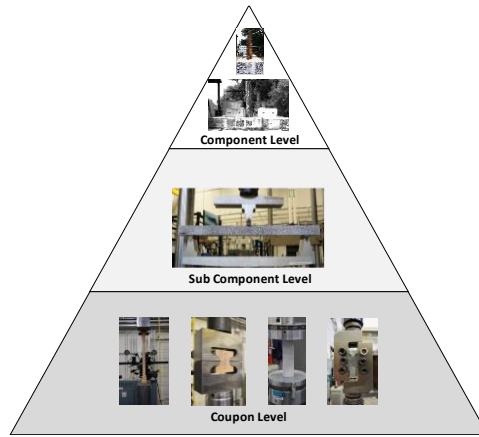


Figure 1.6 Birch Tree Material Model Definition – Building block approach

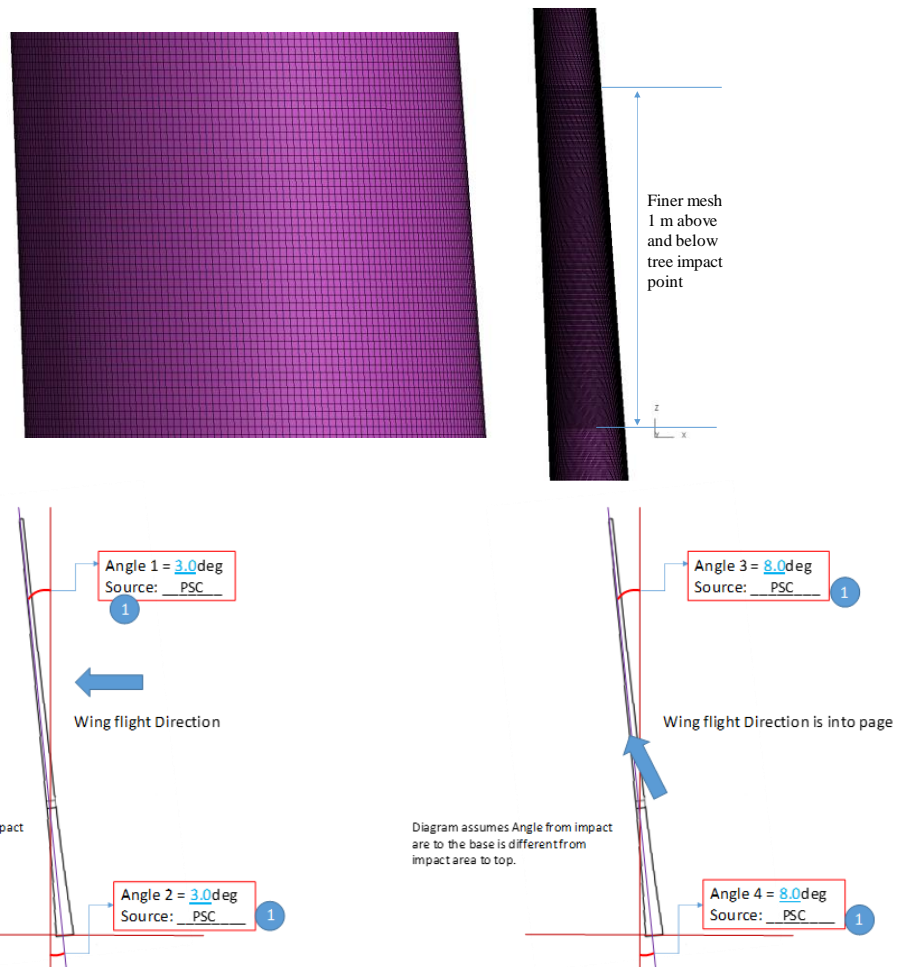


Figure 1.7 Bodin Birch Tree FEA Model and Geometry

1.3 Accident Reconstruction Deliverables

A copy of all the deliverables required per agreement No 261/2018/DA of 29/05/2018 has been uploaded to ftp site: <https://transfer.niar.wichita.edu/>. Username and password to this ftp site has been provided to Mr. Antoni Macierewicz (Chairman of the Sub-Committee to re-investigate the aircraft accident) through email.

The structure of the FTP site and its contents is as follows:

1. FTP – Poland Final Deliverable

1.1. CAD Model Deliverable

1.1.1. 3DXML

Complete Airplane CAD model in a reduced file format.

This file can be opened using Dassault 3D XML player.

This software can be downloaded at: <https://www.3ds.com/products-services/3d-xml/downloads/>

1.1.2. 2020_02_13_CAD_ModelRevA

Completed Airplane CAD model in native CATIA format.

CATIA V5 R25 was used to develop this model.

1.1.3. OML_CFD

Outer Mold Line CAD model in Step format.

This file can be opened with any CAD or Preprocessing packages (ex. Altair Hyperworks)

1.2. FE Model Deliverable

1.2.1. Ground Impact Condition

LSDYNA Tu-154M and soil full finite element model.

This file can be opened with any preprocessor capable of reading .key files or LSDYNA free preprocessor (<https://lstc.com/download>).

All numerical analysis were executed using LSDYNA mpp s R10.2.0 Revision 135267.

1.3. CFD Model Deliverable

ANSYS FLUENT Tu-154M Computational Fluid Dynamic models for both complete aircraft and damage aircraft (wing tip cut).

These files can be opened with any preprocessor capable of reading .cas files or ANSYS FLUENT (<https://www.ansys.com/products/fluids/ansys-fluent>).

All numerical analysis were executed using ANSYS FLUENT V17.2.

1.4. Final Extended Report

1.4.1. Executive Summary Extended Report TU154M 101 Accident Reconstruction 12182020 IR

1.4.2. Annexes

1.4.2.1. Annex I_TU154M 101 Accident Reconstruction - Reverse Engineering Process, CAD, FEA, and CFD Models 12_18_2020 IR

1.4.2.2. Annex II_TU154M 101 Accident Reconstruction - Trajectory Analysis_12_09_2020 IR



- 1.4.2.3. Annex III_TU154M 101 Accident Reconstruction -
TreeMaterial_Component_BirchImpact 12_18_2020_IR
 - 1.4.2.4. Annex IV_TU154M 101 Accident Reconstruction Ground Collision
12_18_2020 IR
 - 1.5. Final Presentation Package
 - 1.5.1. 0 - Table of Contents 07_01_2020
 - 1.5.2. Ch 1 - Accident Reconstruction Process - 07_01_2020
 - 1.5.3. Ch 2 - Aircraft Reverse Engineering Process - 07_01_2020
 - 1.5.4. Ch 2.1 Aircraft Reverse Engineering - CAD - 07_01_2020
 - 1.5.5. Ch 2.2 - Aircraft Reverse Engineering - FEA - 07_01_2020
 - 1.5.6. Ch 2.2.1 - Aircraft Reverse Engineering - Fasteners - 07_01_2020
 - 1.5.7. Ch 2.2.2 – Aircraft FEA Model Weight and Balance Documentation -
07_01_2020
 - 1.5.8. Ch 2.2.2.1 Weight and Balance - MassIdentification - 07_01_2020
 - 1.5.9. Ch 2.2.2.2 Weight and Balance - MassApplication - 07_01_2020
 - 1.5.10. Ch 2.2.3 -
AircraftFEAModel_MaterialReverseEngineeringDocumentation_Testing_and_Buil
dingBlockValidation_07_01_2020
 - 1.5.11. Ch 2.2.4 - Seat Model Reverse Engineering and Testing - 07_01_2020
 - 1.5.12. Ch 2.3 - FEM Verification using building block approach 11_19_2020
 - 1.5.13. Ch 3.1 Data_Recorder_Analysis 07_01_2020
 - 1.5.14. Ch 3.2 Accident_Site_Landmarks 07_01_2020
 - 1.5.15. Ch 3.3 Trajectory_Analysis_Methodology 07_01_2020
 - 1.5.16. Ch 3.4.1 Trajectory_Analyses_Documentation_and_Results_Low_Trajectory
07_01_2020
 - 1.5.17. Ch 3.4.2 Trajectory_Analyses_Documentation_and_Results_High_Trajectory
07_01_2020
 - 1.5.18. Ch 3.5 CFD Analysis for Tu-154M 07_01_2020
 - 1.5.19. Ch 3.6 Engine Thrust Calculations for Tu-154M 07_01_2020
 - 1.5.20. Ch 4.1 Bodin_Tree_Impact_Condition 07_01_2020
 - 1.5.21. Ch 4.2 Birch Tree FEA Model Definition 12_03_2020
 - 1.5.22. Ch 4.2.1 FEA Birch Tree Geometry 12_03_2020
 - 1.5.23. Ch 4.2.2 Birch Tree Material Documentation, Testing and Building-Block
Validation 12_03_2020
 - 1.5.24. Ch 4.2.3 Birch Tree Impact Analysis 12_15_2020
 - 1.5.25. Ch 5.0 Ground Impact Accident Reconstruction 12_18_2020
 - 1.5.26. Ch 6.0 MAK Report Discrepancies 07_01_2020
-



1.4 Summary of Factual Information Based on Official Accident Investigation Report

This section summarizes the factual information of the accident based on the accident report by the Interstate Aviation Committee of Russia also known as MAK [1].

1.4.1 Flight History

In accordance with the request from the Embassy of Poland on March 2010, two aircraft were scheduled to fly from Warsaw (EPWA) to Smolensk “Severny” airdrome (XUBS) on April 10th of 2010. The flights received the following reference numbers: PLF 101 (Tu-154M with tail number 101) and PLF 031 (Yak-40 with tail number 044). The objective of this trip was defined as “the visit of Polish delegation headed by the President of the Republic to Katyn participation in the celebrations in the Memorial Complex”. The PLF 101, which crashed near the boundaries of the Smolensk airdrome, had 96 occupants onboard, all of them citizens of the Republic of Poland: 4 flight crew members, 3 cabin crew personnel, 88 passengers and 1 security officer.

The airplane departed the Warsaw (EPWA) airport to Smolensk (XUBS) at 09:27 Smolensk local time on April 10th, 2010. During the flight descent, PLF 101 flight crew was in contact with air traffic controllers at Minsk, Moscow and Smolensk. The crew also maintained contact with the crew of the Yak-40 (PLF 031 flight) that landed at Smolensk airbase 90 minutes ahead of the presidential flight.

At 10:09 Smolensk time, PLF 101 crew requested estimated descent to 3,900 m, which was cleared by the Minsk Control. At 10:14 Smolensk time, Minsk Control informed PLF 101 crew of 400 m visibility under fog at the Smolensk “Severny” Airdrome. At 10:23 Smolensk local time, PLF 101 established contact with Smolensk “Severny” Control. Weather update still remained as fog and 400 m visibility.

At 10:25, PLF 101 flight crew requested trial approach, being cleared by the controller with a warning of not descending under 100 m and being ready for the scenario of a missed approach. During the decent maneuver, the flight crew contacted the PLF 031 crew, which already landed at Smolensk. The PLF 031 crew informed of a 200 m visibility at the time in the Smolensk airdrome. Despite the warnings, the crew of the Tu-154M continued to approach to the airdrome and initiated final descent.

At 1,100 m from the runway and an approximate deviation of 35 m to the left of the extended centerline runway, the PLF 101 flight hit the top of a tree at 11 m height from the ground. Due to the difference in terrain elevation prior to the runway, the Tu-154M was below the runway elevation at the time. At 245 m from the accident site, the Tu-154M hit a birch trunk of 30-40 cm of diameter, damaging severely the left wing. At 10:41:06 Smolensk local time, the PLF 101 flight crashed inverted and was destroyed prior to the Runway 26 mark in a forest area near the airdrome.

1.4.2 Aircraft Information

The operational details of the aircraft involved in the accident is listed in Table 1.1 below. The overall dimensions of the aircraft are presented in Figure 1.8 and Figure 1.9.

Table 1.1 Information of aircraft involved in crash [1]

Type	Tu – 154 M
Manufacturer Serial Number	90A837
Manufacture	Kuybyshev Aviation Plant
Date of manufacture	June 29, 1990
Registration	Tail number 101, Republic of Poland
Certificate of Registration	January 24, 2005
Owner	Republic of Poland
Operator	Ministry of Defense, Republic Of Poland
Certificate of Airworthiness	Not known
Life in Service by Aug 04, 2010	5143 hours, 3899 landings
Remaining Service Life	24857 hours, 5 years 8 months
Service Life Limit	30000 hours, 25 years 6 months
Center of gravity	25.3% MAC

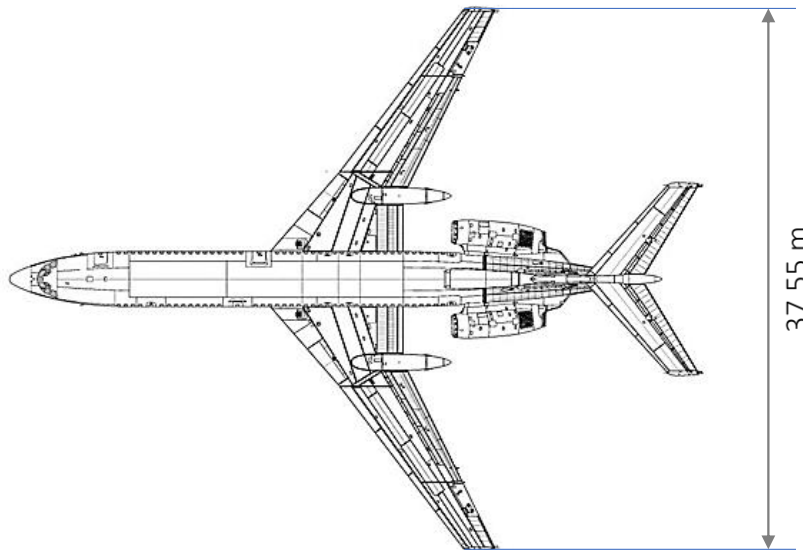


Figure 1.8 Tu-154M Aircraft dimensions – top view

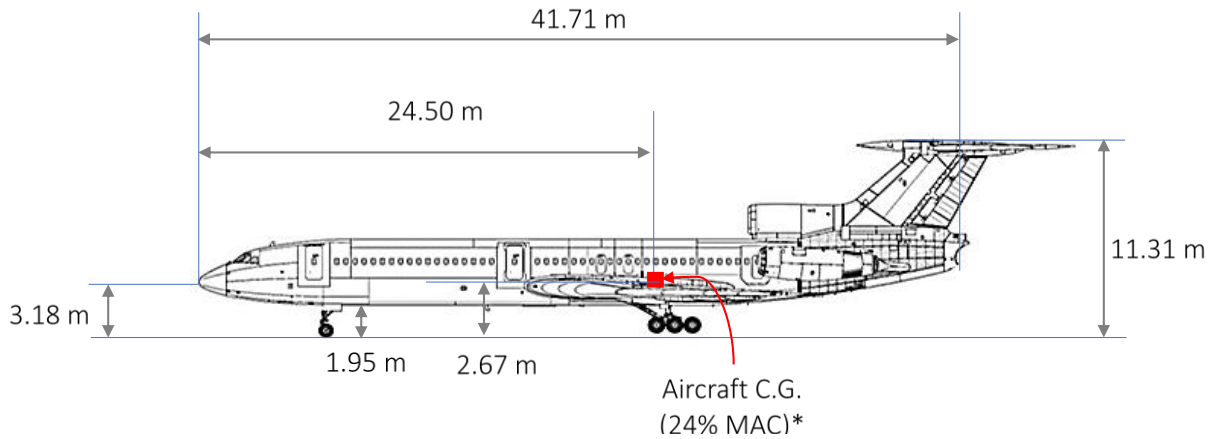


Figure 1.9 Tu-154M Aircraft dimensions – side view

1.4.3 Injuries to Persons

All the 89 passengers and 7 crew, a total of 96 persons on board, died during the time of collision due to multiple mechanical injuries [1].

1.4.4 Damage to Aircraft

Major destruction of the aircraft was caused by the impact forces during the obstacle and ground collisions. The layout of damaged parts, shown in Figure 1.10, reveals that the aircraft was disintegrated into multiple pieces due to the impact with trees and ground.

1.4.4.1 Sequence of Events

Sequentially, the first impact was with the top of a tree at the height of 11 m as shown in Figure 1.11. No parts of the aircraft were found at the first location. After the first impact and a distance of 244 m further with a lateral deviation of 61 m left from the centerline of the extended runway and at the height of about 5 meters, the aircraft wing hit a birch with a trunk of diameter measuring 30-40 cm (Figure 1.12). The investigation team found a left detachable part of the wing about 6.5 m long (Figure 1.13) at the area of impact. Followed by a hard left roll, and the aircraft further departed towards left. While rolling and moving further, the aircraft structure impacted with other trees and impacted the ground at a distance of 580 m from the first impact. The traces on the ground, shown in Figure 1.14, reveals that the impact occurred when aircraft was rolling towards left, and on impact, the aircraft was upturned with a left bank of about 200° - 210° [1].



Figure 1.10 Damage layout [1]



Figure 1.11 Aircraft first impact on a tree top [1]



Figure 1.12 Birch tree impacted by left wing [1]



Figure 1.13 Detached part of left wing [1]



Figure 1.14 Traces of impact on ground [1]

1.4.4.2 Damaged Aircraft Parts on Debris Field

The right stabilizer panel with elevator, the fin, stabilizer, tail cone ripped off on impact. These parts were found at a distance of 590-620 m after the first impact (Figure 1.15).

The whole wreckage area with multiple fragments of aircraft systems and airframe was at a distance of 670-680 m from the first impact and spread across 30-50 m wide and 130 m long along the path of the aircraft (Figure 1.16).

The aircraft was further damaged while moving upside down on the ground. The tail part of the aircraft with engines and other fragments is at a distance of 436 m from the runway threshold and turned 180 ° (Figure 1.17).

A part of the nose landing gear in an extended position is at a distance of 397 m from the runway threshold (Figure 1.18). Fragments of the aircraft revealed no signs of burning. Owing to unforeseen load factors, the aircraft got destroyed on contact with trees, land, and the ground surface during its further flight [1].



Figure 1.15 Detached right stabilizer panel [1]



Figure 1.16 Multiple fragments of aircraft systems and airframe [1]



Figure 1.17 Damaged engine mount [1]



Figure 1.18 Nose landing gear [1]

1.4.5 Accident Site Information

The accident site is at Smolensk “Severny” Airdrome, a military airbase in Russia, a crossed terrain with hills and forest, trees around 25 m with an elevation 230-260 m above the sea level. The impact occurred before the middle marker and 1,050 m distance from the runway 26 threshold [1].

The Center of the wreckage area is located at N 54° 49.450’ and E 32° 03.041’.

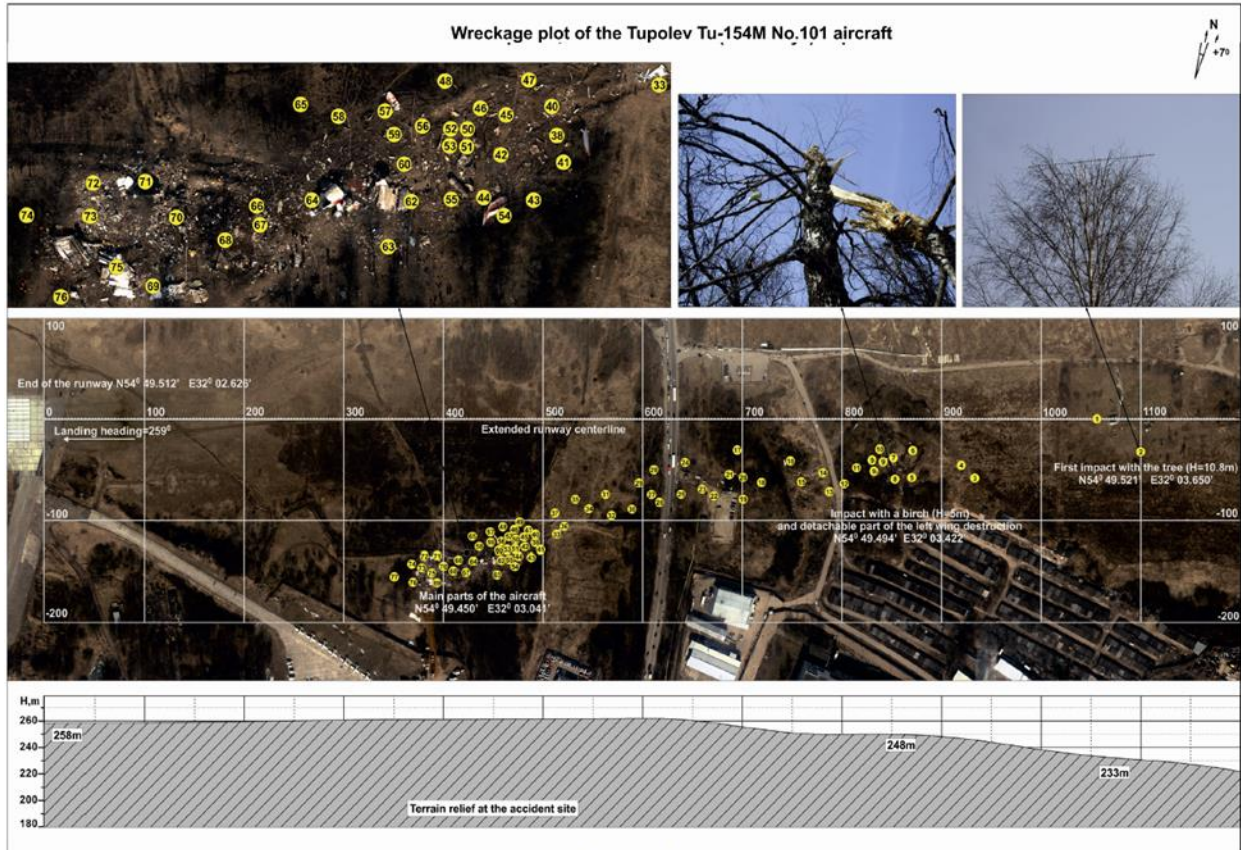


Figure 1.19 Wreckage plot [1]

1.4.6 Impact Conditions

The pilots attempted to land in a thick fog at Smolensk North Airport, a former military airbase with visibility limited to about 500 meters (1,600 ft).

At a distance approximately 1,100 m from the RWY 26 threshold and 35 m left of the extended centerline of the runway, the plane initially struck a tree 11 m above ground level. The estimated speed of impact was around 265 Km/hr. Subsequently, at a height of about 5 m a second impact with a large birch tree, 30 to 40 cm (12 to 16 in) diameter, resulted in about 6.5 meters (21 ft) of the left-wing (including the left aileron) separating from the airplane.

The resulting asymmetric lift produced an uncontrolled roll to the left. Within 5 seconds, the aircraft was rolled inverted and impacted the ground. The remaining outboard end of the left-wing initially impacted the ground, followed shortly by the nose section. The impact on the nose resulted in forces exceeding 100 g, which instantly killed everyone on board. The aircraft was violently ripped apart by impact forces after the nose impact. About 200 meters (660 ft.) before the runway threshold and slightly south of its centerline, the wreckage came to rest upside down. The forward part of the tail section came to rest pointed opposite the flight direction [1].

2 Trajectory Analysis

2.1 Summary of Reconstruction Methodology

A trajectory analysis methodology has been established to determine reasonable flight conditions at both the Bodin birch tree impact and initial ground impact locations for the flight of Tu-154M P101, from Warsaw to Smolensk, on April 10, 2010. A rigorous mathematical approach was needed in order to establish the flight conditions since [i] no GPS coordinates are available from the Flight Data Recorder (FDR) log; and [ii] barometric and radio altitudes from the FDR data cannot be trusted during unusual attitudes that create sensor limitations (during the last 3-4 seconds of flight). An inertial or acceleration-based trajectory analysis method was preferred in this study over an aerodynamic trajectory analysis method, since the complete aerodynamic and performance data for the Tu-154M aircraft is not available in the published literature as well as in the technical manuals. The assumptions and limitations of the methodology have been stated. Due to the lack of optimal quality of the available flight data and uncertainty on the recorded times of the TAWS alerts, the criteria, used to perform checks on the aircraft passing through the landmarks and TAWS/FMS alerts, has been therefore set to ± 5 m.

The FDR log provided to NIAR by Polish Sub-Committee (PSC) has been analyzed to identify the available channels, the sample frequency of the channels, and the stop time of the channels. A list of all the available channels has been documented and the discrepancies with the International Civil Aviation Organization (ICAO) FDR requirements have been highlighted. It has been observed that critical flight parameters required for accident reconstruction including longitudinal accelerations, groundspeeds, aircraft positions (GPS coordinates), and the left aileron deflections are not available from the FDR log.

The flight parameters from the Terrain Awareness and Warning System (TAWS) and Flight Management System (FMS) log relevant to the trajectory analysis have been identified and documented. The time-shift between the FDR time and TAWS/FMS time has been determined to be: $\text{FDR time} = \text{TAWS/FMS time} + 2 \text{ h}:2.75 \text{ s}$. An uncertainty of +1.0 s has been established for the recorded times of the TAWS alerts based on the methodology of recording the Universal Coordinated Time (UTC).

It is not possible to accurately determine the exact time of Bodin birch impact based solely on data available from the FDR and TAWS/FMS logs. A range of Bodin birch tree impact time has been determined based on the time claimed in the MAK report [1]. In this study, the Bodin birch impact time has been determined using a trial and error approach from the trajectory calculations, in which the aircraft is required to satisfy the constraint of impacting the ground-marks. The calculated Bodin birch impact time in this study has been also found to be dependent on the following parameters: longitudinal accelerations, the individual time-shift of the TAWS alerts and the time-shift between FDR and UTC.



Two trajectories have been defined based on the selection of the initial conditions in this study – the low trajectory and the high trajectory. The low trajectory assumes that the aircraft impacts the Bodin birch tree at the known height and location. The high trajectory assumes that the aircraft passes through the height corresponding to the TAWS 38 barometric altitude and the location corresponding to the TAWS 38 GPS coordinates.

In the case of the low trajectory, it has been observed that the aircraft impacts (within the 5 m accuracy) all the landmarks that are observed to be damaged at the accident site from the available photographs. It has also been observed that the aircraft CG height at the time of the TAWS 38 alert is about 15 m lower than the TAWS 38 barometric altitude. In the case of the high trajectory, it has been observed that the aircraft does not impact (within the 5 m accuracy) any of the landmarks that are observed to be damaged at the accident site from the available photographs except for the ground-marks.

The major takeaway from this study is that it is not possible to define a unique trajectory for the flight of Tu-154M P101, from Warsaw to Smolensk, on April 10, 2010, based only on the FDR and TAWS/FMS logs. However, using the location of landmarks at the accident site such as the ground-marks and the Bodin birch in combination with the FDR and TAWS/FMS logs, it has been possible to establish two sets of initial conditions that have resulted in the proposed low and high trajectories presented herein. The purpose of the trajectory analysis is therefore to be used as a complementary tool to the other aspects of accident reconstruction of the Tu-154M crash including the debris field analysis, the birch tree impact analysis and the ground impact analysis.

All the details for the FDR analysis, numerical methodology and in-depth results analysis for the two trajectories are provided in the Annex II trajectory analysis report [10]. In this report, the low trajectory results are summarized in Section 2.2. the flight conditions including velocity, orientation, control surface deflections, and aerodynamic and thrust loads at both the Bodin birch tree impact and the initial ground impact are summarized in Section 2.3. In Section 2.4, the discrepancies between the findings of this study and the findings of the MAK report [1] are discussed.

2.2 Case: Low Trajectory

The results for the Case Low trajectory are described in this section. The trajectory assumes the Bodin birch tree impact to be true. This implies that the initial conditions in the algorithm are adjusted such that the left wing of the aircraft passes through the desired height and location of the Bodin birch tree. The height above the ground where the left wing first impacts the Bodin birch is assumed to be 6.75 m [11]. The location of the Bodin birch tree, obtained from the satellite picture, is found to be 850 m away from the Runway 26 threshold in direction parallel to the runway centerline, and 75 m away in the perpendicular direction. The point on the left wing that makes contact with the Bodin birch tree is assumed to be 6.5 m away from the left wing tip based on the MAK report [1], page no. 76. The time of the Bodin birch tree impact is determined to be 06:40:57.1875 UTC time. It is determined that shifting the TAWS 34 alert by + 0.75 s, results in a trajectory that satisfies the constraint of the aircraft left wing impacting with the ground-mark. The trajectory calculations are based on optimization of accelerations to achieve the best trajectory fit with the barometric heights of TAWS 34 – 37, GPS coordinates of TAWS 34, and height and position of the left wing ground-mark. The conditions that are enforced in the Case Low trajectory are summarized in Table 2.1.

Table 2.1 Enforced conditions in the Case Low trajectory

Impact Height at Bodin Birch Tree:	6.75 m
Bodin Birch Tree coordinates in Runway 26 axis-system:	[850 m, -75 m]
Impact Time at Bodin Birch Tree:	06:40:57.1875 UTC
TAWS 34 Time:	06:40:03.75 UTC (+ 0.75 s)

The trajectory of the Tu-154M P101 aircraft is reconstructed for approximately the last 60 s of its flight. The start point of the trajectory coincides approximately with the TAWS 34 event in time. The end point of the trajectory coincides with the first impact of the aircraft with ground. The path of the aircraft CG, beginning from 1150 m away from Runway 26 threshold, is shown on the satellite picture in Figure 2.1. The vertical position of the aircraft CG with respect to the Runway 26 threshold height and the terrain profile for the path based on SRTM data are also shown Figure 2.1.

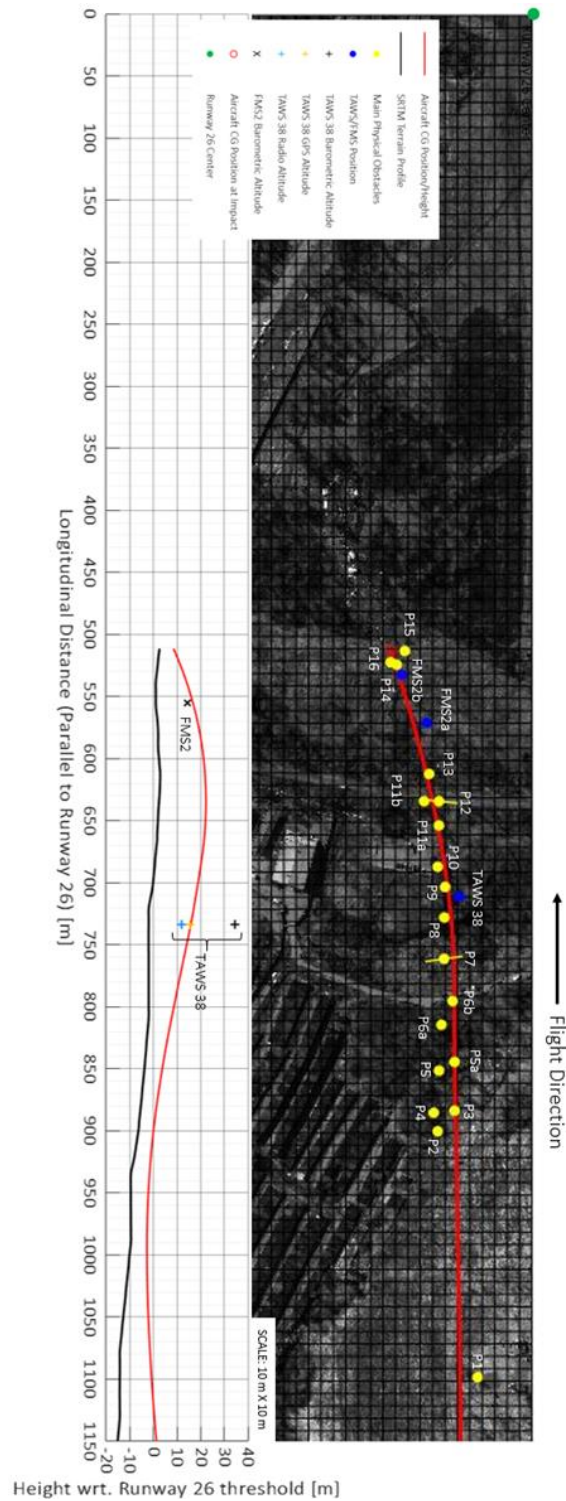


Figure 2.1 Case Low: Aircraft CG positions on the satellite image and CG heights

The two-dimensional horizontal and vertical trajectories of the aircraft with respect to the distance from the Runway 26 threshold are shown in Figure 2.2 and Figure 2.3 respectively. Various positions on the aircraft including the nose, wing tips, landing gear, etc. are tracked during the trajectory reconstruction and their paths are plotted in these figures. The following observations are made from Figure 2.2, Figure 2.3, and Figure 2.4:

- For the Case Low trajectory, the part of the aircraft that makes the initial impact with the ground is the left severed wing (with the outboard ~ 6.5 m section separated). The left severed wing impacts at the left wing ground-mark on the terrain. The aircraft nose impacts at almost the same time as the left severed wing impacts.
 - The Case Low vertical trajectory satisfies the constraint of passing through the TAWS 34 – 37 barometric altitudes. The maximum difference of the aircraft CG heights from the TAWS barometric altitudes, at the time of the TAWS 34 – 37 alerts, is less than 5 m.
 - The aircraft CG height at the time of the TAWS 38 alert is about 15 m lower than the TAWS 38 barometric altitude. The aircraft CG height is much closer to the TAWS 38 GPS and radio altitudes with the maximum difference being less than 5 m. It should be noted that the radio altimeter reading at the time of the TAWS 38 alert is not considered reliable since the roll angle of the aircraft at this time is greater than 20°.
 - The aircraft CG height is significantly lower than the barometric altitude of the FMS2 event at its recorded time. The aircraft CG height does get close to the FMS2b barometric altitude (within 5 m distance), but earlier in time compared to the recorded time of FMS2 alert. The aircraft CG height is significantly lower (~ 20 m) than the barometric altitude corresponding to the one second before the FMS2 event at its recorded time.
 - In the Case Low horizontal trajectory, the aircraft nose passes through the TAWS 34 – 36 longitudinal positions (maximum difference is less than 5 m). The deviation of the aircraft nose positions from the TAWS 37 longitudinal position is greater than 5 m. The aircraft nose deviates significantly from the TAWS 35 – 37 lateral positions but still passes through the TAWS 34 lateral position.
 - The aircraft nose significantly deviates from both the longitudinal and lateral positions of the TAWS 38, FMS2a and FMS2b positions at their respective recorded times. The aircraft nose does pass through the FMS2b position (within 5 m distance), but earlier in time compared to the recorded time of FMS2 alert.
-

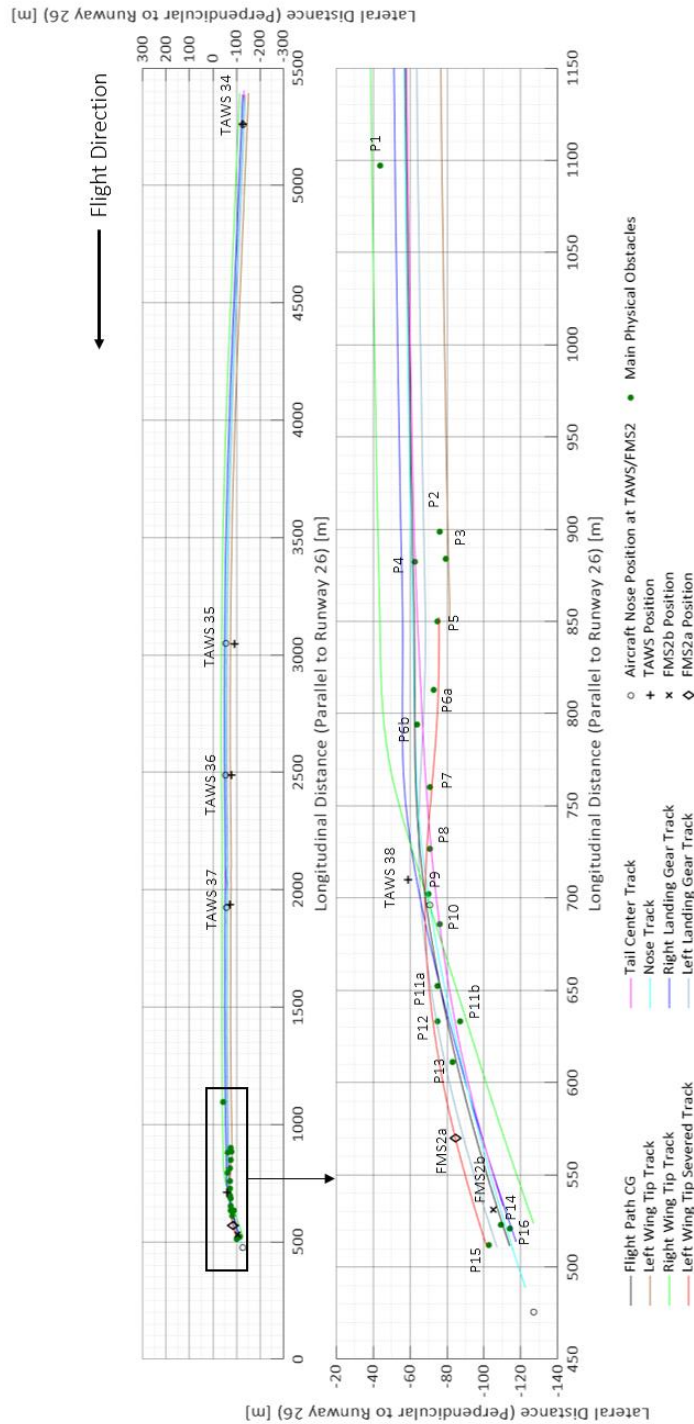


Figure 2.2 Case Low: Aircraft horizontal trajectory with respect to distance from Runway 26 threshold

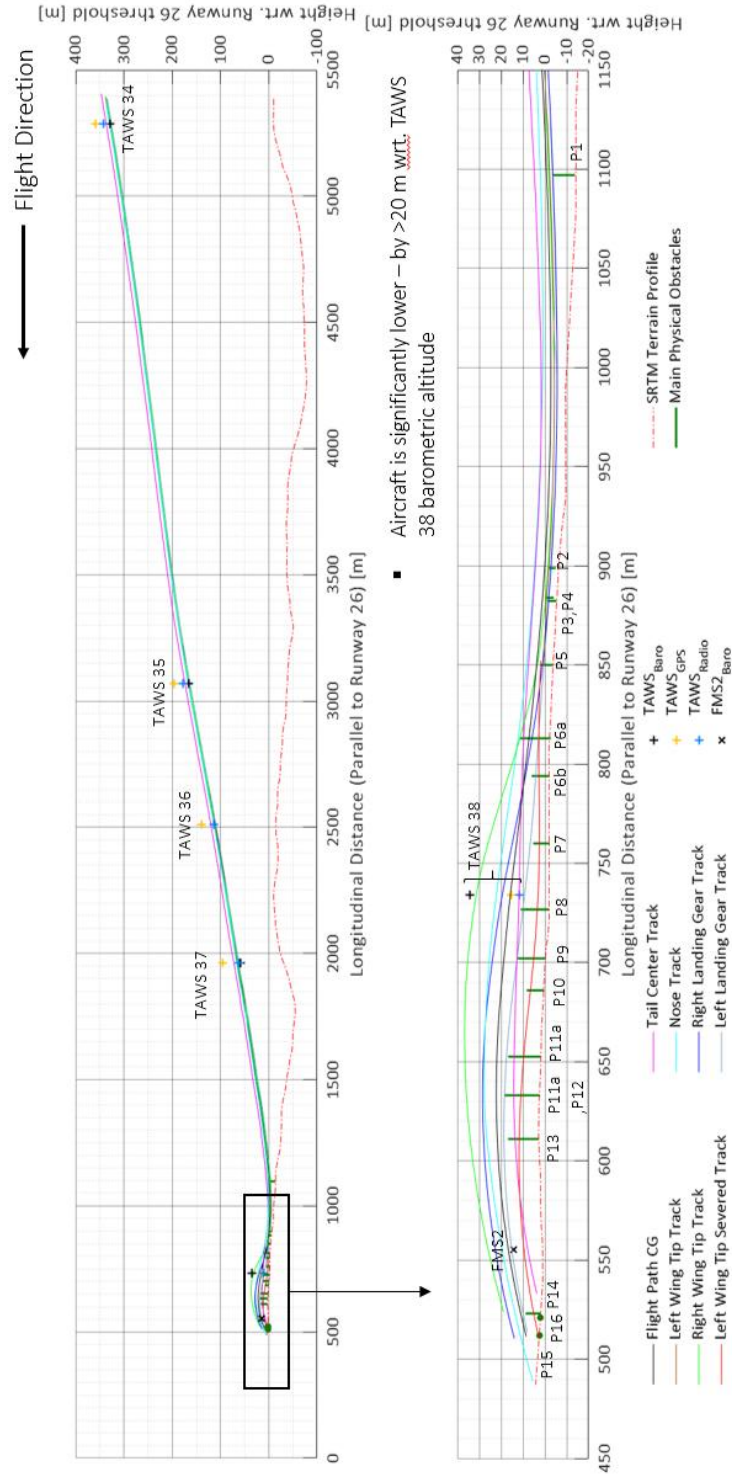


Figure 2.3 Case Low: Aircraft vertical trajectory with respect to distance from Runway 26 threshold

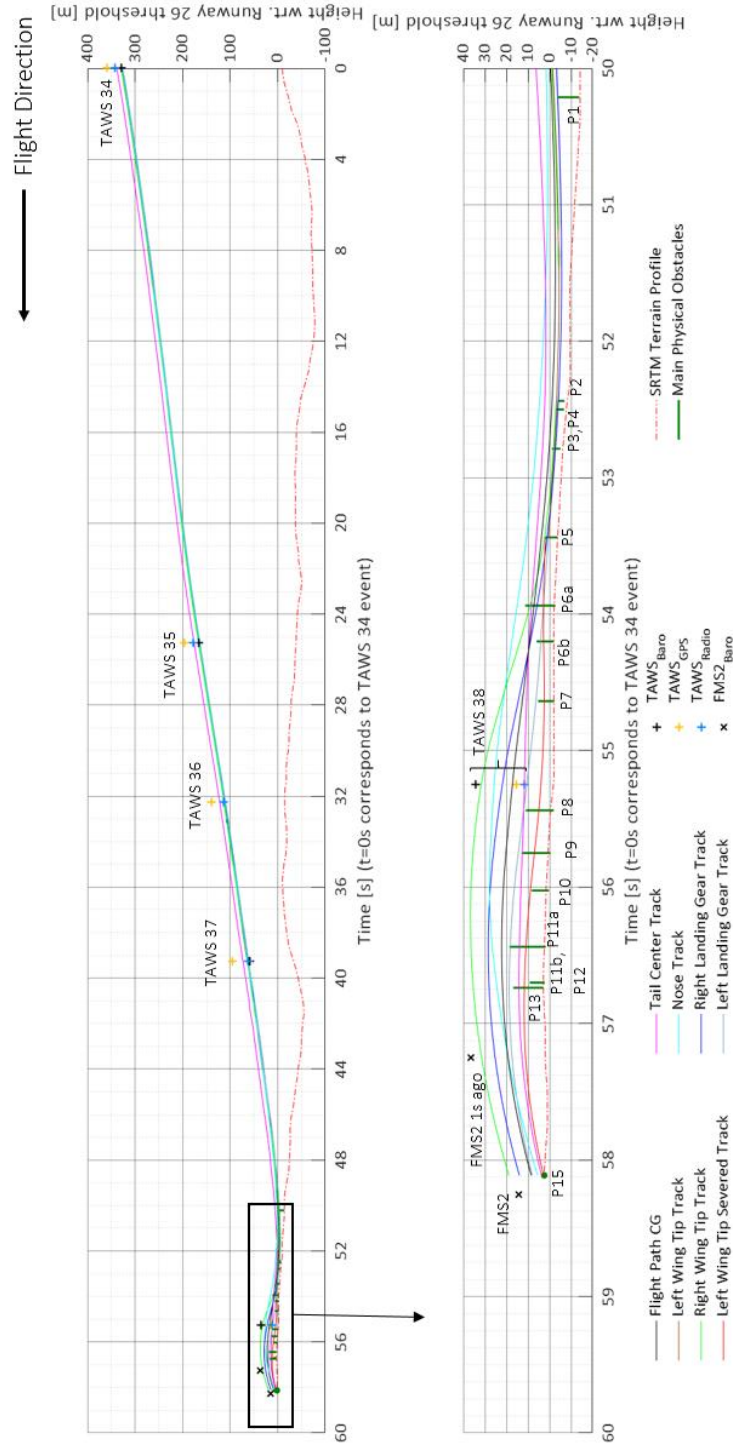


Figure 2.4 Case Low: Aircraft vertical trajectory with respect to time elapsed from the TAWS 34 event

A three-dimensional visualization of the trajectory is shown in Figure 2.5, Figure 2.6, and Figure 2.7. The three-dimensional position of the aircraft, beginning from 1,150 m away from the Runway 26 threshold, is shown in these figures using the CAD model of the Tu-154M aircraft in the landing configuration. The main landmarks in the path of the trajectory are shown in these figures using their approximate CAD models. The longitudinal axis for the plots is parallel to the Runway 26 centerline. The lateral axis of for the plots is perpendicular to the Runway 26 centerline. The height of the aircraft is plotted with respect to the Runway 26 threshold altitude.

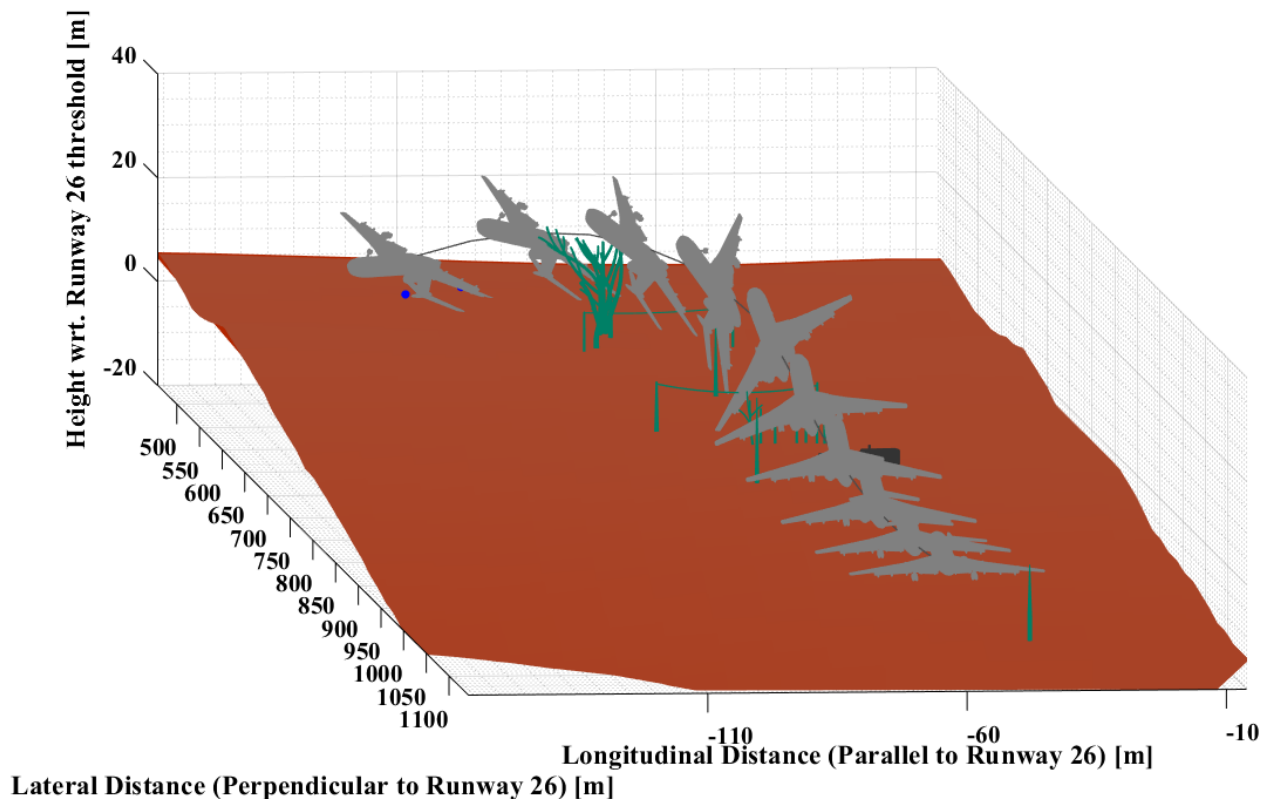


Figure 2.5 Case Low: Isometric view of aircraft 3D trajectory with respect to distance from Runway 26 threshold

Longitudinal Distance (Parallel to Runway 26) [m]

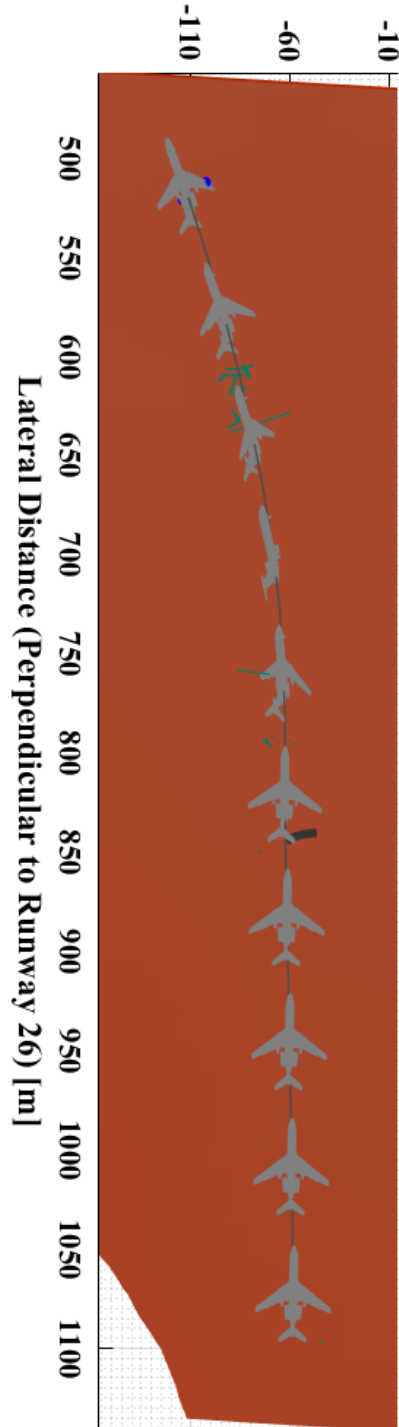


Figure 2.6 Case Low: Top view of aircraft 3D trajectory with respect to distance from Runway 26 threshold

Height wrt. Runway 26 threshold [m]

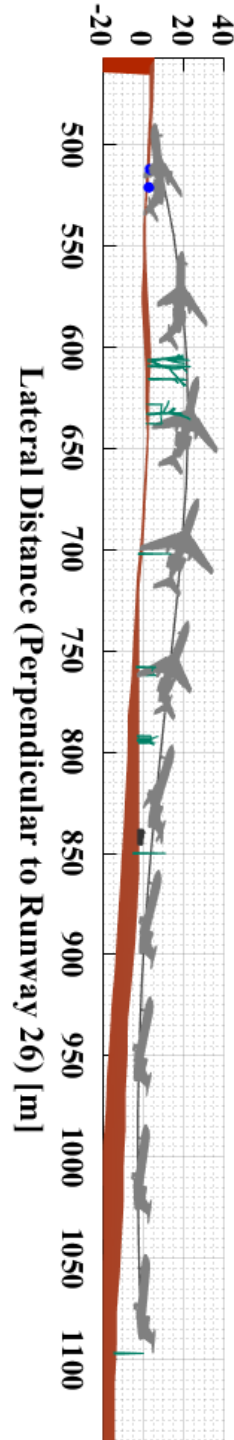


Figure 2.7 Case Low: Side view of aircraft 3D trajectory with respect to distance from Runway 26 threshold



In Table 2.2, checks on the aircraft heights and positions passing through the corresponding heights and positions of TAWS/FMS2 and major accident landmarks are summarized.

Table 2.2 Case Low: Summary of checks on aircraft heights and positions passing through corresponding heights and positions of TAWS/FMS2 and major accident landmarks

	Height* (± 5 m)	Longitudinal Position along Runway 26 centerline** (± 5 m)	Lateral Position along Runway 26 centerline** (± 5 m)
TAWS 34	✓	✓	✓
TAWS 35	✓	✓	✗
TAWS 36	✓	✓	✗
TAWS 37	✓	✗	✗
TAWS 38	✗	✗	✗
FMS2	✗	✗	✗

*For the TAWS alerts, Barometric altitude is used for the height; For the FMS2 alert, altitude corresponding to System Status is used for the height;

**For the FMS2 alert, GPS Position corresponding to Digital Outputs is used (FMS2b) to compute the longitudinal and lateral positions along the Runway 26 centerline;

	Physical Objects Impact Height (± 5 m)	Physical Objects Position (± 5 m)
P1: First-cut Birch	✓	✓
P5: Bodin Birch	✓	✓
P6b: Trees near Gubenko st.	✓	✓
P7: Powerline near Gubenko st.	✓	✓
P9: Mid-field Birch	✓	✓
P11b: Poplar east of Kutuzova st.	✓	✓
P12: Powerline near Kutuzova st. (no impact)	✓	✓
P13: Trees west of Kutuzova st.	✓	✓
Ground-marks Position (± 5 m)		✓
Ground-marks Orientation		✓

2.3 Impact Conditions

In this section, the impact conditions for the aircraft with the Bodin Birch tree (Case Low trajectory only) and with the ground are described. The parameters of interest that are calculated at these events include aircraft linear and angular velocities, aircraft orientation, aircraft control surface deflections, aircraft engine low and high compressor speeds, and aircraft engine thrust. For the Case Low trajectory, the aerodynamic loads are also calculated at these events.

The aircraft velocities are defined with respect to the Runway 26 axis-system (see Section 4.2 of the Annex II trajectory analysis report [10]). The heading or the yaw angle represents the true heading of the aircraft. The control surface deflections at these events are based FDR log, except for the deflection of slats, which is not available from the FDR log and is therefore based on the technical manual for the Tu-154M aircraft [9]. For the engine data, only the low compressor speed (N1) is available from the FDR log. The calculations for the high compressor speed (N2) and the engine thrusts are based on the information provided in the technical manual for the Tu-

154M aircraft. A brief description of these calculations is provided in Appendix A of the Annex II trajectory analysis report [10]. The calculation of the aerodynamic loads is based on Computational Fluid Dynamics (CFD) analysis of the Tu-154M aircraft. A validation of the CFD analysis is performed with the available wind tunnel results for a scaled model of Tu-154M aircraft. The methodology and results for the CFD analysis are provided in Appendix B of the Annex II trajectory analysis report [10].

2.3.1 Bodin Birch Tree Impact Condition

The velocities and orientation of the aircraft when it impacts the Bodin birch tree, obtained from the Case Low trajectory are depicted in Table 2.3. When the aircraft impacts the Bodin birch tree, it is in a climb flight phase with a vertical velocity of ~ 6 m/s and a pitch angle of about 15° . The groundspeed of the aircraft is about 73 m/s. The aircraft is slightly rolled at $\sim 3^\circ$ with the left wing down. The heading of the aircraft is almost identical to the heading of the Runway 26 centerline. The control surface deflections of the aircraft at the time of impact with Bodin birch tree are depicted in Table 2.4. The engine low and high compressor speeds and engine thrust of the aircraft at the time of impact with Bodin birch tree are depicted in Table 2.5. The aerodynamic loads for the aircraft at the time of impact with Bodin birch tree are depicted in Table 2.6. Figure 2.8 shows the position and orientation of the aircraft in the vicinity of the Bodin birch tree.

Table 2.3 Case Low: Aircraft velocities and orientations at impact with the Bodin birch

CG Linear Velocity		CG Angular Velocity		Orientation (Euler Angles)	
V_{x_r}	-73.2 m/s	ω_{x_r}	0.168 rad/s	Roll (ϕ)	-3.0°
V_{y_r}	-1.1 m/s	ω_{y_r}	0.065 rad/s	Pitch (θ)	15.4°
V_{z_r}	6.1 m/s	ω_{z_r}	-0.039 rad/s	Heading (ψ)	267.7°

Table 2.4 Case Low: Aircraft control surface deflections at impact with the Bodin birch

Left Aileron:	12.6°	Rudder:	7.9°
Right Aileron:	-12.6°	Flaps:	35.8°
Left Elevator:	-22.4°	Slats:	22°
Right Elevator:	-21.8°		

Table 2.5 Case Low: Aircraft engine low and high compressor speeds, and thrust at impact with the Bodin birch

	N1		N2		Thrust
Engine-1:	78.4 %	4215 rpm	90.6 %	9883 rpm	63.7 kN
Engine-2:	71.7 %	3856 rpm	88.8 %	9689 rpm	51.6 kN
Engine-3:	77.6 %	4170 rpm	90.4 %	9864 rpm	61.9 kN

Table 2.6 Case Low: Aircraft aerodynamic loads at impact with the Bodin birch

Body-fixed axis-system		Wind axis-system		Aerodynamic Angles	
FA_{x_b}	9.8 kN	Drag	136.3 kN	Angle of Attack	10.4°
FA_{y_b}	6.4 kN	Side Force	6.4 kN	Sideslip Angle	-2.5°
FA_{z_b}	-875.3 kN	Lift	864.7 kN		

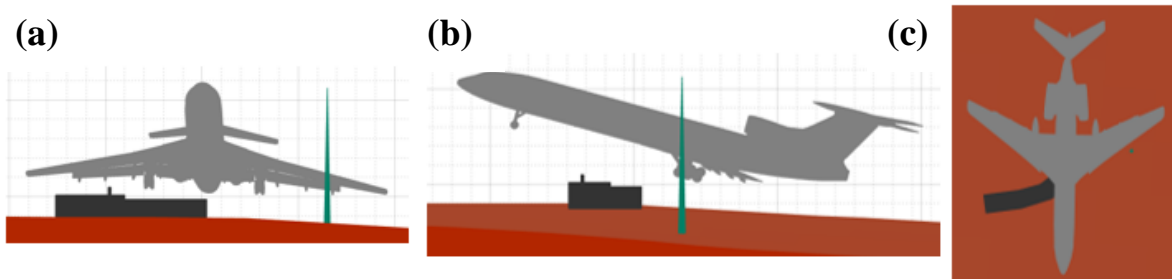


Figure 2.8 Case Low: Aircraft orientation at impact with the Bodin birch tree (a) Front view (b) Side view (c) Top view

2.3.2 Ground Impact Condition

The velocities and orientation of the aircraft at the time of impact with the ground, obtained from the Case Low trajectory, are depicted in Table 2.7. The left severed wing (without the ~ 6.5 m outboard section) makes the initial impact with the ground. The aircraft at the time of impact is almost inverted, with a roll angle of ~ -150°. The aircraft nose impacts almost at the same time as the left severed wing. The aircraft at the time of impact has a pitch angle of ~ -6°. The aircraft at the time of impact has a true heading of 246.8°. The effective yaw angle of the aircraft with respect to the Runway 26 centerline is therefore ~ -20°. The aircraft has a vertical velocity of ~ 17 m/s and a groundspeed of ~ 79 m/s at impact. The control surface deflections of the aircraft at impact, depicted in Table 2.8, correspond to the last recorded values from the FDR log. The FDR log (8 Hz channels) terminates ~ 1 s before the initial impact of the aircraft with the ground for the Case Low trajectory. The engine low and high compressor speeds, and engine thrust of the aircraft at the time of impact with the ground are depicted in Table 2.9. The low compressor speeds N1 (%) are extrapolated linearly from the end of the FDR log until the point of impact (~ 1 s). The aerodynamic loads for the aircraft at the time of impact with the ground are depicted in Table 2.10. Figure 2.9 shows orientation of the aircraft with respect to the local terrain at the time of impact with the ground.

Table 2.7 Case Low: Aircraft velocities and orientations at impact with the ground

CG Linear Velocity		CG Angular Velocity		Orientation (Euler Angles)	
V_{x_r}	-75.0 m/s	ω_{x_r}	0.169 rad/s	Roll (ϕ)	-150.5°
V_{y_r}	-25.2 m/s	ω_{y_r}	0.049 rad/s	Pitch (θ)	-6.2°
V_{z_r}	-17.3 m/s	ω_{z_r}	-0.012 rad/s	Heading (ψ)	246.8°

Table 2.8 Case Low: Aircraft control surface deflections at impact with the ground

Left Aileron:	N/A	Rudder:	1.7°
Right Aileron:	-5.1°	Flaps:	35.8°
Left Elevator:	24.4°	Slats:	22°
Right Elevator:	1.0°		

Table 2.9 Case Low: Aircraft engine low and high compressor speeds, and thrust at impact with the ground

	N1		N2		Thrust
Engine-1:	10.0 %	533 rpm	27.6 %	3015 rpm	1.3 kN
Engine-2:	86.9 %	4676 rpm	91.6 %	9990 rpm	83.9 kN
Engine-3:	80.8 %	4348 rpm	91.0 %	9932 rpm	68.6 kN

Table 2.10 Case Low: Aircraft aerodynamic loads at impact with the ground

Body-fixed axis-system		Wind axis-system		Aerodynamic Angles	
FA_{x_b}	-105.4 kN	Drag	93.4 kN	Angle of Attack	-4.7°
FA_{y_b}	51.1 kN	Side Force	44.4 kN	Sideslip Angle	-4.2°
FA_{z_b}	-184.4 kN	Lift	192.4 kN		

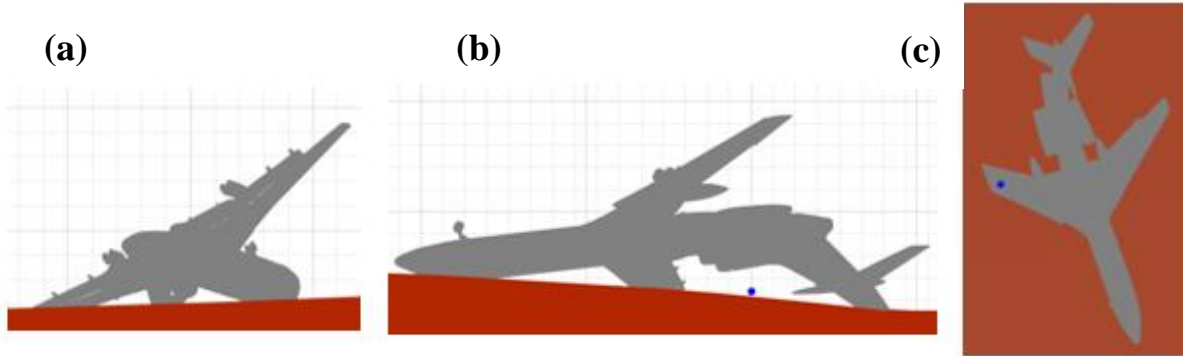


Figure 2.9 Case Low: Aircraft orientation at initial impact with the ground (a) Front view (b) Side view (c) Top view

The velocities and orientation of the aircraft at the time of impact with the ground, obtained from the Case High trajectory, are depicted in Table 2.11. The left severed wing (without the ~ 6.5 m outboard section) makes the initial impact with the ground. The aircraft at the time of impact is almost inverted, with a roll angle of ~ -150°. The aircraft nose impacts almost at the same time as the left severed wing. The aircraft at the time of impact has a pitch angle of ~ -6°. The aircraft at the time of impact has a true heading of 247.2°. The effective yaw angle of the aircraft with respect to the Runway 26 centerline is therefore ~ -20°. The aircraft has a vertical velocity of ~ 25 m/s and a groundspeed of ~ 79 m/s at impact. The control surface deflections of the aircraft at impact, depicted in Table 2.12, correspond to the last recorded values from the FDR log. The FDR log (8 Hz channels) terminates ~ 1.75 s before the initial impact of the aircraft with the ground for the Case High trajectory. The engine low and high compressor speeds, and engine thrust of the aircraft at the time of impact with the ground are depicted in Table 2.13. The low compressor speeds N1 (%) are extrapolated linearly from the end of the FDR log until the point of impact (~ 1.75 s). Figure 2.10 shows orientation of the aircraft with respect to the local terrain at the time of impact with the ground.

Table 2.11 Case High: Aircraft velocities and orientations at impact with the ground

CG Linear Velocity		CG Angular Velocity		Orientation (Euler Angles)	
V_{x_r}	-73.3 m/s	ω_{x_r}	0.040 rad/s	Roll (ϕ)	-149.5°
V_{y_r}	-28.7 m/s	ω_{y_r}	-0.010 rad/s	Pitch (θ)	-6.0°
V_{z_r}	-25.0 m/s	ω_{z_r}	-0.008 rad/s	Heading (ψ)	247.2°

Table 2.12 Case High: Aircraft control surface deflections at impact with the ground

Left Aileron:	N/A	Rudder:	1.7°
Right Aileron:	-5.1°	Flaps:	35.8°
Left Elevator:	24.4°	Slats:	22°
Right Elevator:	1.0°		

Table 2.13 Case High: Aircraft engine low and high compressor, speeds and thrust at impact with the ground

	N1		N2		Thrust
Engine-1:	10.0 %	533 rpm	27.6 %	3015 rpm	1.3 kN
Engine-2:	91.2 %	4907 rpm	91.3 %	9965 rpm	94.8 kN
Engine-3:	80.1 %	4309 rpm	90.9 %	9919 rpm	66.8 kN

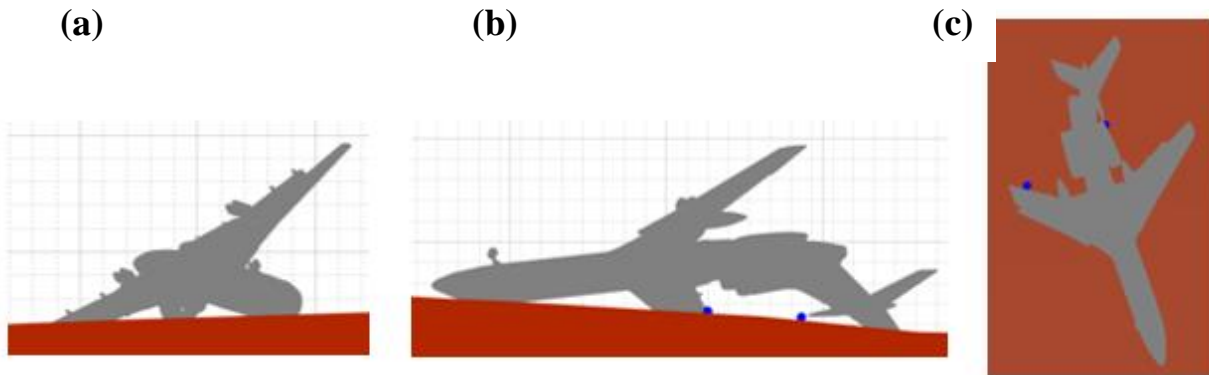


Figure 2.10 Case High: Aircraft orientation at initial impact with the ground (a) Front view (b) Side view (c) Top view

2.4 MAK Report Discrepancies

The main discrepancies observed in the MAK report [1] relevant to the trajectory analysis are described below:

- The flight data obtained from the MAK report [1] (via plot-digitization) has an offset in time of about 0.500-0.625 s with respect the MLP recorder log. This offset varies for different channels of the FDR log. The procedure for extracting the raw data from the FDR log is not explained in the MAK report [1]. Therefore, the reasons for the offset in time for the flight data provided in the MAK report [1] are not known.



- Based on analysis of the FDR log, a total of only 42 channels are available. Critical flight parameters required for accident reconstruction including longitudinal accelerations, groundspeeds, aircraft positions (GPS coordinates), and the left aileron deflections are not available from the FDR log. This is a violation of the ICAO Annex 6 Chapter 6.3.1 requirements that require these parameters to be recorded in the FDR. The MAK report [1] does not address this issue and provides no explanation as to why only a total of 42 channels are available in the FDR log.
 - According to the MAK report [1], page no. 75, the left wing of the aircraft impacted the Bodin birch tree at a height of 5 m above the ground. The height of 5 m is inconsistent with the findings of the prosecutor report [11], which claims the height to be 6.75 m. For the impact height of 5 m, right main landing gear of the aircraft needs to impact with the Bodin hut. However, from the photographs of the accident site (refer to Annex II trajectory analysis report [10] for details) it can be observed that the Bodin Hut was not impacted by the aircraft.
 - The magnetic heading data from the FDR does not correspond to actual locations of the initial ground-marks and subsequent wreckage scatter, and no explanation is provided in the MAK report [1] as to why this is the case. Based on the information provided in the Annex 4 to Miller report, the magnetic heading of the aircraft is determined to be 239° at the time of impact with the ground. The last recorded value of the magnetic heading from the FDR log is 216°. The magnetic heading at the time of impact with the ground through linear extrapolation is less than 200°. This value would result in the aircraft impacting sideways, and therefore direction of the wreckage scatter would be completely different to what is observed from the accident site photographs.
 - The pitch angle from the FDR does not correspond to actual locations of the initial ground-marks and subsequent wreckage scatter, and no explanation is provided in the MAK report [1] as to why this is the case. Based on the information provided in the Annex 4 to Miller report, the pitch angle of the aircraft is determined to be -6° at the time of impact with the ground. The last recorded value of the pitch angle from the FDR log is 0°. The pitch angle at the time of impact with the ground through linear extrapolation is more negative than -20°. This value would result in the aircraft impacting with the nose first, and therefore the left wing and horizontal stabilizer would miss the ground-marks observed from the accident site photographs.
 - The GPS coordinates of Bodin birch tree provided in the MAK report [1], in Table 1 on page no. 83 are not consistent with the location of the tree found on the satellite picture provided to NIAR by PSC. This is also true for the position of a lot of the landmarks provided in Table 1 of the MAK report [1]. The position is documented with respect to the longitudinal and lateral position from the Runway 26 centerline. There is a significant difference between these values compared to the locations found on the satellite picture provided to NIAR by PSC.
-



- According to the MAK report [1] on page no. 106, there were only four TAWS alerts recorded during the approach of the flight of TU-154M P101 at the Smolensk airport. This is inconsistent with the findings of the NTSB report [12], [13]. According to the manufacturer of the TAWS system – Universal Avionics, five TAWS alerts were recorded during the approach of the flight of TU-154M P101 at the Smolensk airport. The MAK report [1] completely ignores the TAWS 38 alert in its analysis. It should be noted that the TAWS 38 alert is controversial because of the barometric altitude and the GPS position of the aircraft recorded during this event. From the Case Low trajectory presented in this study, it is seen that the aircraft is much lower in height at the TAWS 38 time compared to the recorded barometric altitude. The aircraft also does not pass through the recorded TAWS 38 GPS coordinates.
 - According to the MAK report [1], on page number 106, the time-shift between TAWS alerts (UTC time) and FDR time is $FDR\ time = TAWS/FMS\ time + 2\ h:3.00\ s$. No additional information is provided in the MAK report [1] on how this time-shift is determined. In this study and according to the information provided by PSC, the time-shift is determined to be 2.75 s instead of the 3 s.
 - In Table 2.14, checks on the aircraft heights and positions passing through the corresponding heights and positions of the most important accident landmarks are summarized for the low trajectory. The location and height data for the landmarks used in this study are based on information provided by PSC. Checks are also performed against the positions and heights of the landmarks that are mentioned in the MAK report [1] (page number 83-84, Table 1). It can be seen that the aircraft will not pass through the landmarks including the ground-marks, when considering the positions (within the 5 m accuracy) provided in the MAK report [1]. These discrepancies are due to the inaccuracies in the measurements of the landmark positions provided in the MAK report [1]. The difference in the measurements provided in the MAK report [1] to ones provided by PSC to NIAR are shown in Table 2.15. The discrepancy in the aircraft orientation at time of ground impact is mainly due to the heading angle. The MAK report [1] does not mention of any correction that would be required in the magnetic heading angle in order for the aircraft to impact the ground with the right orientation (refer to Annex II trajectory analysis report [10] for details).
-

Table 2.14 Summary of checks on aircraft heights and positions passing through corresponding heights and positions of major accident landmarks for the low trajectory

	Physical Objects Impact Height (± 5 m)	Physical Objects Position (± 5 m)	Physical Objects Impact Height (± 5 m)	Physical Objects Position (± 5 m)
	(based on data provided by PSC [15])		(based on data provided in MAK report [1])	
P1: First-cut Birch	✓	✓	✓	✗
P5: Bodin Birch	✓	✓	✓	✗
P6b: Trees near Gubenko st.	✓	✓	N/A	N/A
P7: Powerline near Gubenko st.	✓	✓	N/A	✗
P9: Mid-field Birch	✓	✓	✓	✗
P11b: Poplar east of Kutuzova st.	✓	✓	N/A	✗
P12: Powerline near Kutuzova st. (no impact)	✓	✓	N/A	N/A
P13: Trees west of Kutuzova st.	✓	✓	N/A	N/A
Ground-marks Position (± 5 m) (based on data provided by PSC [15])	✓		Ground-marks Position (± 5 m) (based on data provided in MAK report [1])	
Ground-marks Orientation (based on data provided by PSC [15])	✓		Ground-marks Orientation (based on data provided in MAK report [1])	

Table 2.15 Distance of the major accident site landmarks from Runway 26 threshold/reference

Physical Obstacle ID	Physical Obstacle Description	MAK Report [1] Table 1 (Pg. 83-84)		Annex-4 to Miller Report [14], Table 2 (Pg. 4)		Data based on information provided by PSC on 01/15/2020 [15]	
		x _r (m)	y _r (m)	x _r (m)	y _r (m)	x _r (m)	y _r (m)
P1	First-cut Birch	1100	-35	1099	-39	1097.0	-44.0
P5	Bodin Birch	856	-61	855	63	850.0	-75.0
P6b	Trees near Gubenko st.	N/A	N/A	808	-57	794.0	-64.0
P7	Powerline near Gubenko st.	760	-56	777	-59	760.0	-71.0
P9	Mid-field Birch	715	-58	709	-68	702.0	-70.0
P11b	Poplar east of Kutuzova st.	635	-70	640	-76	633.0	-87.0
P12	Powerline near Kutuzova st.	N/A	N/A	N/A	N/A	633.0	-75.0
P13	Trees west of Kutuzova st.	N/A	N/A	616	-82	611.0	-83.0
P15	Left wing ground-mark	511	-96	518	-93	512.0	-102.5
P16	Horizontal Stab. ground-mark	520	-104	535	-105	521.0	-114.0

3 Bodin Birch Tree Accident Reconstruction

3.1 Bodin Birch Tree Impact Condition Definition

The MAK report does not specify all of the flight parameters required to define the initial conditions at the time of impact with the Bodin Birch. The only flight parameters available in the flight data plots provided in the MAK report [1] are indicated air speed, pitch, roll, and yaw angles of the aircraft. Other flight parameters required to define the initial conditions including ground speed, vertical velocity, and body axis angular rates of the aircraft are not available from the FDR log [16]. These parameters were determined from the trajectory analysis documented in detail in Annex II trajectory analysis report [10].

The MAK report, on page no. 167 [1], claims the time of the Bodin birch tree impact to be 10:41:00 hours local time (equivalent to 06:40:57 hours UTC time, based on MAK report time-shift of 4 h:3.00 s). The report does not give specific details on how the time of impact with the Bodin birch tree is determined. It is observed from the trajectory calculations that when the MAK time is used, the aircraft does not yaw enough to impact in an orientation consistent with the direction of the ground-marks and the subsequent wreckage scatter. The initial conditions for the birch tree impact were calculated based on the time of impact established in the trajectory analysis i.e. 06:40:57.1875 UTC. The trajectory analysis is documented in detail in the Annex II trajectory analysis report [10].

In this section, the impact conditions for the aircraft with the Bodin Birch tree (Case Low only) and with the ground are described. The parameters of interest that are calculated at these events include aircraft linear and angular velocities, aircraft orientation, aircraft control surface deflections, aircraft engine low and high compressor speeds, and aircraft engine thrust. For the Case Low trajectory, the aerodynamic loads are also calculated at these events. The aircraft velocities are defined with respect to the Runway 26 axis-system shown in Figure 3.1 [10]. The heading or the yaw angle represents the true heading of the aircraft. The control surface deflections at these events are based FDR log [16], except for the deflection of slats which is not available from the FDR log and is therefore based on the technical manual for the Tu-154M aircraft [18]. For the engine data, only the low compressor speed (N1) is available from the FDR log [16]. The calculations for the high compressor speed (N2) and the engine thrusts are based on the information provided in the technical manual for the Tu-154M aircraft. A description of these calculations is provided in the trajectory annex report [10]. The calculation of the aerodynamic loads is based on Computational Fluid Dynamics (CFD) analysis of the Tu-154M aircraft. A validation of the CFD analysis is performed with the available wind tunnel results for a scaled model of Tu-154M aircraft. The methodology and results for the CFD analysis are also provided in the trajectory annex report [10].

3.1.1 Aircraft Orientation and Velocities

The velocities and orientation of the aircraft when it impacts the Bodin birch tree, obtained from the Case Low trajectory [10], are summarized in Table 3.1. When the aircraft impacts the Bodin

birch tree, it is in a climb flight phase with a vertical velocity of ~ 6 m/s and a pitch angle of about 15°. The ground speed of the aircraft is about 73 m/s. The aircraft is slightly rolled at ~ 3° with the left wing down. The heading of the aircraft is almost identical to the heading of the Runway 26 centerline. The control surface deflections of the aircraft at the time of impact with Bodin birch tree are summarized in Table 2.4. Figure 3.2 shows the position and orientation of the aircraft in the vicinity of the Bodin birch tree.

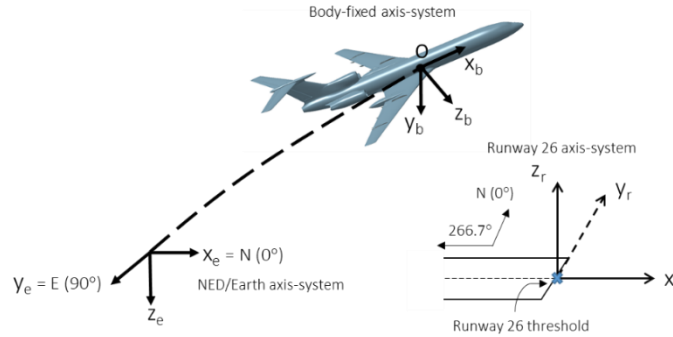


Figure 3.1 Aircraft coordinate system

Table 3.1 Case Low: Aircraft velocities and orientations at impact with the Bodin birch.

CG Linear Velocity		CG Angular Velocity		Orientation (Euler Angles)	
V_{x_r}	-73.2 m/s	ω_{x_r}	0.168 rad/s	Roll (ϕ)	-3.0°
V_{y_r}	-1.1 m/s	ω_{y_r}	0.065 rad/s	Pitch (θ)	15.4°
V_{z_r}	6.1 m/s	ω_{z_r}	-0.039 rad/s	Heading (ψ)	267.7°

Table 3.2 Case Low: Aircraft control surface deflections at impact with the Bodin birch.

Left Aileron:	12.6°	Rudder:	7.9°
Right Aileron:	-12.6°	Flaps:	35.8°
Left Elevator:	-22.4°	Slats:	22°
Right Elevator:	-21.8°		

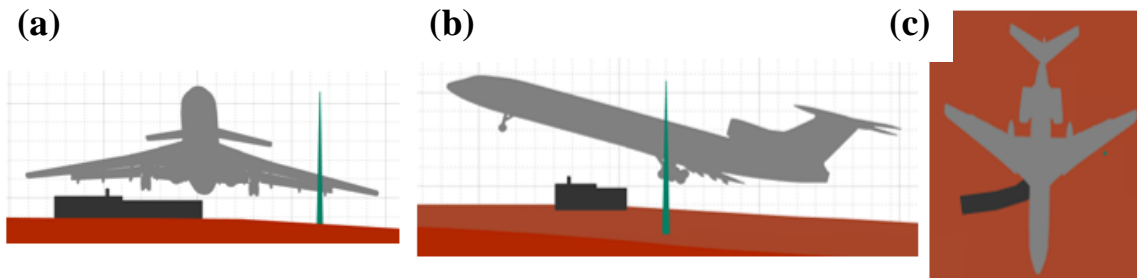


Figure 3.2 Case Low: Aircraft orientation at impact with the Bodin birch tree (a) Front view (b) Side view (c) Top view

3.1.2 Engine Thrust Loads

N1 for the three engines are based on the FDR data [16]. Beyond the end of the FDR log, N1 is determined using linear extrapolation until the ground impact. The lower limit for the value of N1 is capped to zero during the extrapolation. N2 is determined from the relationship between N1 and N2 obtained from information provided in the Tu-154M engine manual. RPMs for N1 and N2, and thrust values are determined based on information provided in the Tu-154M engine manual.

The values for N1, N2, and thrust are tabulated in Table 3.3. The thrust was kept constant for the entire duration of the Bodin birch tree analysis.

Table 3.3 Engine rpm and thrust for Bodin birch impact condition

	N1		N2		Thrust
Engine-1:	78.4 %	4215 rpm	90.6 %	9883 rpm	63.7 kN
Engine-2:	71.7 %	3856 rpm	88.8 %	9689 rpm	51.6 kN
Engine-3:	77.6 %	4170 rpm	90.4 %	9864 rpm	61.9 kN

3.1.3 Aerodynamic Forces

A CFD Analysis was conducted to define the aerodynamic forces. These calculations are discussed further in the trajectory analysis report [10]. The resulting forces are summarized in Table 3.4.

Table 3.4 Case Low: Aircraft aerodynamic loads at impact with the Bodin birch.

Body-fixed system	axis-	Wind axis-system	Aerodynamic Angles		
FA _{x_b}	9.8 kN	Drag	136.3 kN	Angle of Attack	10.4°
FA _{y_b}	6.4 kN	Side Force	6.4 kN	Sideslip Angle	-2.5°
FA _{z_b}	-875.3 kN	Lift	864.7 kN		

3.2 Bodin Birch Tree FEA Model Definition

The definition of the tree is critical in predicting the outcome of the tree impact. The definition of the tree geometry is documented in section 3.2.1. Information for the tree material model definition is summarized in section 3.2.2.

3.2.1 Tree Geometry

The only information about the tree available in the MAK report [1] is that the impact height was 5 m, the tree diameter at the impact height was 30 – 40 cm, and that it was a birch tree. As shown in the trajectory analysis report and chapter 3.5, the impact height of 5 m is not feasible as the aircraft would impact the “Bodin hut” (see Figure 3.41). Images from the site, such as Figure 3.42, show that the “Bodin hut” was not damaged by the aircraft. In addition, several sources of information were analyzed regarding the tree geometry and all data showed that the tree impact height was greater than 6 m. Thus detailed discussions were held with the PSC to discuss the geometry of the tree that would be used for the impact reconstruction.

The information for the tree geometry and angles was provided by the PSC through email attachments received on November 7th 2019 [17]. The dimensions of the tree are shown in Figure 3.3. The angle and orientation of the tree is shown in Figure 3.4. Note that branches of the tree were not modeled and it was agreed with the PSC members to simplify the tree model to a cone shape.

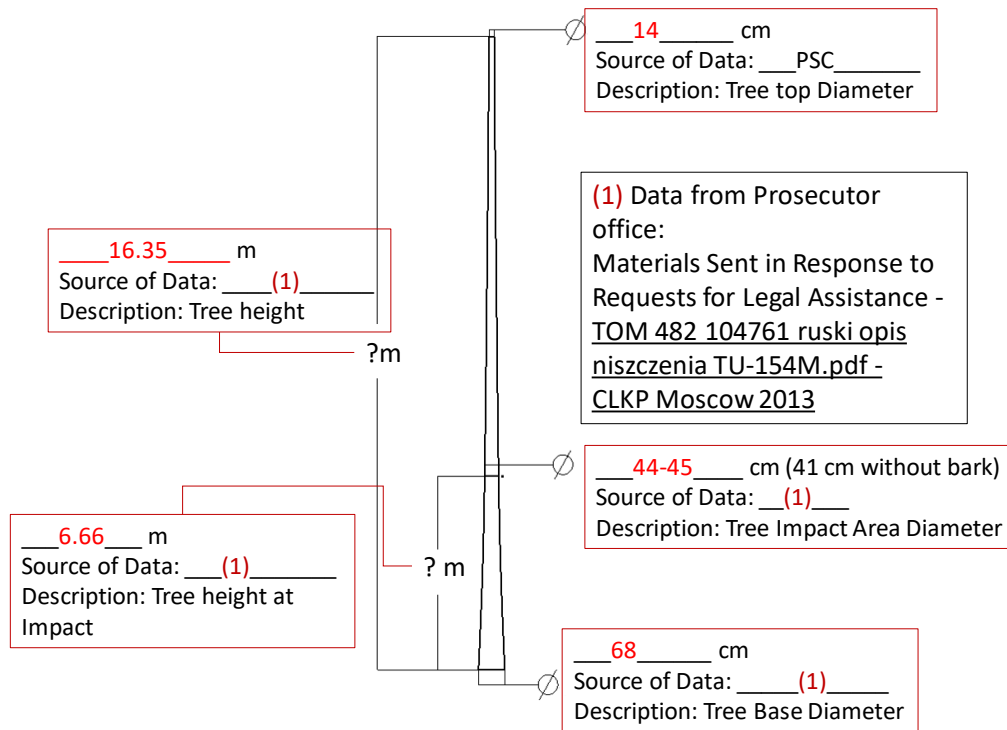


Figure 3.3 Tree geometry provided by the PSC [17]

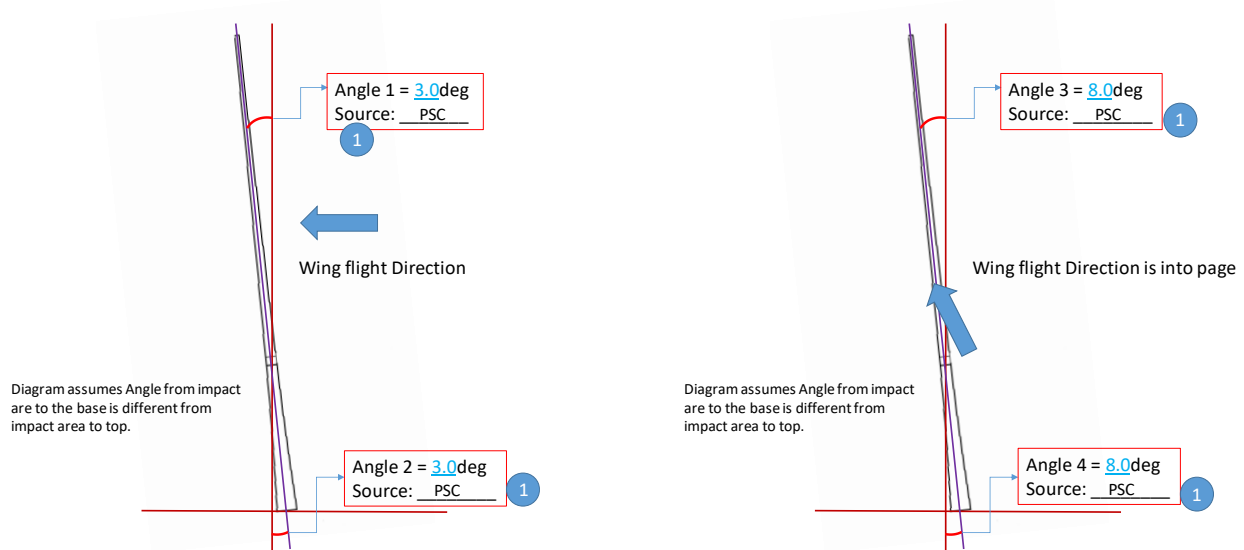


Figure 3.4 Tree angle and orientation provided by the PSC [17]

3.2.2 Tree Material Definition

The development of tree material model for LS-DYNA analysis is documented in Chapter 2 of the annex III report. The material card was calibrated and validated against coupon, sub-component, and component level tests (see Figure 1.6 Building Block Approach). The coupon level tests included tensile, shear and compression coupon tests. The sub-component level test was a three-point bending test, and the component level tests for birch trees of various diameters were impact tests conducted by NIAR at Southwest Research Institute and by the PSC at the University of Akron. A summary of the correlation of the material model to test data is summarized in Section 2.4 of the annex III report.

3.2.3 Tree FEA Model

The birch tree model was discretized using 8-noded solid elements, as shown in Figure 3.5. The LS-DYNA constant stress element formulation [24] was used to define the section properties of the tree elements. The minimum element length in the tree is 1.187 mm in length and the maximum element length is 9.9 mm. At the impact area, the element length was maintained between 3.4 – 6 mm, as shown in Figure 3.6. There are a total of 12,548,288 solid elements in the tree FEM.

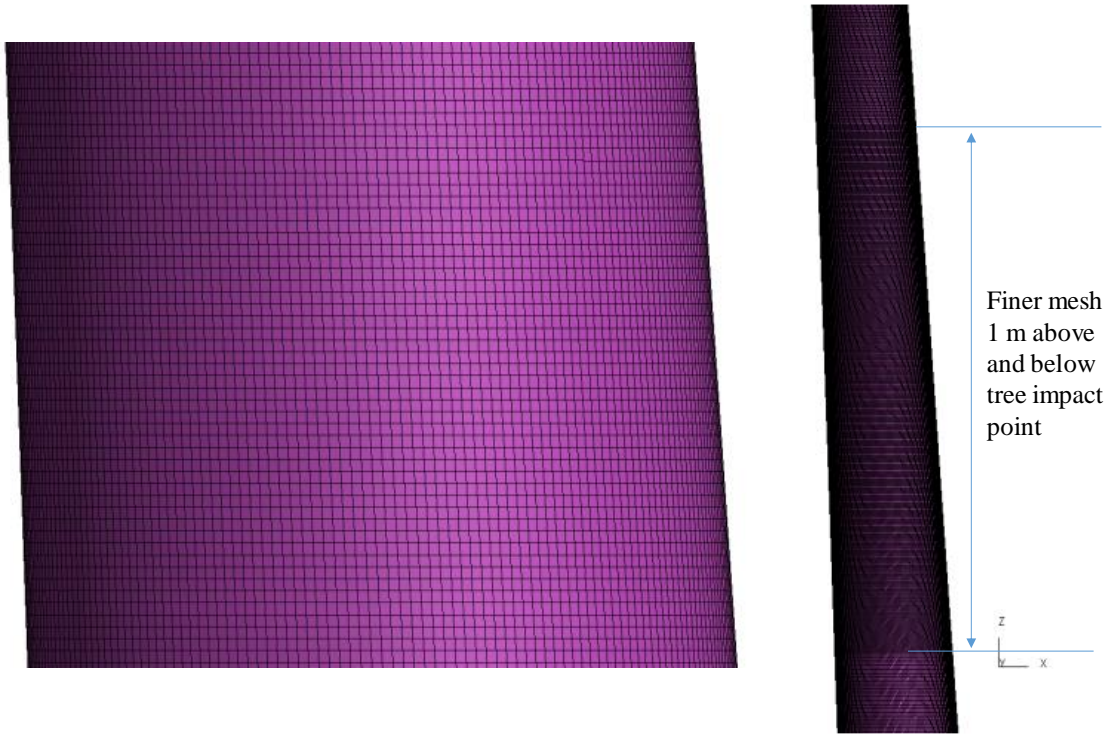


Figure 3.5 Tree FEM discretization

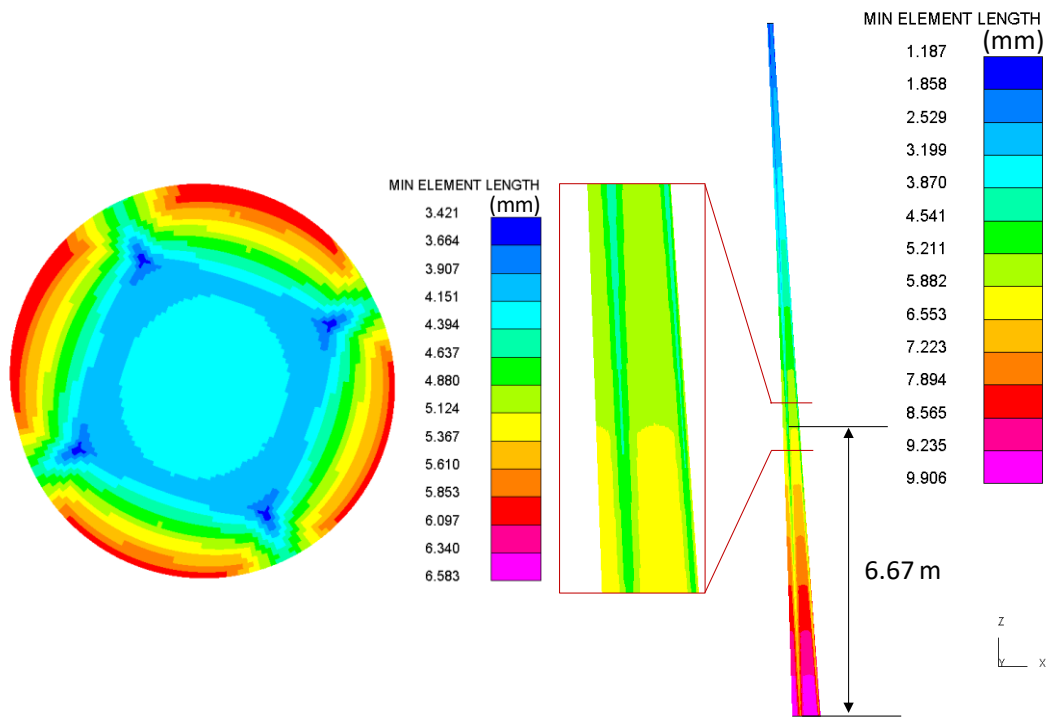


Figure 3.6 Tree FEM element length

3.3 Bodin Birch Tree Impact Analysis Setup

The impact location on the wing was defined based on a detailed analysis and discussion with the PSC. Based on the discussion and approval by the PSC, the impact location on the wing was set, as shown in Figure 3.7. This data was provided by the PSC through email attachments received on November 7th 2019 [17].

The setup of the analysis model with the loads (see Table 4.3 and 4.4) and initial velocities (see Table 4.1) is shown in Figure 3.8 and Figure 3.9. Note that the remaining weight (73.76 tons) of the full aircraft was applied at the CG node. The engines total thrust force (per Table 4.3) was also applied at the CG node. The tree was constrained in all degrees of freedom at the base. Control surfaces of the wing were also deflected per the data provided by the trajectory analysis, as shown in Figure 3.10.

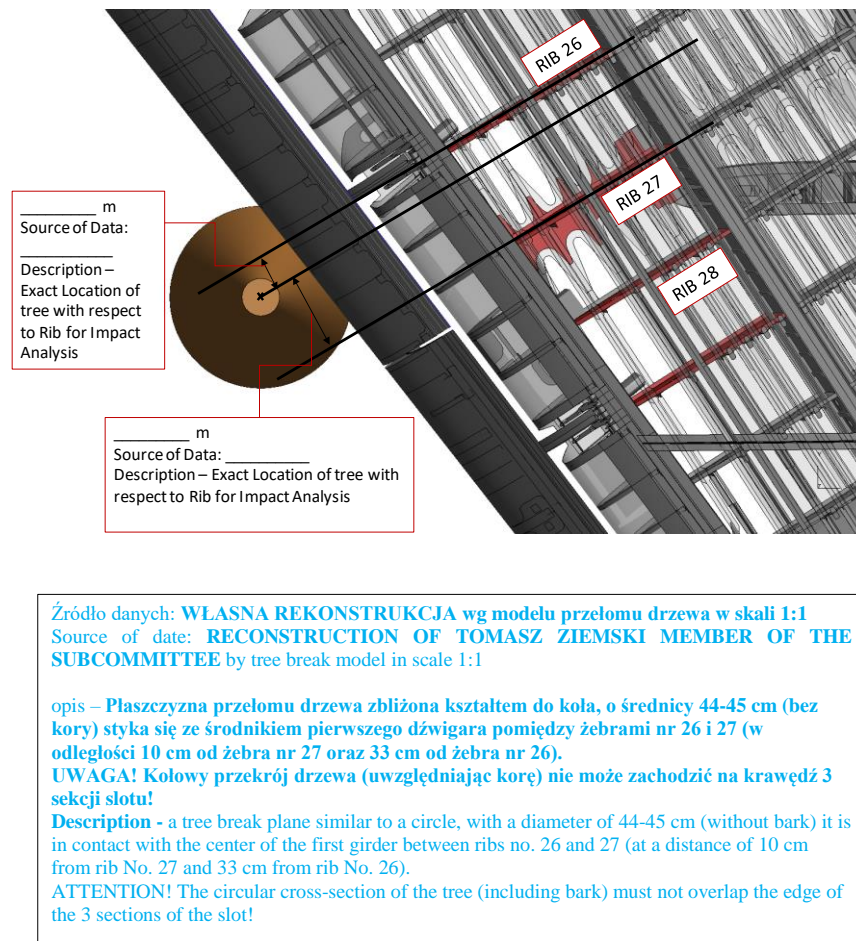


Figure 3.7 Tree impact location definition for analysis by the PSC [17]

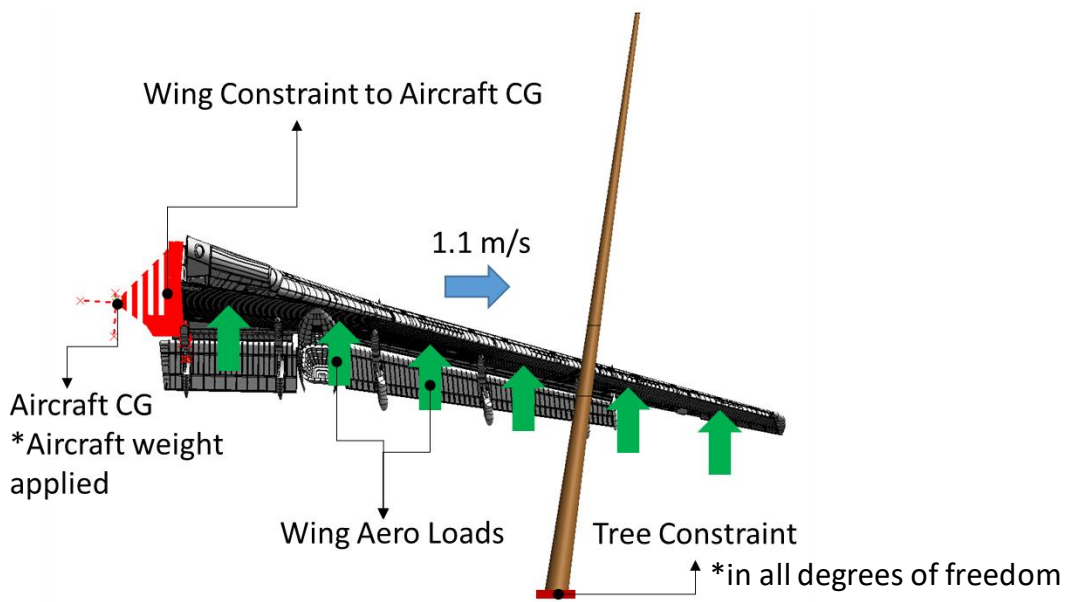


Figure 3.8 Tree impact analysis setup – front view

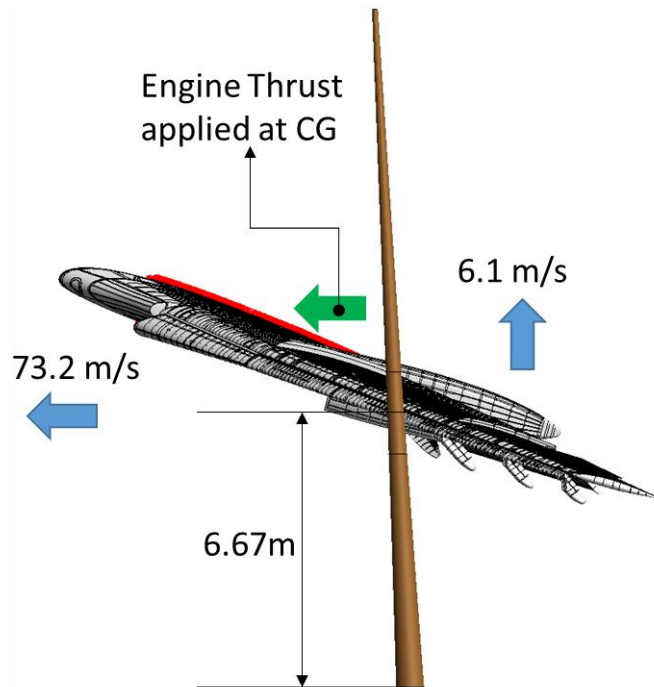


Figure 3.9 Tree impact analysis setup – side view

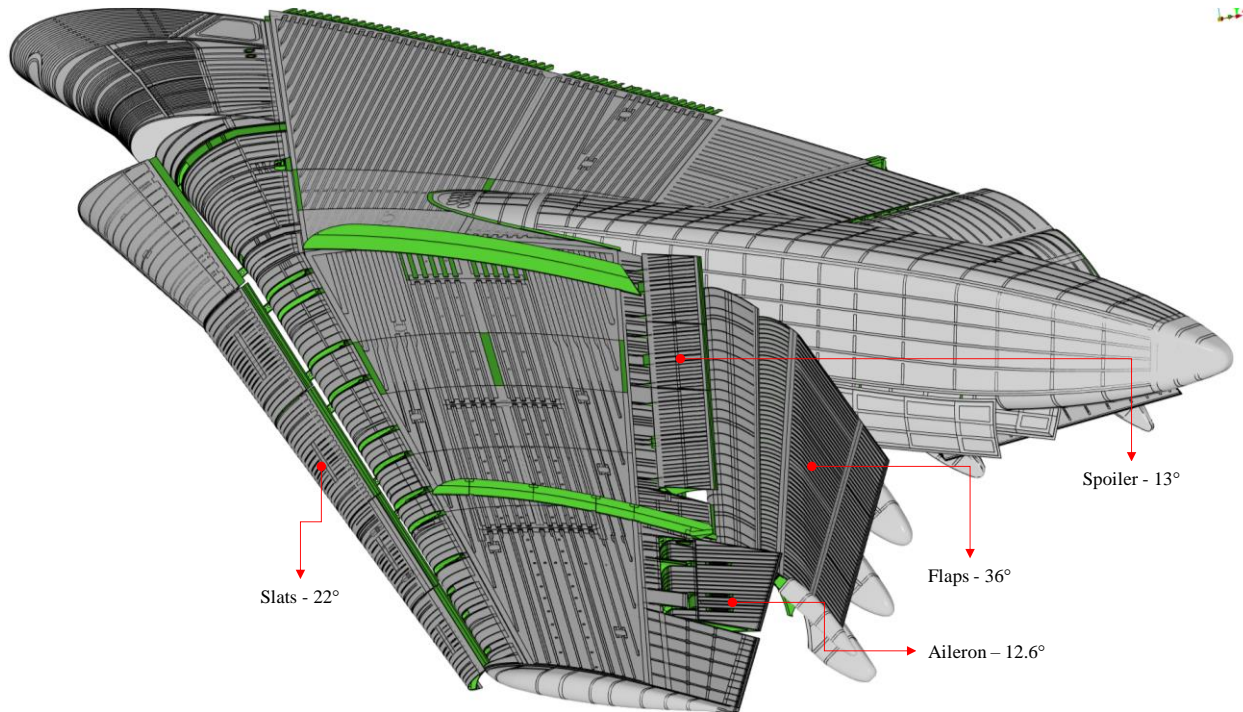


Figure 3.10 Tree impact analysis setup – control surface orientations

3.4 Bodin Birch Tree Impact Analysis Results

This section presents the analysis results of the Bodin birch tree impact reconstruction and a comparison with the data provided in the MAK Report [1] and by the PSC [4].

3.4.1 Left Wing to Bodin Birch Tree Impact Kinematics Analysis.

The following events were observed during the impact event between the Bodin birch tree and the left wing (see Figure 3.11 to Figure 3.17):

- From 0 to 10 ms: Initial Bodin birch tree contact with left wing slat
- From 10 to 20 ms: Interaction between the Bodin Birch tree and front spar (Spar 1)
- From 20 to 26 ms: The front spar (spar 1) fails

- From 27 to 30 ms: Interaction between the Bodin Birch tree and middle spar (Spar 2)
 - From 30 to 40 ms: The middle spar (spar 2) fails
 - From 40 to 50 ms: The Bodin Birch tree starts failing in the impact height location (~6.66 meters)
 - At 50 ms: The Bodin tree fails and separates in two parts (upper and lower trunk, see Figure 3.17)
 - From 50 to 58 ms: Interaction between the Bodin Birch tree and rear spar (Spar 3)
 - From 58 to 91 ms: The upper trunk contacts with the rear spar (Spar 3) and the bottom trunk upper surface contacts the bottom wing and flap surfaces
 - At 91 ms: The bottom trunk of the birch tree is no longer in contact with the flaps and the upper part of the Bodin birch tree starts separating from the rear spar (Spar 3)
 - From 91 to 110 ms: The upper trunk is still in contact with the rear spar (Spar 3)
 - At 110 ms: The upper trunk separates from the rear spar (Spar 3), and contact between the left wing and the Bodin Birch tree terminates
 - From 110 ms to the end of the simulation (130 ms) the upper and lower birch tree trunks continue to separate as the left wing moves in the direction of flight. It should be noted that the rear spar (Spar 3) did not fail completely. The margin of safety for Spar 3 is 0.08 as shown in Table 3.5. Minor changes in Birch tree geometry and material, or wing aerodynamic loads could introduce additional forces that would be sufficient to fail spar 3.
-

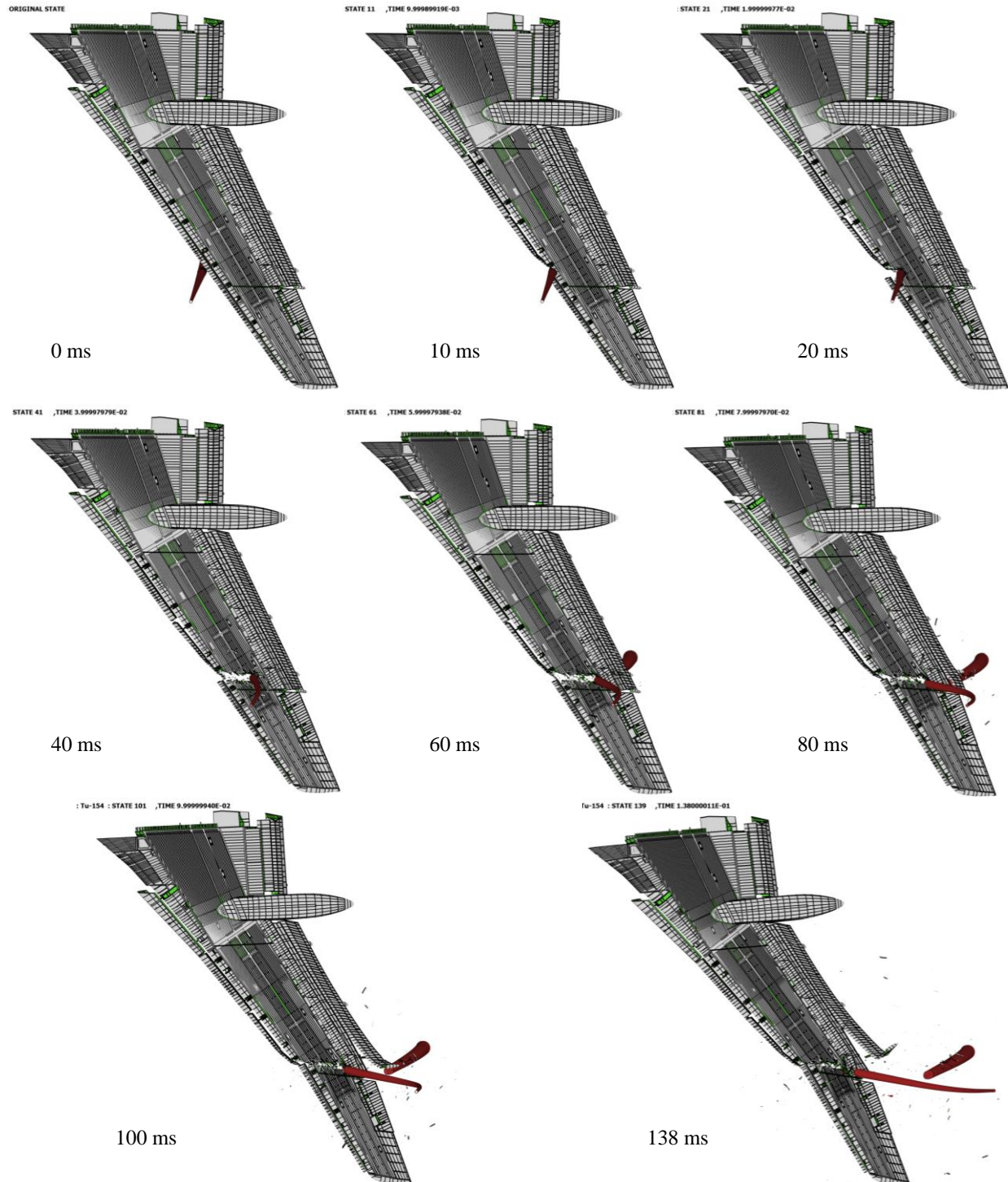


Figure 3.11 Tree impact analysis kinematics – top view

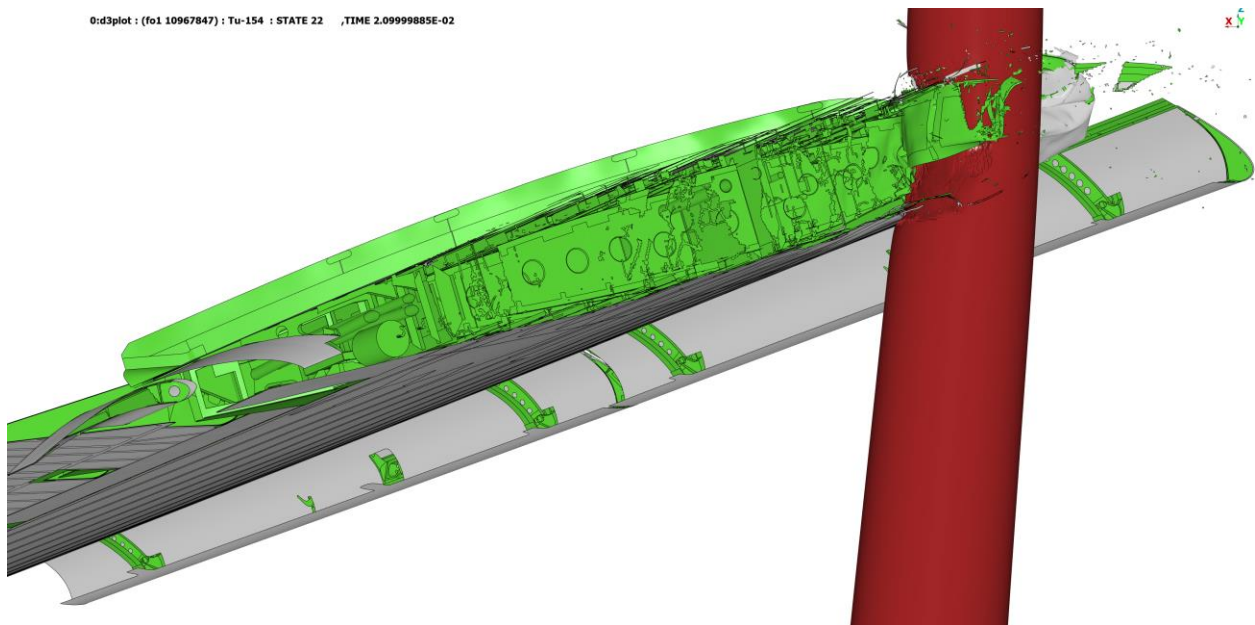
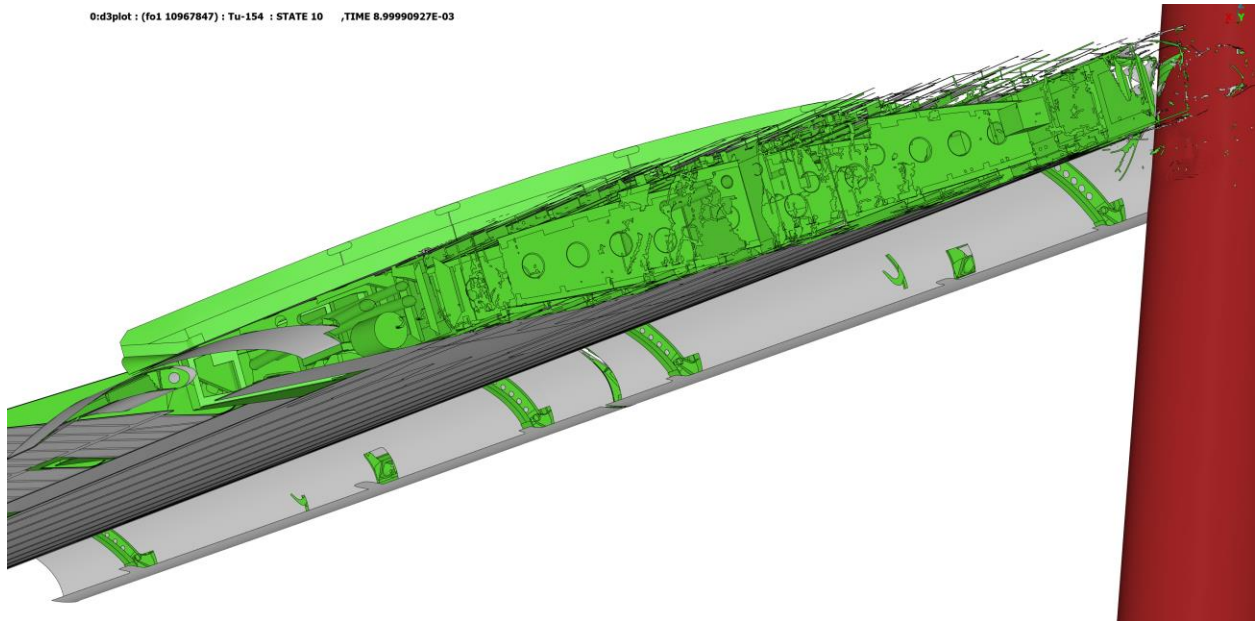


Figure 3.12 Tree impact analysis kinematics – section view (9 and 20 ms)

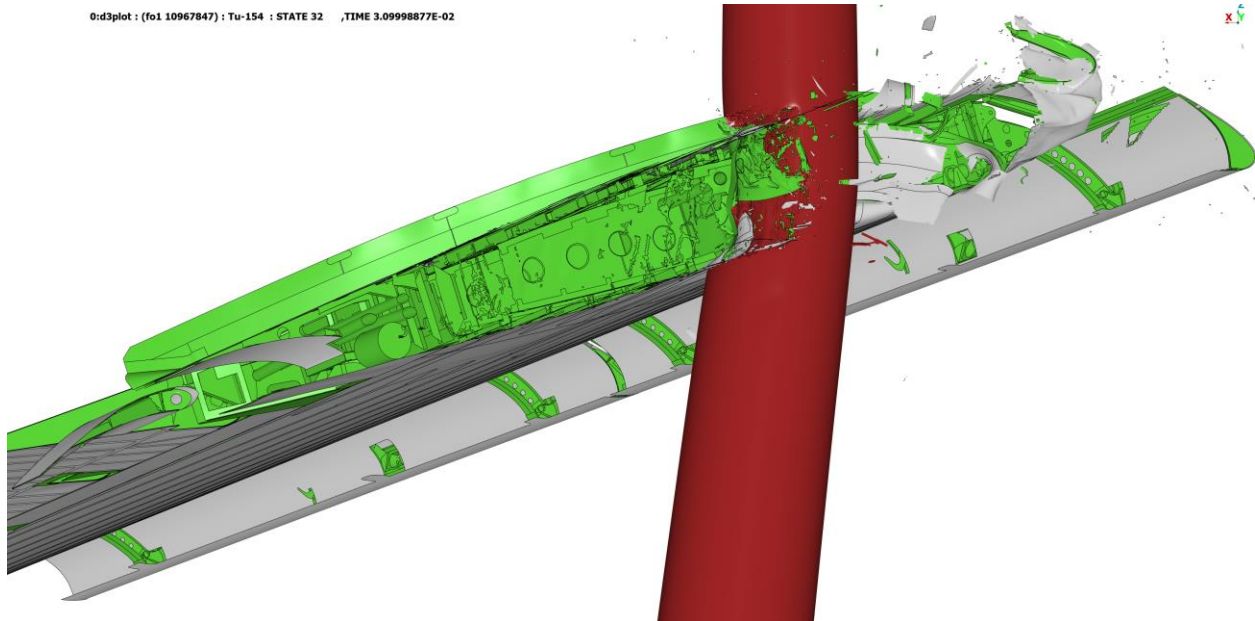
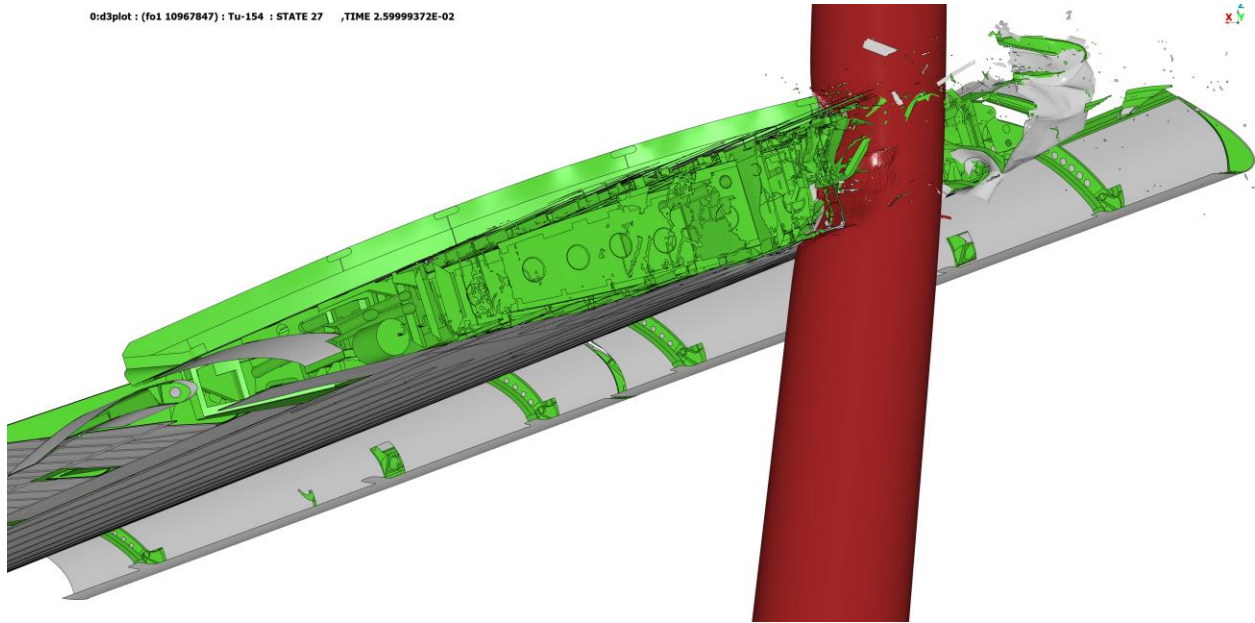


Figure 3.13 Tree impact analysis kinematics – section view (26 and 31 ms)

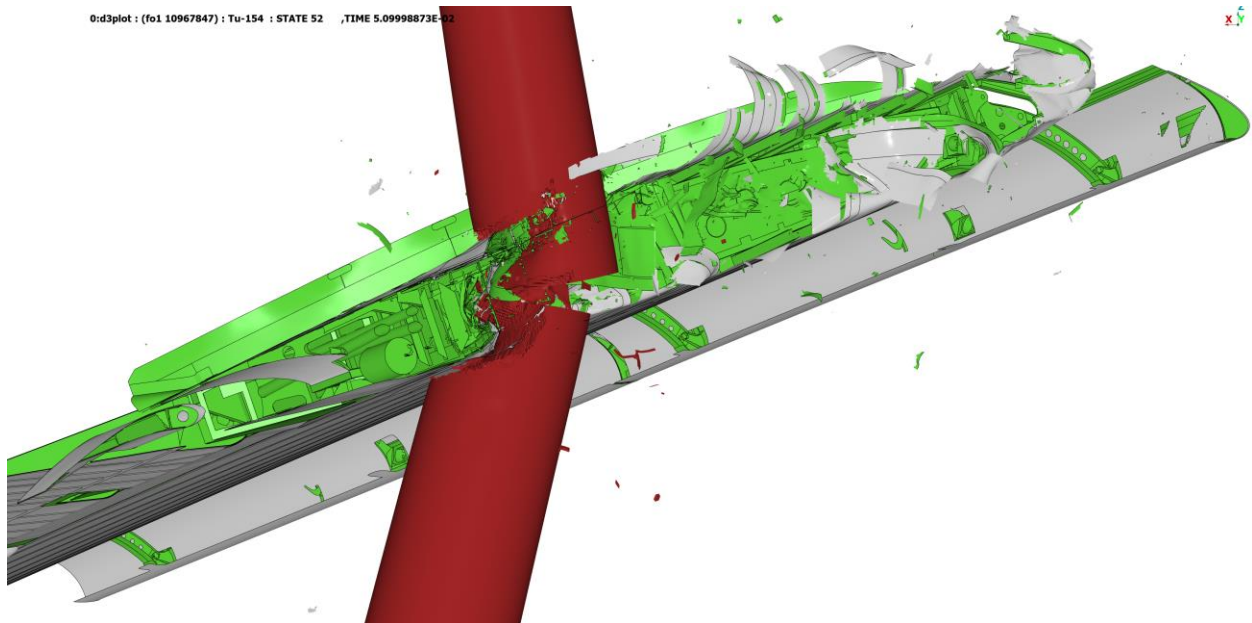
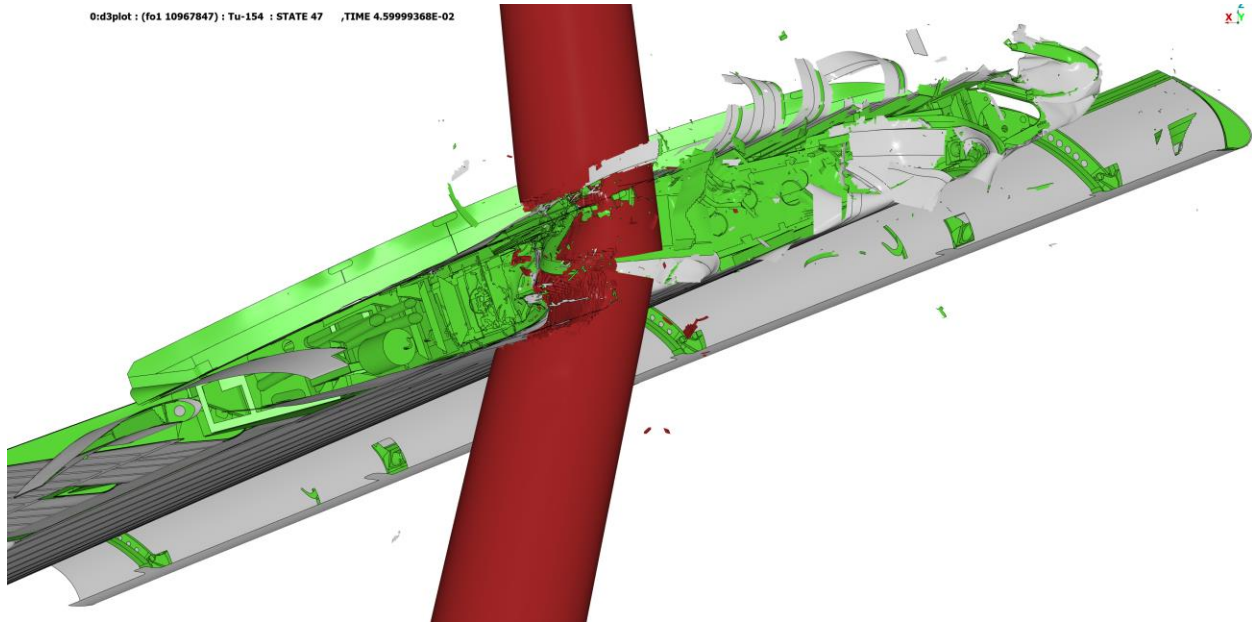


Figure 3.14 Tree impact analysis kinematics – section view (46 and 51 ms)

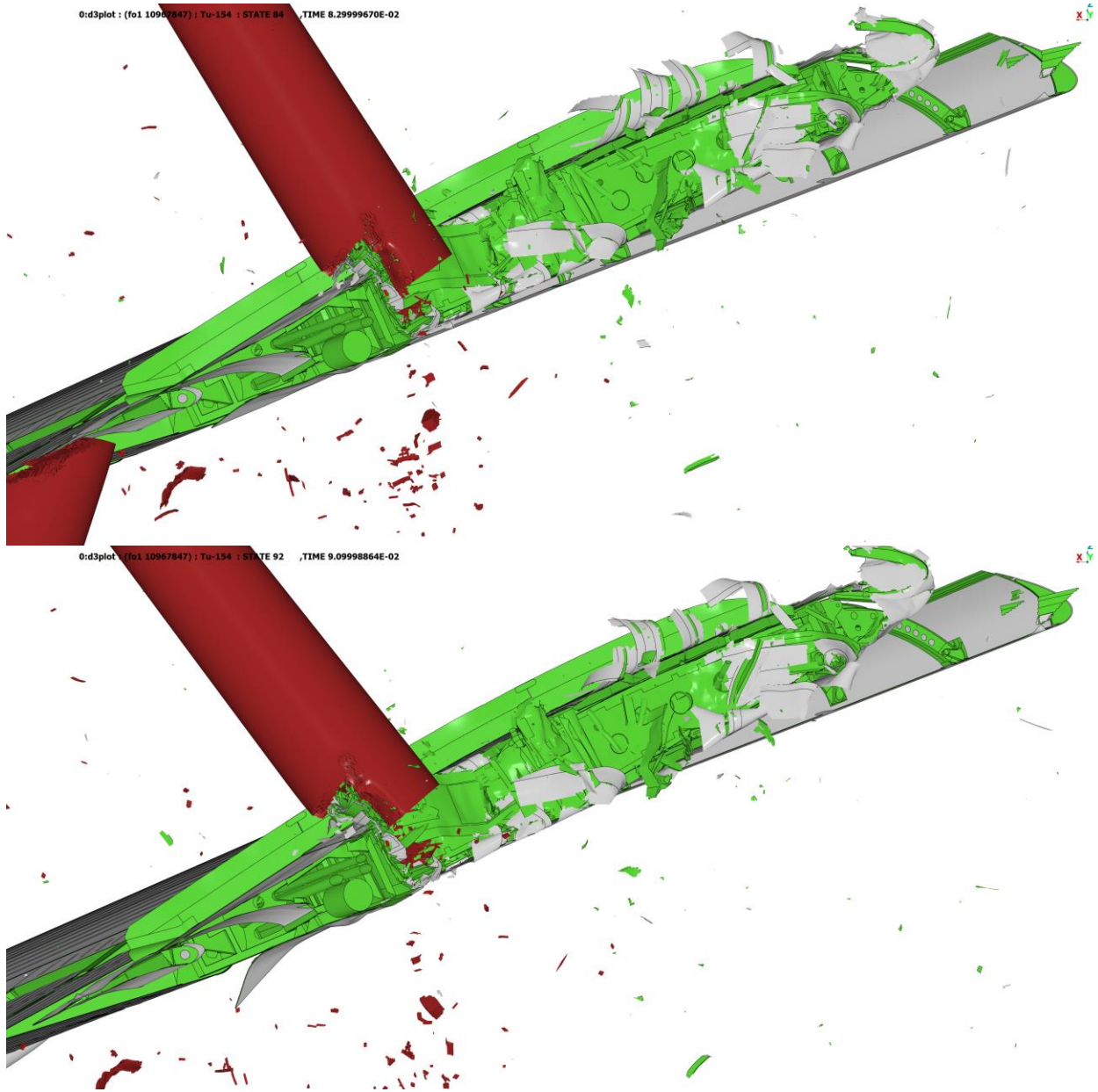


Figure 3.15 Tree impact analysis kinematics – section view (83 and 91 ms)

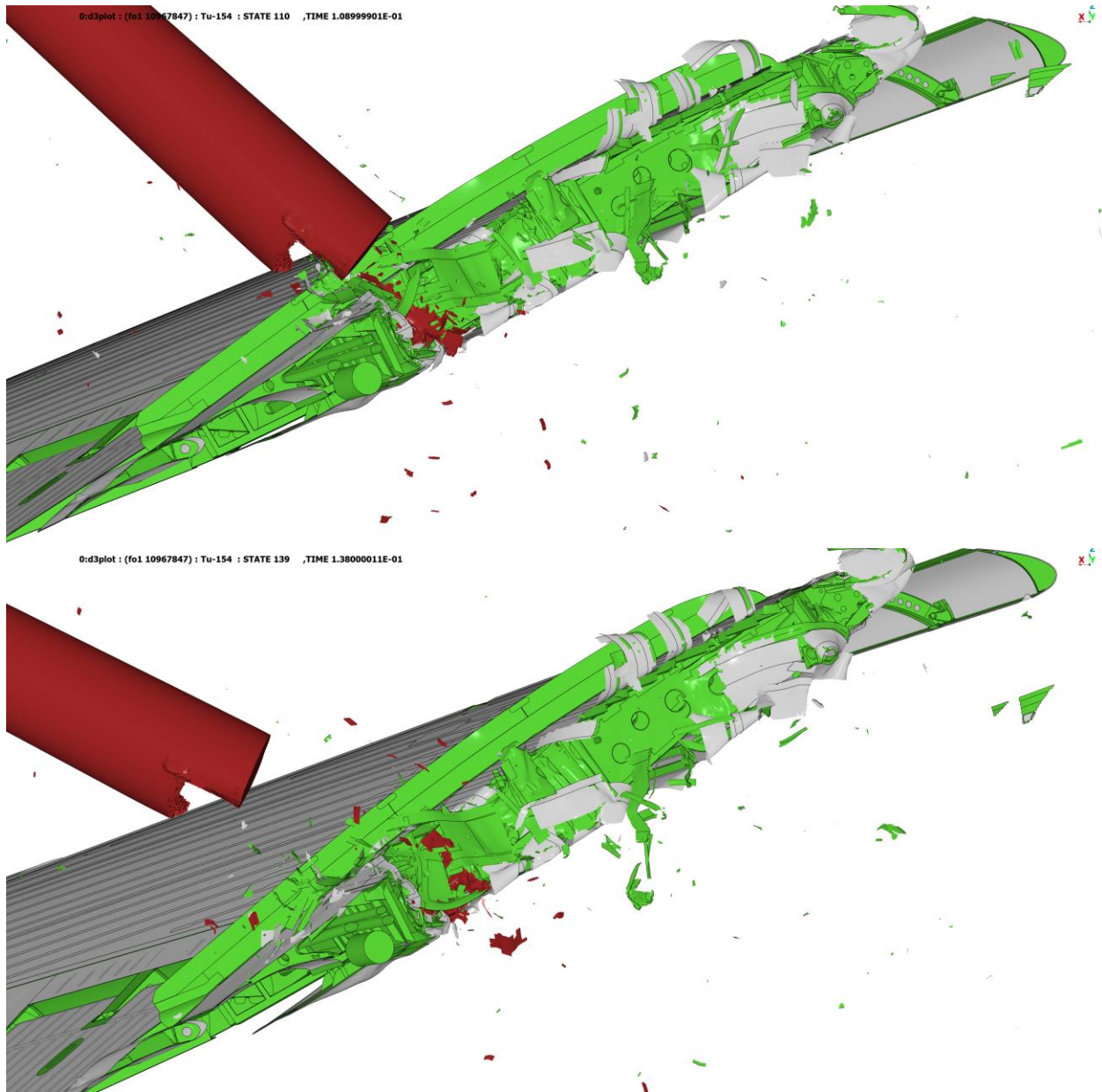


Figure 3.16 Tree impact analysis kinematics – section view (109 and 138 ms)

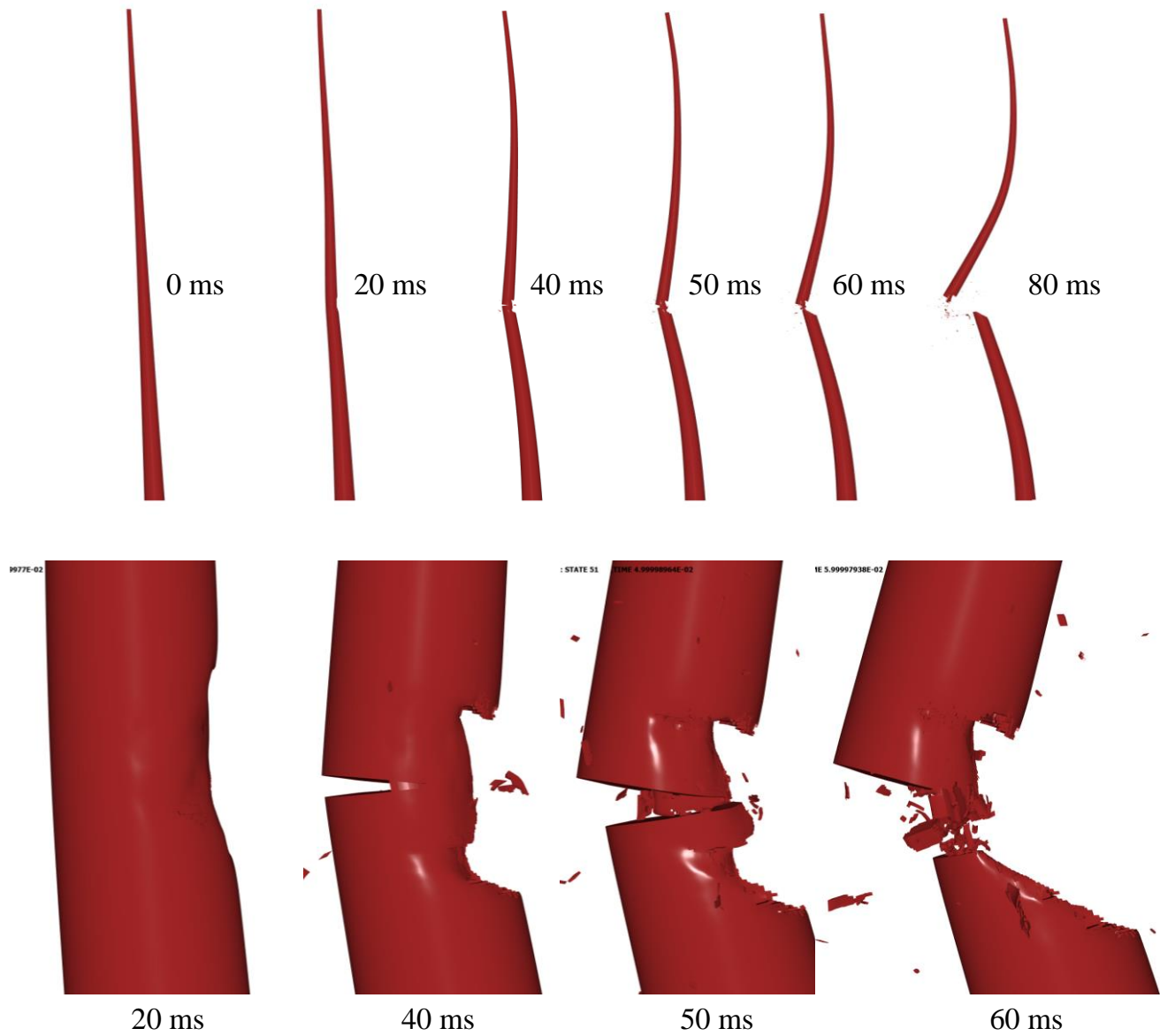


Figure 3.17 Tree impact analysis kinematics – tree kinematics from side view

Table 3.5 Margin of safety on remaining attached parts of wing – Time: 138ms

Components IDS	Part	Material	Max Plastic Strain	Max-Von Mises Stress(MPa)	Failure Strain	True Ultimate tensile stress(MPa)	Margin Of Safety (Stress)
252781	Trailing Edge (TE) Skin Rib	PA-E8-12A-0X	0.1750	559.00	0.1920	574.19	0.03
252791	TE Skin	PA-E8-16A-0X	0.0940	443.00	0.0940	581.73	0.31
253021		PA-E8-16A-0X	0.0940	546.00	0.0940	581.73	0.07
217091	Aft Tube3	Aluminum	0.1920	410.00	0.1920	574.19	0.40
217141	Aft MiddleTube	Aluminum	0.1920	580.00	0.1920	574.19	-0.01
217171	Aft Upper Tube	Aluminum	0.1524	399.00	0.1920	574.19	0.44
202311	Spar 3	PA-E8-62A-0X	0.1353	518.00	0.1353	561.57	0.08
202312		PA-E8-62A-0X					
202331	Spar 3 Upper Stiffener	PA-E8-62A-0X	0.0918	450.00	0.1353	561.57	0.25
202335		PA-E8-62A-0X					
254351	TE Span Wise Stiffener Aft	PA-E8-17C-0X	0.0000	196.00	0.1071	666.03	2.40
254341	TE Span Wise Stiffener FWD	PA-E8-17C-0X	0.0000	209.60	0.1071	666.03	2.18
254141	TE Ribs/Stiffeners	PA-E8-64A-0X	0.1944	460.90	0.1944	543.96	0.18
254280	TE Wedge	PA-E8-16A-0X	0.0000	169.00	0.0940	581.73	2.44

3.4.2 Wing Damage Evaluation

The impact of the left wing with the Bodin Birch tree was presented in the MAK Report [1] as the cause of the left wing tip being separated from the aircraft, which resulted in an abrupt roll of the aircraft. However, the damage to the wing or the Birch tree were not adequately documented, and the only picture or analysis data available is shown in Figure 1.12 and Figure 1.13. Additional data was provided by the PSC [19][20] and has been used to compare the damage predicted by the simulation.

The sequence of interactions between the Bodin Birch Tree and the left wing impact are described below. The damage observations are divided into four regions as shown in Figure 3.18:

- Region 1:
 - From 0 to 10 ms: Initial impact of Bodin birch tree contact with left wing slat. No significant damage is sustained on the left slat portion of the wing as shown in Figure 3.20. The results of the simulation agree with the post impact pictures provided by the PSC [19][20].

- Region 2:
 - From 10 to 20 ms: Interaction between the Bodin Birch tree, leading edge and spar (Spar 1). As shown in Figure 3.19 the leading edge is plastically deformed due to the compressive loads exerted by the tree impact. Similar deformations are observed in the pictures provided by the PSC [19][20].
 - From 20 to 26 ms: The front spar (spar 1) fails (see Figure 3.32).

 - Region 3:
 - From 27 to 30 ms: Interaction between the Bodin Birch tree displacing towards the middle spar (Spar 2). Failures of the wing skin, stringers and ribs occur as the tree moves towards spar 2. Similar failure mechanisms are shown when compared with the post impact wing pictures provided by the PSC (see Figure 3.27).
 - From 30 to 40 ms: The middle spar (spar 2) fails (see Figure 3.33).
 - From 40 to 50 ms: The Bodin Birch tree starts failing at the impact height location (see Figure 3.36).
 - At 50 ms: The Bodin tree fails and separates in two parts (upper and lower trunk)

 - Region 4:
 - From 50 to 58 ms: Interaction between the Bodin Birch tree and rear spar (Spar 3)
 - From 58 to 91 ms: The upper trunk contacts with the rear spar (Spar 3) and the bottom trunk upper surface contacts the bottom wing and flap surfaces.
 - At 91 ms: The bottom trunk from the birch tree is no longer in contact with the flaps, and the upper part of the Bodin birch tree starts separating from the rear spar (Spar 3)
 - From 91 to 110 ms: The upper trunk is still in contact with the rear spar (Spar 3)
 - At 110 ms: The upper trunk separates from the rear spar (Spar 3) and the contact between the wing and Bodin Birch tree terminates.
-

- From 110 ms to the end of the simulation (130 ms): The upper and lower birch tree trunks continue to separate as the left wing moves in the direction of flight. It should be noted that the rear spar (Spar 3) did not fail completely as shown on the pictures provided by the PSC (See Figure 3.19). The margin of safety for Spar 3 is 0.08, as shown in Table 3.5. Minor changes in Birch tree geometry and material, or wing aerodynamic loads could introduce additional forces that would be sufficient to fail spar 3.

The damage to the outboard part of the wing from the analysis was compared to the severed part of the wing from the debris field [19] in Figure 3.23 and Figure 3.24. The analysis model shows good correlation to the damage observed on the post-impact wing pictures. Further images of the separated wing were provided to NIAR by the PSC [20], which show more detail of the wing damage. Comparisons to these pictures are shown in Figure 3.19 and Figure 3.23 through Figure 3.28.

Figure 3.27 shows the similarities observed in the curling of the wing. The top part of the wing shows outwards curling, which is captured by the simulation model. The first curl on the bottom of the wing is also captured by the model as shown in Figure 3.27.

It should also be noted that some discrepancies were observed when comparing the simulation results to the post-impact pictures provided by the PSC:

- A closer look at Figure 3.26 shows that some curled edges on the bottom of the wing do not curl outwards as shown in the wing post impact pictures. Note that the wing debris images used for comparison in Figure 3.25, Figure 3.26 and Figure 3.27 are taken at a storage facility and NIAR does not have any documentation on any damage that the wing debris could experience during transportation or storage. NIAR recommends the PSC to request or conduct a detail failure surface analysis of the lower skin to confirm whether the outward curling of the lower skin was due to the tree impact loads.
- Another difference that was observed between the simulation and the post impact pictures provided by the PSC is highlighted in Figure 3.28. In this picture, the wing rupture line on the outboard portion of the left wing is much closer to the wing boundary layer fence compared to the simulation. This indicates that small variations in the aircraft orientation prior to the tree impact or the idealized tree geometry could have contributed to these discrepancies.
- The PSC identified pieces of the left wing slat and spar stiffener that were found embedded into the birch tree at time of accident [21]. These are shown in Figure 3.29. The MAK report also notes that the investigation team found, fragments of left wing panel embedded in the tree trunk”[1]. While the MAK report does not identify these fragments, detailed information about the fragments has been provided by the PSC [21]. The top piece is part of the upper fixed leading edge and the bottom piece is a stiffener from the front spar [21]. The kinematics of the top and bottom fragments as observed on the simulation are shown

in Figure 3.30 and Figure 3.31 respectively. In terms of similarities, it can be noted that the two parts of the wing indeed are in the path of the tree in the simulation. The simulation does not show any of the parts remaining embedded in the tree trunk. The fragment of the fixed leading edge fragment bends upwards in the simulation, while in the actual accident, it is bent upwards and embedded into the tree. This is also illustrated in Figure 3.30, which shows that the skin of the front leading edge ruptures at 12 ms allowing direct contact of the top piece with the tree trunk. The spar stiffener fragment, shown in Figure 3.31, also does not get embedded in the tree impact simulation. In the simulation, the stiffener piece is positioned towards the left side of the tree and does not experience a head on impact with the tree trunk. In addition, there are several damaged parts of the slat and leading edge of the wing in-between the stiffener and the tree.

The following reasons explain why the simulation cannot capture the jamming of parts:

- 1) The mesh size of the tree is around 5 mm and the tree model does not take into account the tree fibers. In addition, the FEA model material card for the tree includes element erosion parameters (it is not feasible for simulation models to capture details such as embedded parts).
 - 2) The analysis also indicates that it is likely that the wing orientation at the time of impact was slightly different when compared to the one provided by the PSC and the trajectory analysis work. This could be due to small differences in the initial position of the aircraft or the idealized geometry of the Bodin birch tree.
-

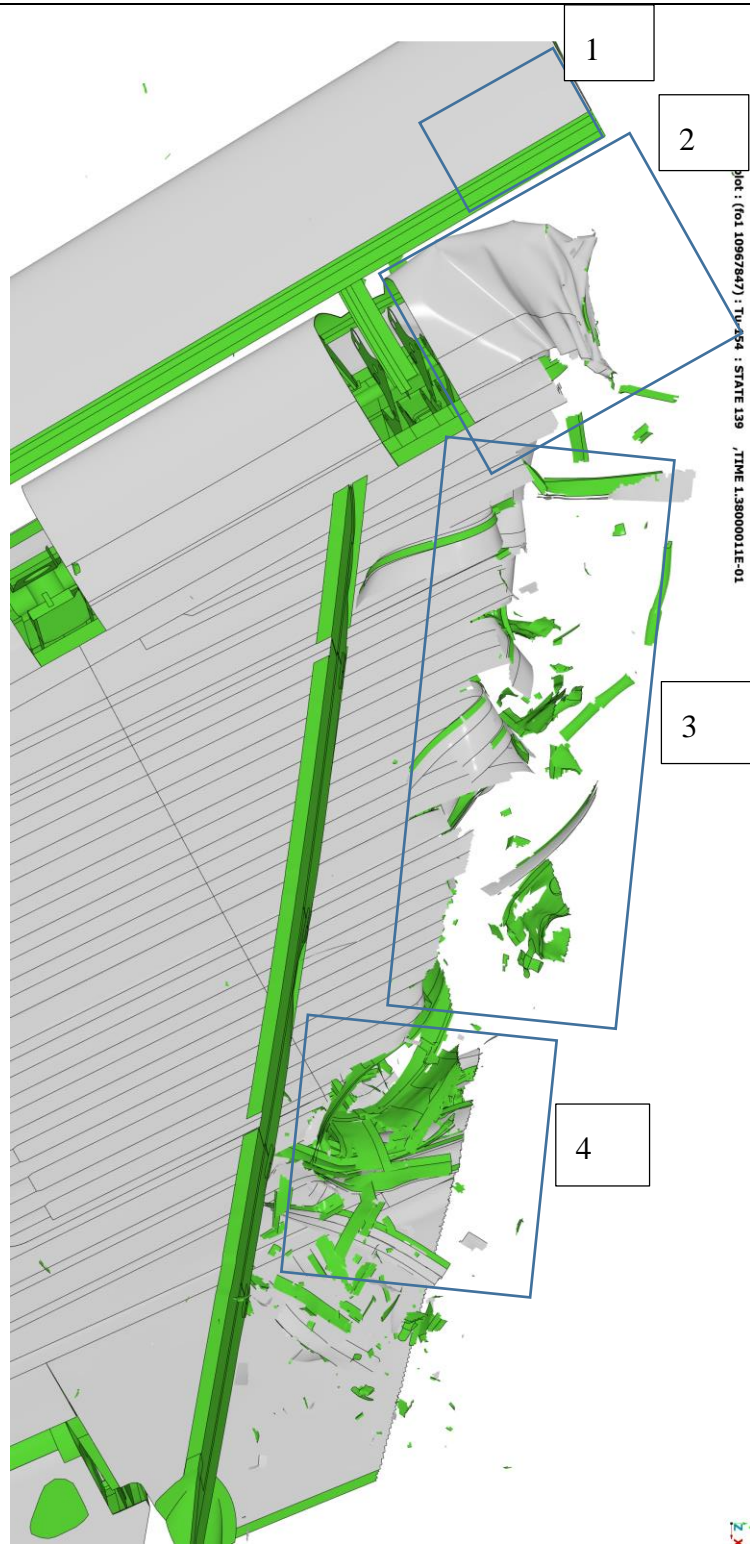


Figure 3.18 Separated wing damage – Top View (138 ms)

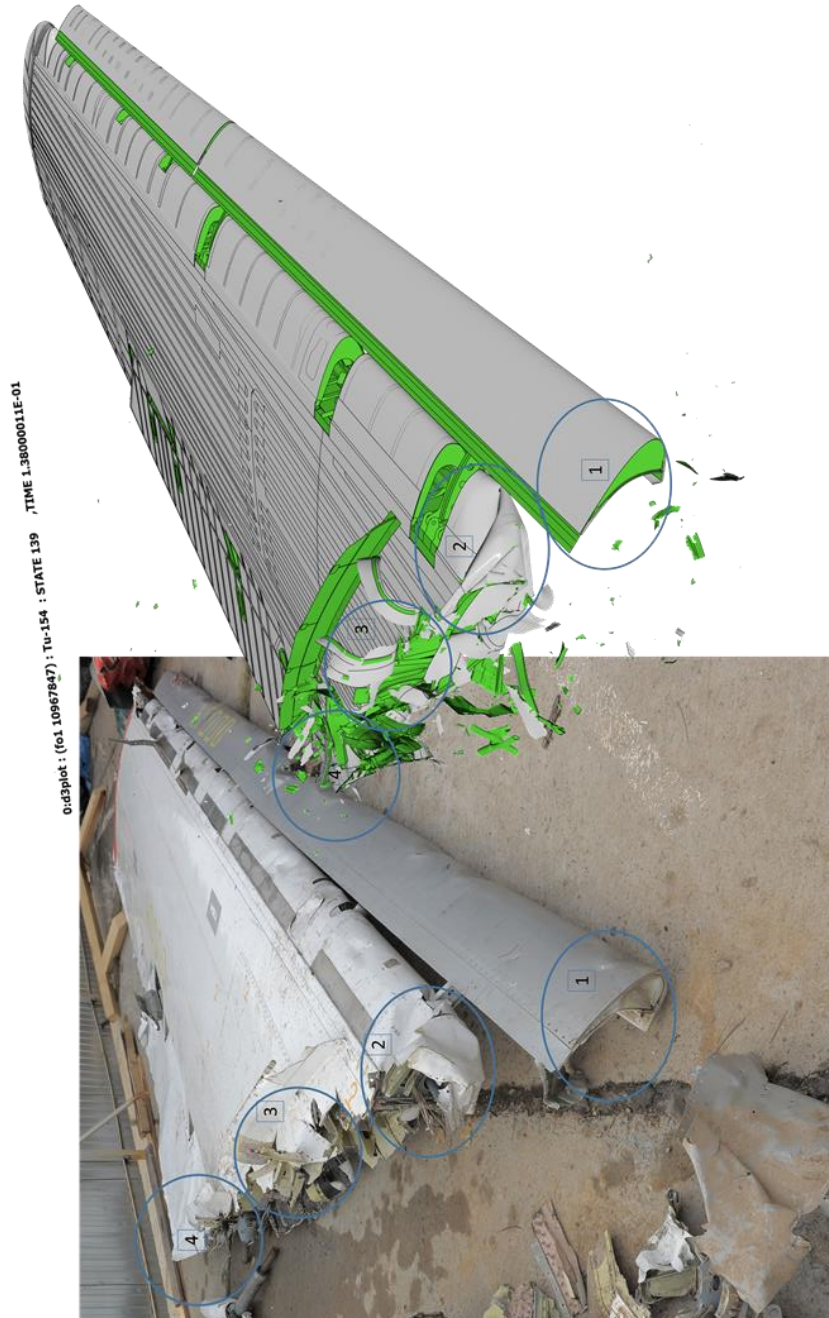


Figure 3.19 Separated wing damage comparison (138 ms) with debris image by the PSC [19]

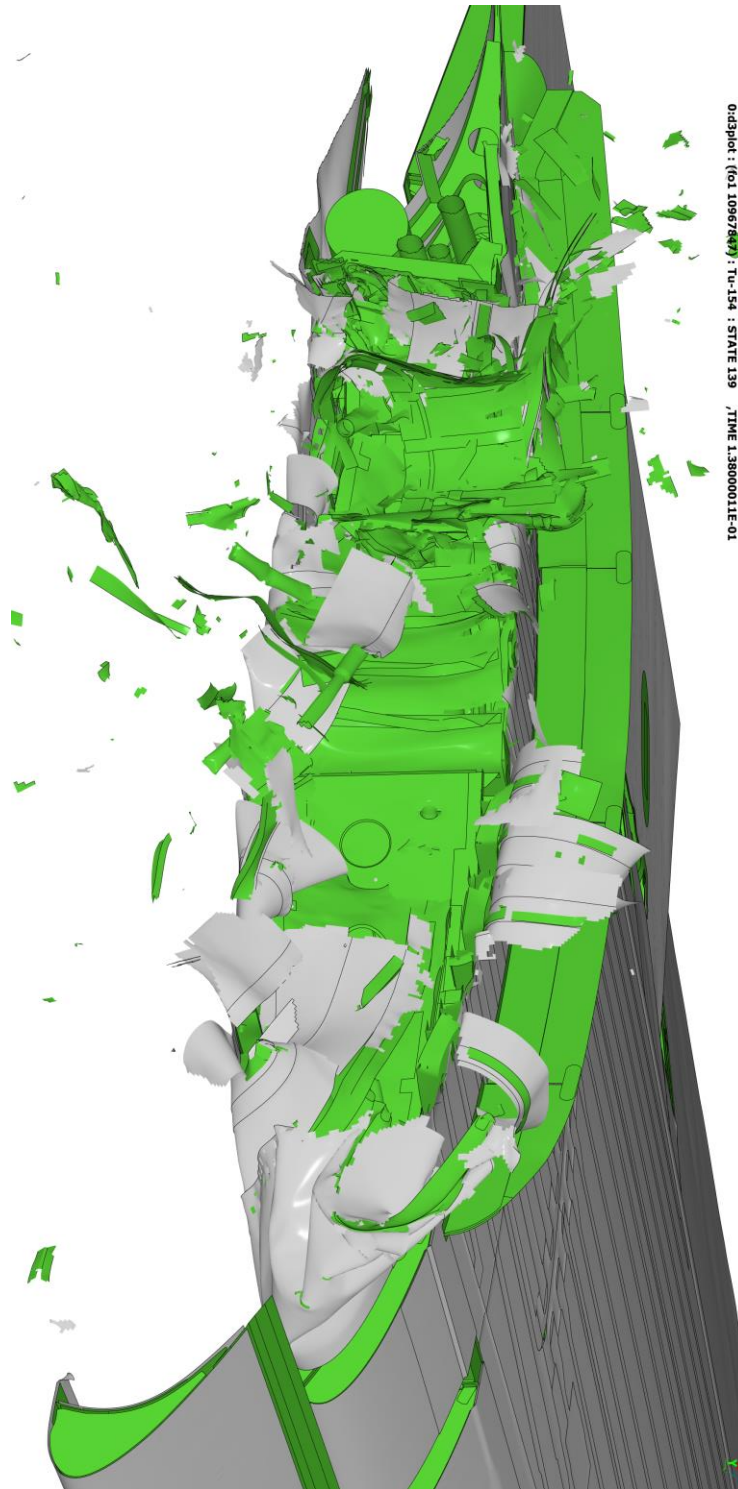


Figure 3.20 Separated wing damage – Side View (138 ms)

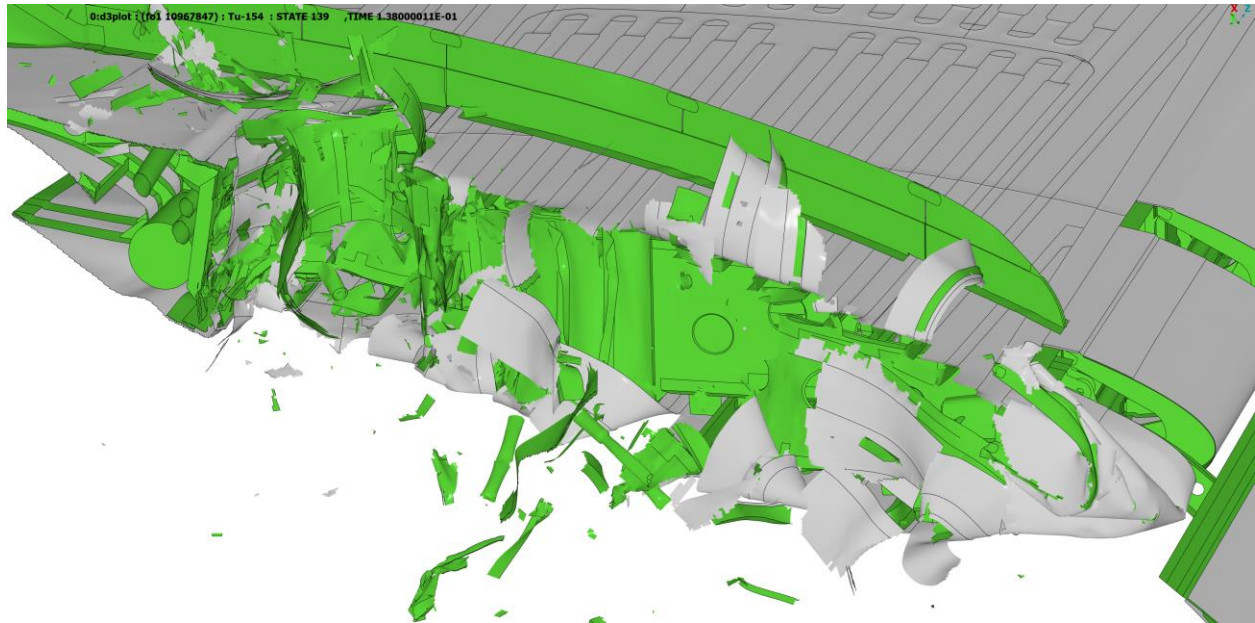
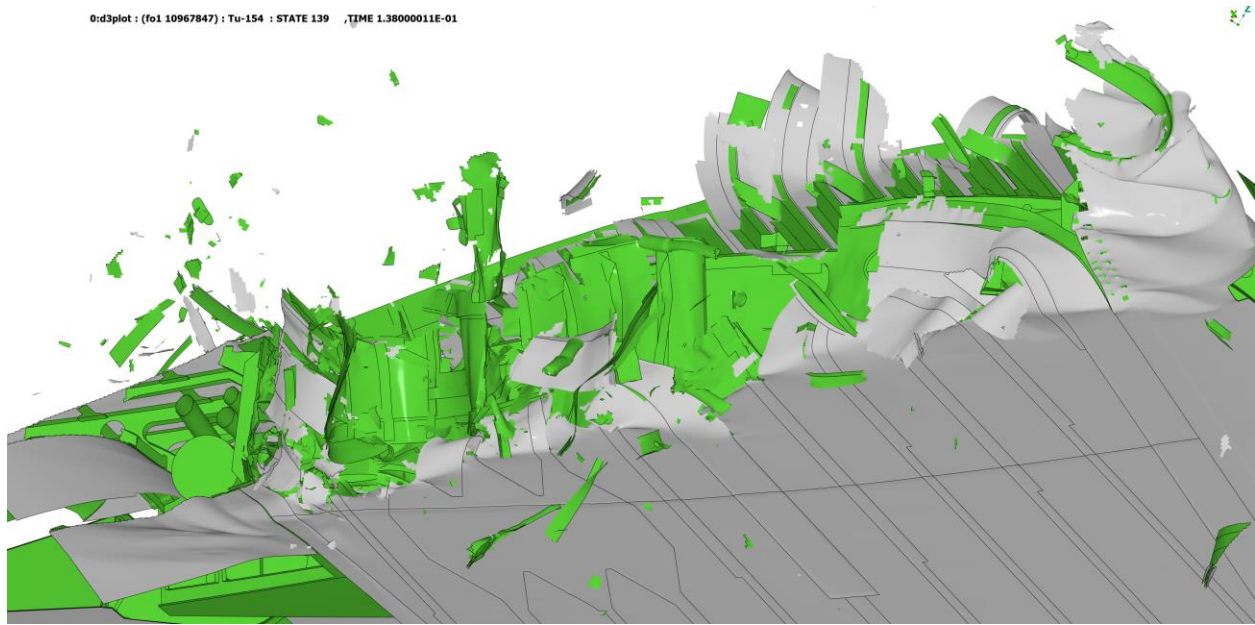


Figure 3.21 Separated wing damage – Upper and Lower Left Side View (138 ms)

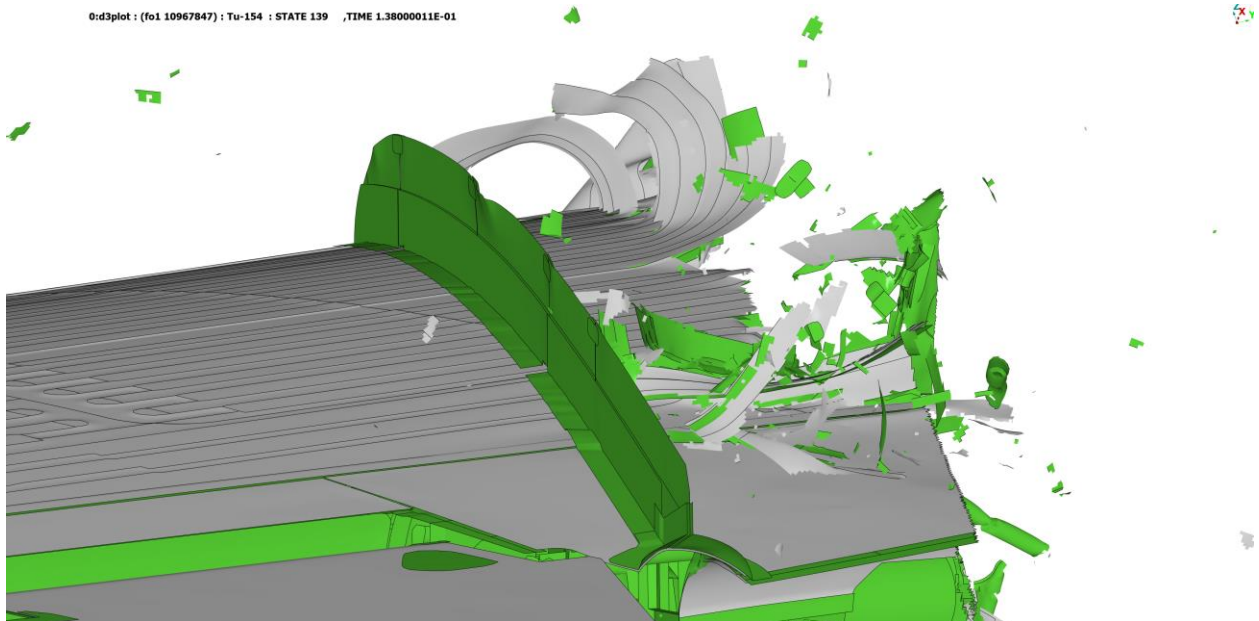
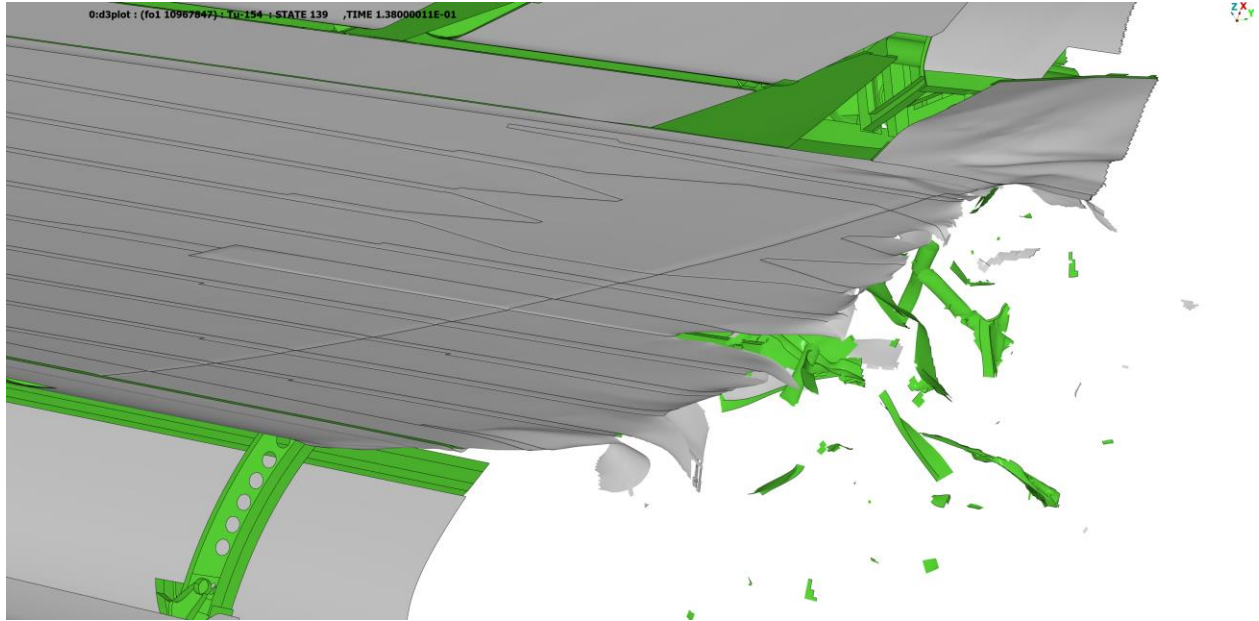


Figure 3.22 Separated wing damage – Upper and Lower Right Side View (138 ms)

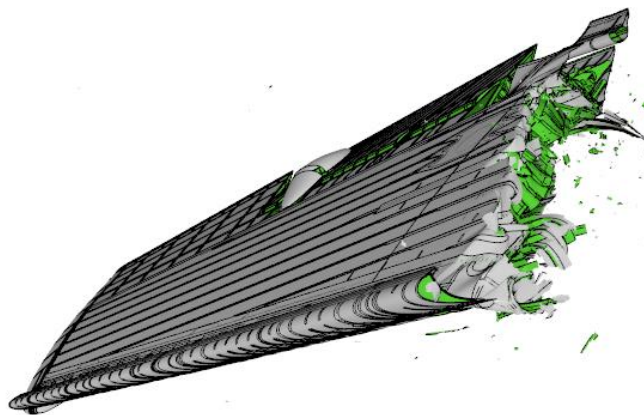


Figure 3.23 Separated wing damage comparison with debris image by the PSC [19]

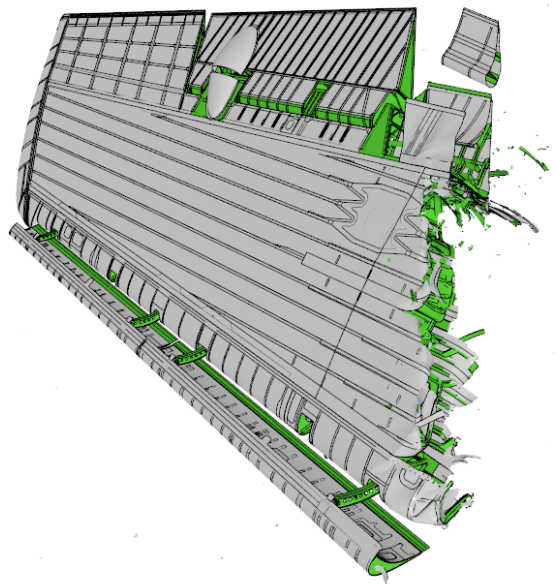


Figure 3.24 Separated wing damage comparison with debris image by the PSC [19]

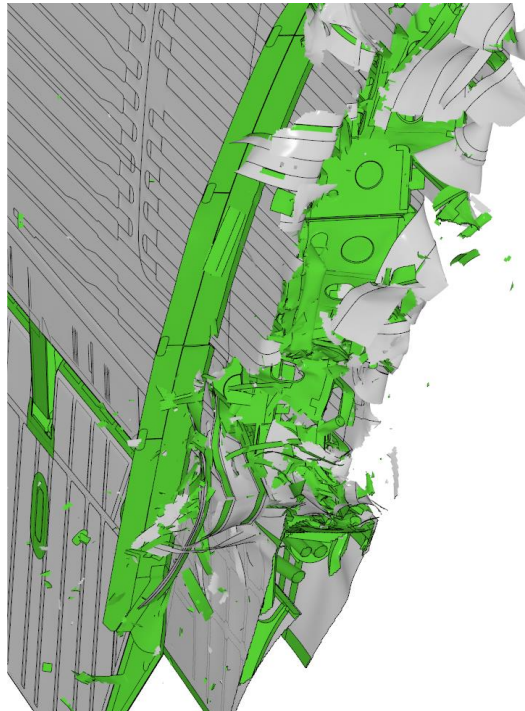


Figure 3.26 Separated wing damage comparison with debris image by the PSC [20]

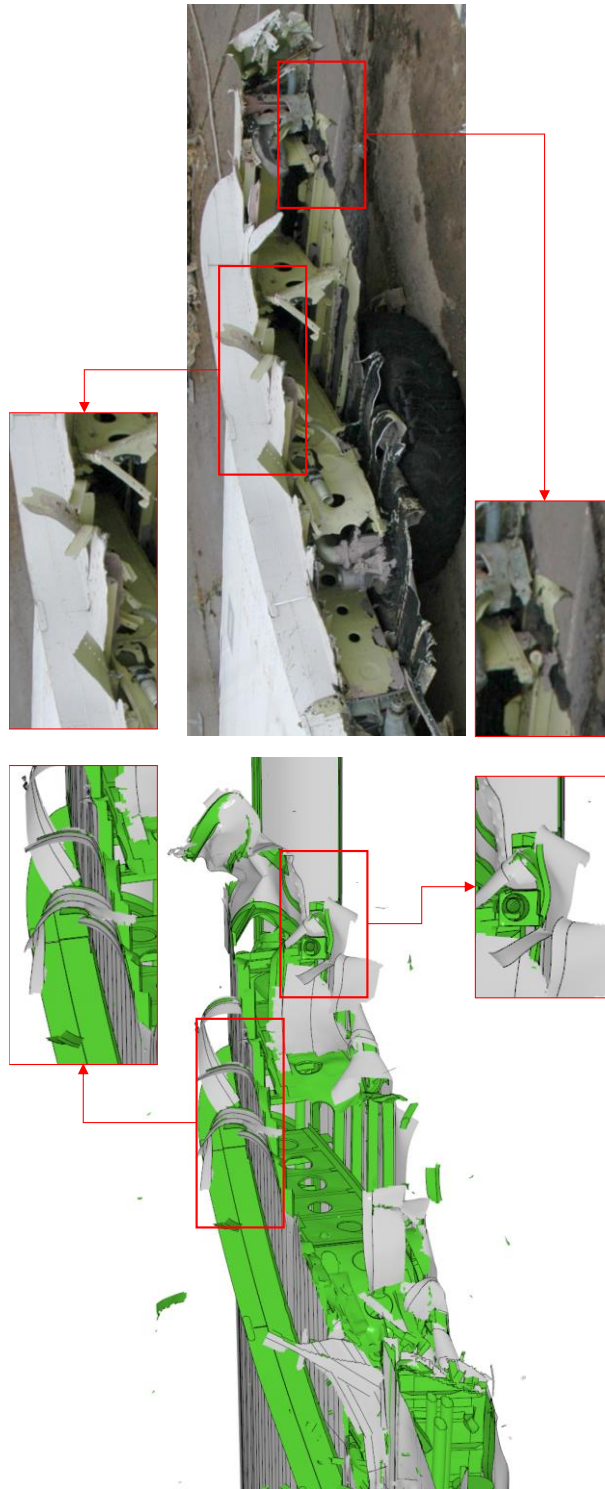


Figure 3.27 Separated wing damage comparison with debris image by the PSC [20]

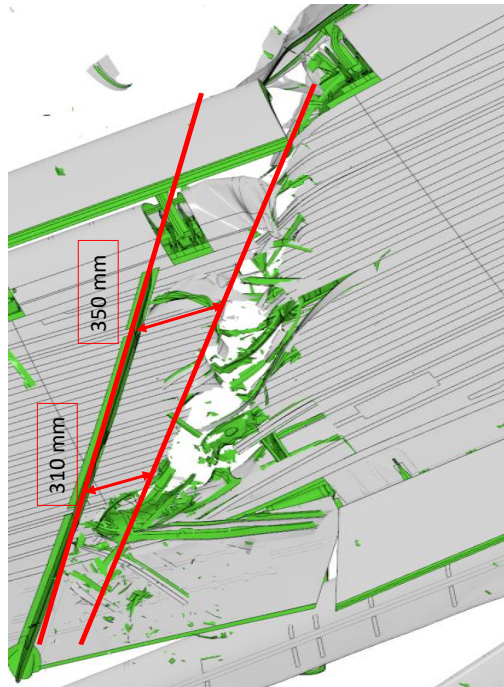


Figure 3.28 Separated wing damage comparison with debris image from the PSC [20]



Figure 3.29 Fragments embedded in birch tree identified by the PSC [21]

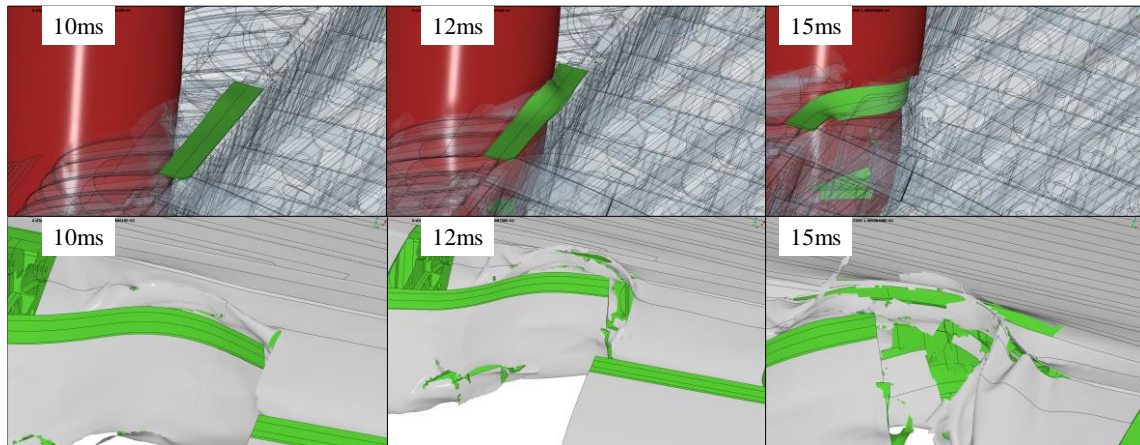


Figure 3.30 Top fragment analysis in tree impact simulation

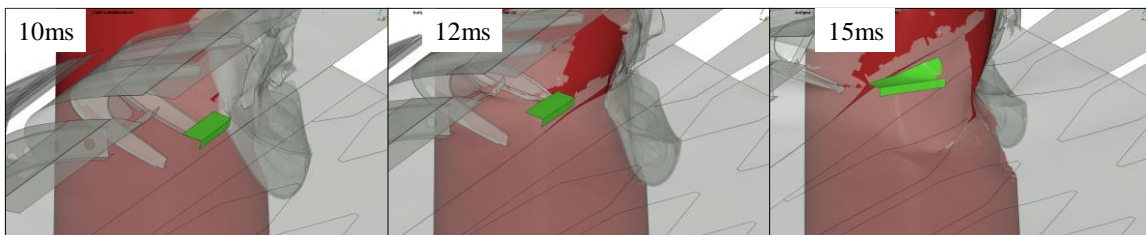


Figure 3.31 Bottom fragment analysis in tree impact simulation

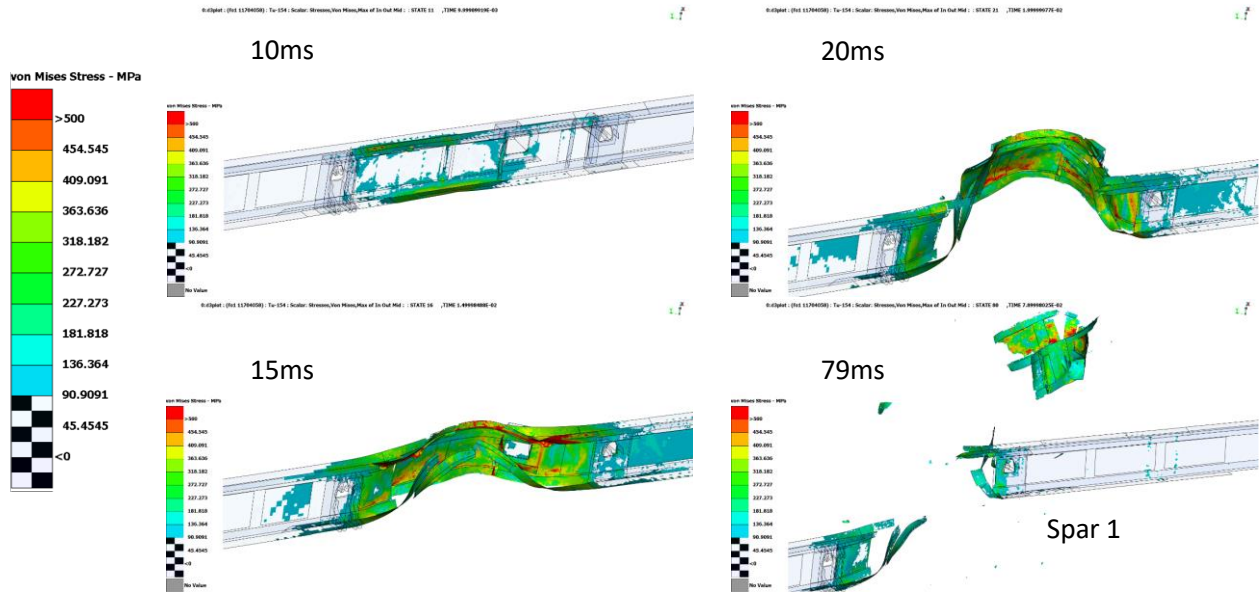


Figure 3.32 Von Mises stresses on Spar 1 - MPa

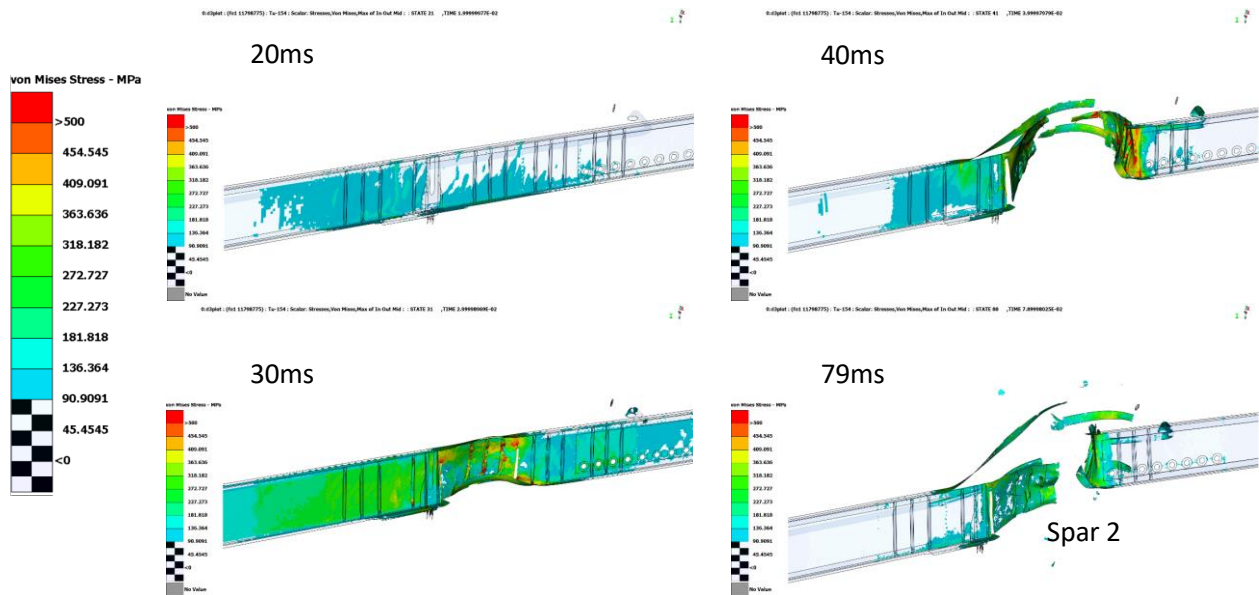


Figure 3.33 Von Mises stresses on Spar 2 - MPa

3.4.3 Tree Top Trunk Trajectory – Simulation

The simulation shows that the tree trunk breaks in two major pieces as observed in the photos reported in the MAK report [1] and those provided by the PSC [19]. The tree splits into two parts at 50 ms after initial impact, as shown in Figure 3.17 and Figure 3.34. Detailed view of the tree damage is shown in Figure 3.35. The analysis does not capture all the failure mechanisms (such as fiber splitting) of the tree because the simulation cannot capture the individual fibers that define the tree structure. Nevertheless, the analysis shows good agreement with the overall tree failure mechanisms.

0:d3plot : Tu-154 : STATE 51 , TIME 4.99998064E-02

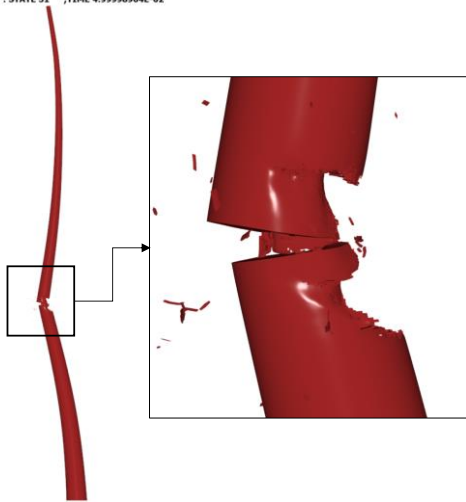


Figure 3.34 Tree impact analysis – tree damage view 1



Figure 3.35 Tree impact analysis – tree damage view 2

In the satellite image of the debris field [19][6], after impact with the wing, the top piece of the tree fell to the side towards the Bodin hut. From the aircraft flight path perspective, the top piece fell towards the right wing of the aircraft as shown in Figure 3.37. Since the wing tree impact reconstruction analysis was not run long enough to see the tree fall to ground, a trajectory analysis was performed by solving the six degrees-of-freedom (6DOF) equations of motion using Matlab Simulink.

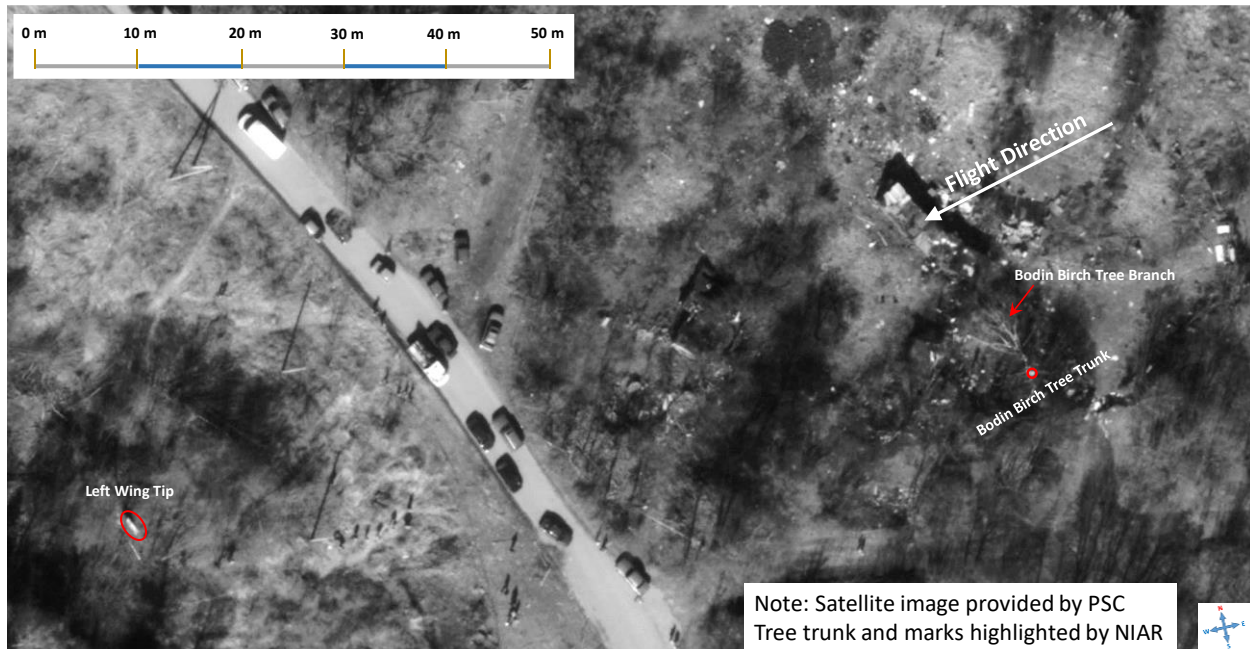


Figure 3.37 Crash site satellite image close-up view of the Bodin birch tree [19]

The trajectory analysis simulation is run until the broken tree piece impacts with the ground. Based on the calculations, the time taken for the broken tree piece to impact with the ground is 0.5 seconds. The top part of the broken tree piece makes first contact with the ground as shown in Figure 3.38 through Figure 3.40.

At the time of impact with the ground, the CG of the broken tree piece has moved 3.9 m in the downward direction, 2.1 m in the direction of flight and 0.8 m in the perpendicular direction of flight away from the Bodin hut.

These results indicate that the trajectory of the broken tree piece is mostly governed by the rotational motion and not the translational motion. The broken tree piece at the time of impact with the ground is very close to the main tree body as observed from the satellite image shown in Figure 3.37. The orientation of the broken piece is different compared to the orientation observed from the satellite and accident site pictures. This difference can be attributed to the simplification of the geometry (branches not being modeled) and not taking into account aerodynamic effects.

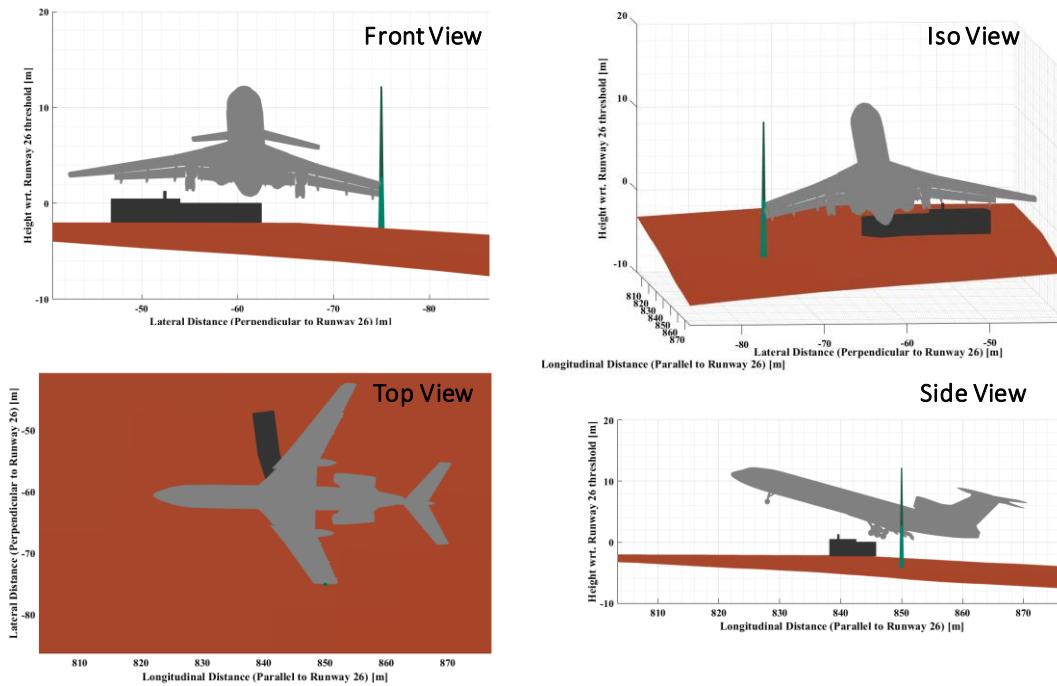


Figure 3.38 Broken simulation tree top piece trajectory analysis – time: 0 (Tree Broken in two pieces, Upper and Lower Trunk)

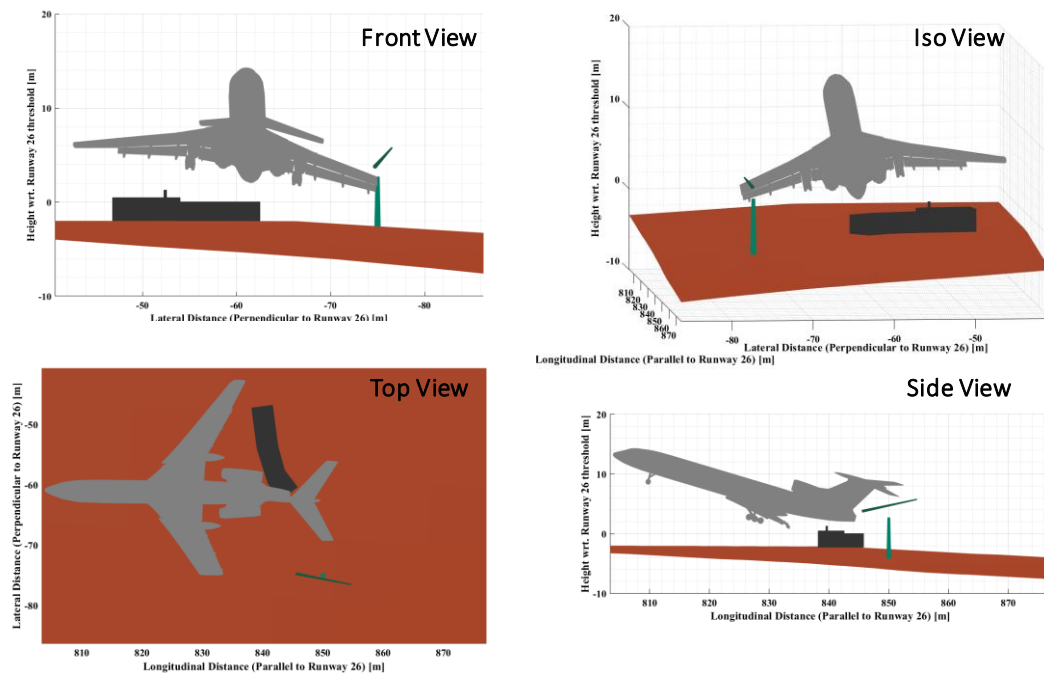


Figure 3.39 Broken simulation tree top piece trajectory analysis – time: 0.25 s

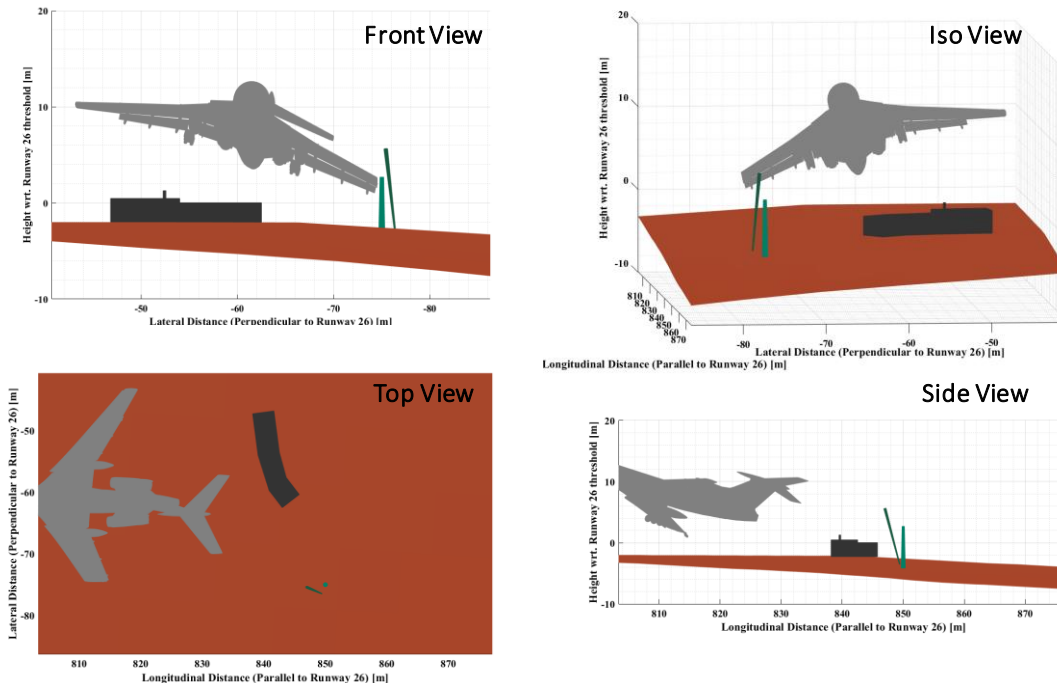


Figure 3.40 Broken simulation tree top piece trajectory analysis – time: 0.5 s

3.5 Comparison to MAK Report

The impact with the birch tree marks a critical point in the accident sequence defined in the MAK report. This impact resulted in the aircraft losing the outboard 6.5m of the left wing and creating a significant aircraft until ground impact. Consequently, the aircraft impacted the ground inverted. This chapter discusses the similarities and differences observed between the MAK report and the accident reconstruction analysis performed by NIAR to analyze the left wing impact against the birch tree trunk.

- According to the MAK report, page no. 75, the left wing of the aircraft impacted the Bodin birch tree at a height of 5 m above the ground. The height of 5 m is inconsistent with the findings of the prosecutor report [11], which claims the height to be 6.75 m. For the impact height of 5 m, the right main landing gear of the aircraft would impact with the Bodin hut as shown in Figure 3.41. This is confirmed by the photographs taken at the accident site where it is shown that the Bodin Hut was not impacted by the aircraft landing gear (see Figure 3.42). Detailed analysis is also shown in Annex II Trajectory analysis report [10].

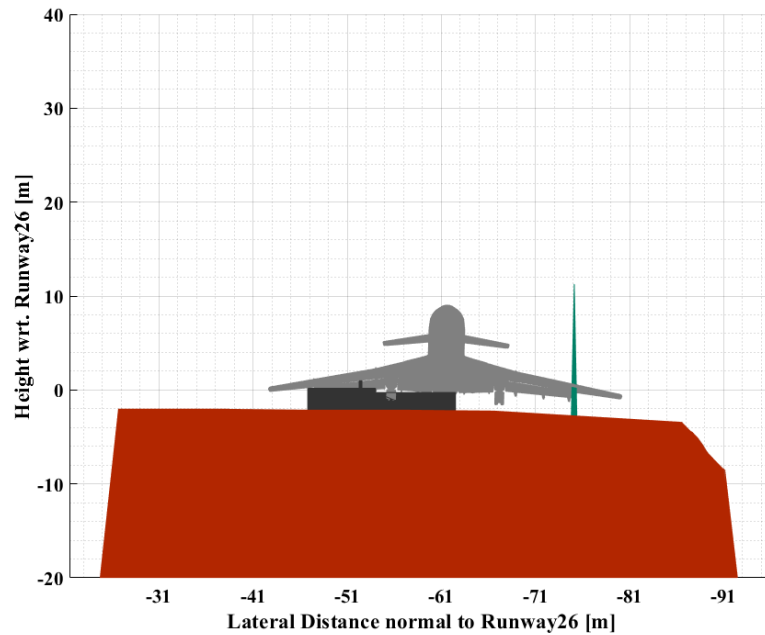


Figure 3.41 NIAR trajectory analysis showing birch tree impact at 5 m height as per MAK report



Figure 3.42 Photograph of Bodin hut provided by the PSC [19]

- According to the MAK report, page no. 74, the aircraft hit a birch tree trunk measuring 30-40 cm in the diameter. The diameter of this tree trunk is underestimated in the MAK report. The documentation obtained in the prosecutor report [11] indicates that the diameter of the tree at impact location was 44-45cm, as shown in Figure 3.43.

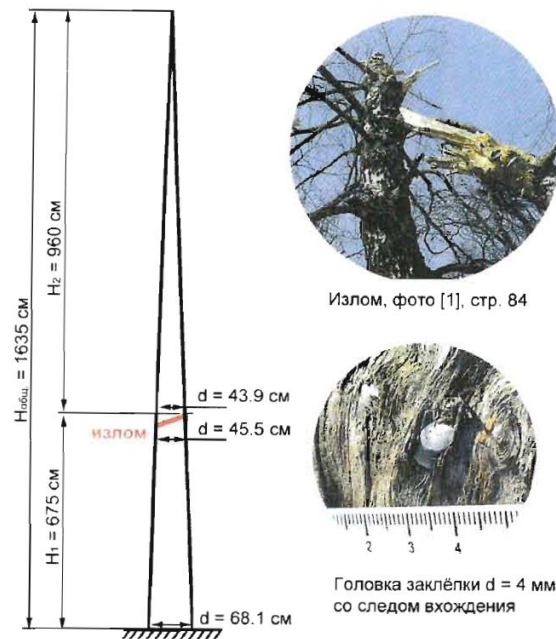


Рис. 1.8. Схема измерений ствола березы (реконструкция на момент столкновения).

Figure 3.43 Tree dimensions drawing in Prosecutor report [11]

- Page 75 on the MAK report states that the investigation team found fragments of the separated left wing panel embedded in the tree trunk. Figure 1.12 shows the image of the tree from the MAK report which also shows the embedded fragments. Detailed information of the embedded fragments was provided by the PSC as documented in section 3.4.2. In the tree impact reconstruction analysis performed by NIAR, it was determined that it is feasible for the top piece of fixed leading edge to get embedded in the trunk. The analysis showed that the second fragment (spar 1 stiffener), does not directly impact the tree as it is blocked by debris from other parts. Details of this analysis are documented in section 3.4.2.
- On page 13, the MAK report states that 245 m from the point of first impact with a lateral deviation of 60 m left from the extended runway centerline the Tu-154M aircraft hit a 30 – 40 cm wide birch tree trunk, which led to the damaged left wing and significant left bank. The aircraft crashed inverted and was totally destroyed. Page 76 of the MAK report states that the outboard 6.5 m of the left wing separated. The analysis performed by NIAR shows that it is feasible for the wing to break upon impact with a birch tree of 44-45 cm diameter for the impact conditions and material presented in this report. The birch tree material was created through a series of experiments and simulations defined by the building block approach. The extensive work of developing the birch tree material response is documented in Chapter 2 of the annex III report. Further, the Tu-154M wing was modeled in detail to represent the actual aircraft. Detailed documentation of the wing can be found in Chapter 4 of the annex III report. The tree impact reconstruction analysis is documented in detail

in Chapter 4 of the annex III. While the analysis shows that at 138 ms the wing only detaches up until spar 3 and does not rupture spar 3, detailed stress analysis on the remaining attached parts show very low margins of safety (0.08) when compared to the ultimate stress of the material. As a result, any additional aerodynamic loading, or differences in tree material/geometry could introduce a complete rupture of the left wing tip.

- According to Table 1 of the MAK report, which consists of the wreckage list, the birch tree impact (item no. 8) occurs at longitudinal and lateral position of 856 m and -61 m, respectively. The fragment of the left outer wing (item no. 16 of Table 1) is found at longitudinal and lateral position of 745 m and -40 m, respectively. This indicates that the separated left wing was found about 111 m (longitudinal) away from the impact site. In a study performed by Ding and Binienda [23], the trajectory of a 5.5 m long wing was analyzed for similar conditions as the birch tree impact (forward velocity – 75m/s, vertical velocity – 11m/s and pitch - 14°) using 6-DOF rigid body motion equations and three dimensional compressible Navier-Stokes equations. The results indicate that the wing tip travels approximately 150 m in the forward (longitudinal) direction towards the flight path [23]. This indicates that it is feasible for the separated left wing, as described in the MAK report, to travel 111 m. NIAR recommends the PSC to apply the same methodology to the Tu-154M detailed wing CAD model provided by NIAR in order to conduct the analysis with the actual mass, geometry, and inertia properties of the separated left wing portion.
- The birch tree post-impact is not analyzed in detail in the MAK report. However, one image on page 75 indicates that the broken top piece of the birch tree (post-impact) is close to the base of the birch tree. Based on the wing tree impact reconstruction, a 6DOF trajectory analysis of the top piece of the tree was performed to understand where it would land based on the initial conditions calculated by the analytical model. The trajectory analysis is documented in section 3.4.3. Based on the analysis, the broken upper tree trunk at the time of impact with the ground is very close to the lower tree trunk observed from the satellite image shown in Figure 3.37. The orientation of the broken piece is different compared to the orientation observed from the satellite and accident site pictures. This difference can be attributed to the simplification of the geometry (branches not being modeled) and not taking into account aerodynamic effects.
- A closer look at Figure 3.25 shows that some fracture edge curls on the bottom wing skin do not curl outwards as shown in the post impact pictures provided by the PSC. Also note that the wing debris images used for comparison in Figure 3.24, Figure 3.25 and Figure 3.26 are taken at a storage facility and NIAR do not have any documented damage that the wing debris could have experienced during transportation or storage [20]. NIAR recommends that the PSC requests or conducts a detail failure surface analysis of the lower skin to confirm whether the outward curling of the lower skin was due to the tree impact loads.

4 Ground Collision Accident Reconstruction

This chapters summarizes the ground impact accident reconstruction. It provides an overview of the survivability and structural evaluation criteria, a description of the analysis model, and the results of the impact simulation.

4.1 Ground Impact Reconstruction Evaluation Criteria

4.1.1 Survivability Evaluation Criteria and Supporting Documentation

A series of criteria will be used to analyze the survivability of the Tu154 accident. The typical criteria that an accident needs to meet in order to be considered “survivable” is presented in section 4.1.1.1. These are well established criteria that have been used in the aerospace industry to study survivability [26] [27] [28]. An injury study was performed by the PSC [7] describing the severity of injuries each occupant experienced. An explanation of the criteria used for this study in presented in section 4.1.1.2

4.1.1.1 Survivability Evaluation Criteria

I. Maintain survivable volume:

Overall survivable space shall be maintained during peak dynamic event as well as any permanent post event deformations. This criterion will be evaluated on a per row basis based on the deformation of the fuselage cross section where each row is located. See Figure 4.2.

II. Maintain deceleration loads to occupants:

Injury criteria limits specified in 14 CFR 25.562 [29] must be maintained:

- Where upper torso straps are used for crewmembers, tension loads in individual straps must not exceed 1,750 pounds. If dual straps are used for restraining the upper torso, the total strap tension loads must not exceed 2,000 pounds.
 - The maximum compressive load measured between the pelvis and the lumbar column of the anthropomorphic dummy must not exceed 1,500 pounds.
 - Where head contact with seats or other structure can occur, protection must be provided so that the head impact does not exceed a Head Injury Criterion (HIC) of 1,000 units.
 - Where leg injuries may result from contact with seats or other structure, protection must be provided to prevent axially compressive loads exceeding 2,250 pounds in each femur.
-

These criteria must be met under the following dynamic emergency landing conditions specified in 14 CFR 25.562 [29] for aircraft seats and occupants:

- “A change in downward vertical velocity (Δv) of not less than 35 feet per second, with the airplane's longitudinal axis canted downward 30 degrees with respect to the horizontal plane and with the wings level. Peak floor deceleration must occur in not more than 0.08 seconds after impact and must reach a minimum of 14g.”
- “A change in forward longitudinal velocity (Δv) of not less than 44 feet per second, with the airplane's longitudinal axis horizontal and yawed 10 degrees either right or left, whichever would cause the greatest likelihood of the upper torso restraint system (where installed) moving off the occupant's shoulder, and with the wings level. Peak floor deceleration must occur in not more than 0.09 seconds after impact and must reach a minimum of 16.”

These criteria will be evaluated in the Tu154 numerical model by analyzing the floor acceleration and velocity levels. These will be extracted from accelerometer elements in the model using floor local coordinates, as shown in Figure 4.1. When cabin floor acceleration levels exceed the levels specified in 14 CFR part 25.562 [29], the seats are expected to fail hence increasing the risk for severe injuries or fatalities to occupants.

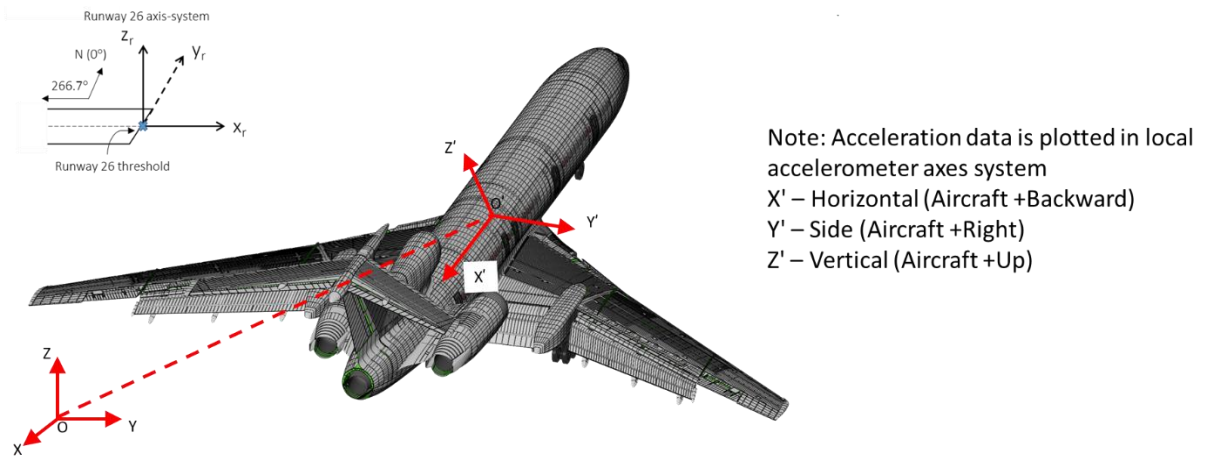


Figure 4.1 Local accelerometer output coordinate system

III. Retention of items of mass

14 CFR part 25.562(c)(7) [29] states “The seat must remain attached at all points of attachment, although the structure may have yielded.”. Other large items of mass, such as overhead bins, must also remain attached to avoid head injuries to occupants.

IV. Maintain egress paths

14 part 25 CFR 25.815 establishes that a minimum aisle distance of 12 to 15 inches must be maintained at all times in order to allow for passenger evacuation. Plastic deformations of the supporting structure near the exit doors should allow for the opening of the exit doors. Floor warping and floor beam failures need to be assessed. They must be able to support passenger weight and allow passenger evacuation.

These criteria will be evaluated in the Tu154 numerical model by examining plastic strains of the floor support structure and exit door support structure.

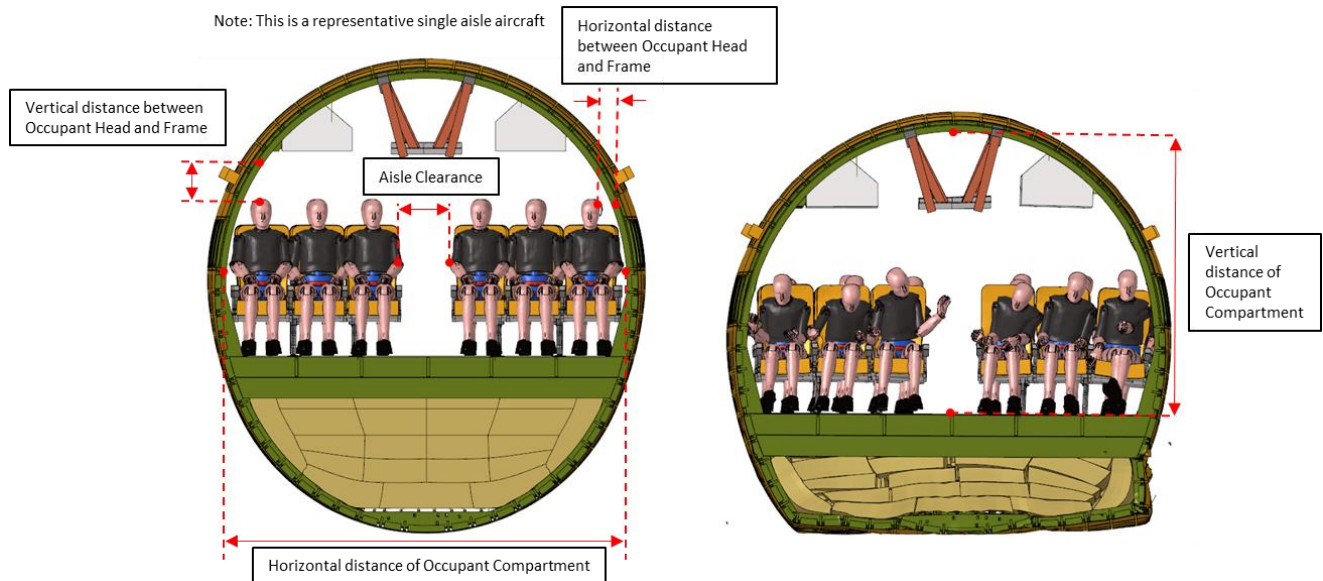


Figure 4.2 Example of evaluation criteria of a survivable event

4.1.1.2 Injury Analysis PSC

PSC shared the work carried out by their team documenting the data available on the passengers' injuries and location of victims at the crash site. Documentation consists of reports and spreadsheets classifying and evaluating the injuries suffered by each occupant according to the autopsies. Some passengers' seating location in the aircraft have been provided by the PSC based on protocol and images taken by the passengers inside the aircraft.

For data protection purposes, each passenger has been assigned a number and all data has been referred to their corresponding passenger number. In accordance to the number of passengers inside the airplane, passenger number nomenclature goes from 1 to 96.

I. Injury Data

The injuries that the victims' bodies experienced has been classified in two categories: bone structure and internal organs. Several types of bones or organs, respectively form each category. Table 4.1 lists the types of bones considered analyzed in the autopsy reports.



Table 4.1 List of documented injured bones [7]

1	Skull	2	Jaw Bone
3	Hyoid Bone	4	Right Collarbone
5	Left Collarbone	6	Right Shoulder Blade
7	Left Shoulder Blade	8	Right Side of Ribs
9	Left Side of Ribs	10	Bridge
11	Neck Spine	12	Chest Spine
13	Lumbar Spine	14	Sacrum
15	Tailbone	16	Right Humerus
17	Left Humerus	18	Right Ulna
19	Left Ulna	20	Right Radius
21	Left Radius	22	Right Wrist Bone
23	Left Wrist Bone	24	Right metacarpal bone
25	Left Metacarpal Bone	26	Finger Bones of the Right Hand
27	Finger Bones of the Left Hand	28	Right Hip Bone
29	Left Hip Bone	30	Right Pubis Bone
31	Left Pubis Bone	32	Pubic Symphysis
33	Right Ischium	34	Left Ischium
35	Right Femur	36	Left Femur
37	Right Kneecap	38	Left Kneecap
39	Right Tibia Bone	40	Left Tibia Bone
41	Right Fibula	42	Left Fibula
43	Right Tarsal Bone	44	Left Tarsal Bone
45	Right Metatarsal	46	Left Metatarsal
47	Right Toe Bones	48	Left Toe Bones

The bone damage is evaluated in a scale from 0 to 4, correlating higher values to more severe injury. Table 4.2 describes the damage level criterion used for the bone structure.

Table 4.2 Bone structure damage level criterion [7]

Level	Description
0	No damage
1	Single fracture, broken bones
2	Multiple breaks and fractures, displacements, splinters
3	Multiple fractures with major displacements, fragmentation or missing bone pieces
4	Amputation, crushing, numerous missing pieces, massive damage

Figure 4.3 shows an example of how PSC collected data related to bone structure damage of passenger #71 [7]. Damage level for each of passenger #71 bones is ranked according to the criterion introduced in Table 4.2.

DAMAGES TO THE BONE STRUCTURE	
skull	4
jaw bone	2
hyoid bone	0
right collarbone	0
left collarbone	1
right shoulderblade	2
left shoulderblade	2
right side of ribs	3
left side of ribs	3
bridge	1
neck spine	3
chest spine	2
lumbar spine	2
sacrum	0
tailbone	0
right humerus	4
left humerus	2
right ulna	1
left ulna	1
right radius	1
left radius	1
right wrist bone	0
left wrist bone	0
right metacarpal bone	0
left metacarpal bone	2
finger bones of the right hand	0
finger bones of the left hand	1
right hip bone	3
left hip bone	4
right pubic bone	3
left pubic bone	3
pubic symphysis	1
right ischium	3
left ischium	3
right femur	1
left femur	3
right kneecap	0
left kneecap	1
right tibia bone	3
left tibia bone	4
right fibula	3
left fibula	4
right tarsal bone	1
left tarsal bone	3
right metatarsal	2
left metatarsal	2
right bones of toes	0
left bones of toe	1

POINTS FOR DAMAGES TO THE BONE STRUCTURE

0 - no mechanical damages	3 - multiple fractures with major displacements, fragmentation or missing pieces of bone
1 - single fractures, broken bones	4 - amputation, crushing, numerous missing pieces, massive damage
2 - multiple breaks and fractures, displacements, splinters	

Figure 4.3 Bone structure damage – Passenger #71 [7]

Likewise the bone damage assessment, PSC classified the internal organs based on the information extracted from the autopsies [7]. Table 4.3 lists the internal organs documented for injury evaluation.

Table 4.3 List of documented internal organs [7]

1	Brain	2	Spinal Chord
3	Mouth	4	Esophagus
5	Stomach	6	Small Intestine
7	Large Intestine	8	Liver
9	Pancreas	10	Thyroid
11	Parathyroid	12	Pleura
13	Genitals and Reproduction Organs	14	Nasal Cavity
15	Throat	16	Trachea
17	Bronchi	18	Lungs
19	Spleen	20	Heart
21	Aorta	22	Kidneys and Adrenal
23	Ureters	24	Bladder

PSC developed a criterion to rank the internal organs damage [7]. This damage level assessment goes from 0 to 4. Table 4.4 describes the level definition for internal organs damage.

Table 4.4 Internal organs damage level criterion [7]

Level	Description
0	No damage
1	Hemorrhage, hematoma no destruction of the continuity of tissue
2	Cracks, split, destruction of the continuity without serious damage to the tissue
3	Massive damage, tearing, crushing
4	Massive damage, crushing, tearing with tissue damage

Figure 4.4 shows an example of how data related to internal organs damage for passenger #71 is collected in the documentation provided by PSC [7].

DAMAGES TO THE INTERNAL ORGANS																							
brain	spinal cord	mouth	esophagus	stomach	small intestine	large intestine	liver	pancreas	thyroid	parathyroid	pleura	genitals and reproductive system	nasal cavity	throat	trachea	bronchi	lungs	spleen	heart	aorta	kidneys and adrenal	ureters	bladder
4	0	3	0	0	2	0	3	1	0	0	3	0	3	0	2	0	3	3	3	3	3	0	2
POINTS FOR DAMAGES TO INTERNAL ORGANS																							
0 - no damages																							
1 - hemorrhage, hematoma, no destruction of the continuity of tissue																							
2 - cracks, splits, destruction of the continuity without serious damage to the tissue																							
3 - massive damages, tearing, crushing																							
4 - massive damages, crushing, tearing with tissue damages																							

Figure 4.4 Internal organs damage – Passenger #71 [7]

II. Injury Evaluation

PSC team has created a criterion to assign a injury severity value to each passenger [7]. This criterion looks at the following numerical aspects:

- *Number of damage areas*: is the count of the individual bones and organs damaged. This value goes from 0 to 72.
- *Sum of injured values*: is the added sum of all the damage level values associated to each passenger’s *damage areas*. This value goes from 0 to 288.
- *Weighted Average*: average of the damage assigned to all the bones and organs. This value is obtained by dividing the *sum of injury values* by the total count of bones and organs (72).

Figure 4.5 summarizes passenger #71 injury values according to PSC injury criterion.

NUMBER OF DAMAGED AREAS (0 to 72)
54
SUM OF INJURY VALUES (0 to 288)
128
WEIGHTED AVERAGE (0 to 4)
1.78

Figure 4.5 Injury values – Passenger #71 [7]

NIAR has created an additional classification methodology using PSC data [7], with the aim of facilitating the visualization and comparison of the injuries suffered by each passengers. Figure 4.6 presents the bone structure and internal organs injury values per body area.

Bone Structure	Body Parts	Internal Organs
4.00	Skull	3.33
1.00	Jaw Region*	
3.00	Neck	0.00
2.00	U. Torso	1.75
1.25	U. Extr.	
2.22	L. Torso	1.17
2.00	L. Extr.	

* Jaw region includes jaw bone and hyoid bone

Figure 4.6 Injury values per body area – Passenger #71

III. Injury Report

Figure 4.7 shows the injury evaluation of passenger #71 based on the data discussed in this section. NIAR has created a color coded body image to facilitate visualization of the data. Color areas in the body images are associated with the values provided in Figure 4.6.

NIAR has created an injury report compiling the data presented in Figure 4.3 through Figure 4.7. Figure 4.8 presents the injury report of passenger #71. NIAR has produced complete injury reports for all passengers based on the data provided by the PSC documentation. The individual injury reports associated to each passenger are attached in Appendix B of the annex IV report.

Bone Structure	Body Parts	Internal Organs
4.00	Skull	3.33
1.00	Jaw Region*	
3.00	Neck	0.00
2.00	U. Torso	1.75
1.25	U. Extr.	
2.22	L. Torso	1.17
2.00	L. Extr.	

* Jaw region includes jaw bone and hyoid bone

Seat Number	71
Aircraft Area	1 Left

NUMBER OF DAMAGED AREAS (0 to 72)	
	54
SUM OF INJURY VALUES (0 to 288)	
	128
WEIGHTED AVERAGE (0 to 4)	
	1.78

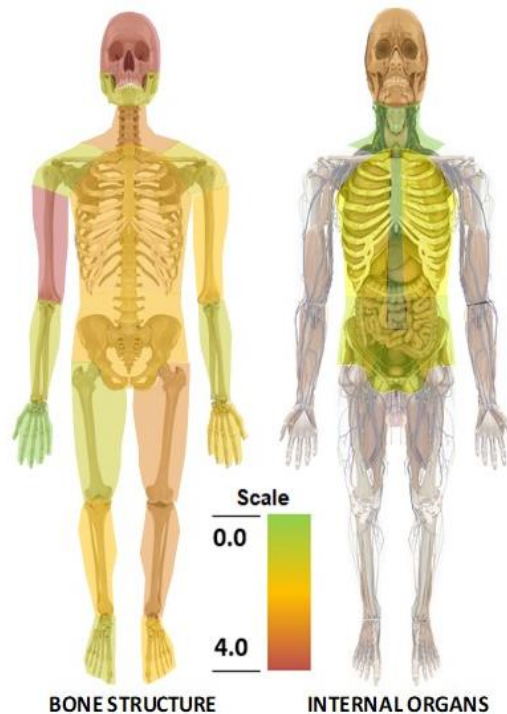


Figure 4.7 Injury assessment – Passenger #71

DAMAGES TO THE BONE STRUCTURE	
skull	4
jaw bone	2
hyoid bone	0
right collarbone	0
left collarbone	1
right shoulderblade	2
left shoulderblade	2
right side of ribs	3
left side of ribs	3
bridge	1
neck spine	3
chest spine	2
lumbar spine	2
sacrum	0
tailbone	0
right humerus	4
left humerus	4
right ulna	2
left ulna	1
right radius	1
left radius	1
right wrist bone	1
left wrist bone	2
right metacarpal bone	0
left metacarpal bone	2
finger bones of the right hand	0
finger bones of the left hand	1
right hip bone	3
left hip bone	4
right pubis bone	3
left pubis bone	3
pubic symphysis	1
right ischium	3
left ischium	3
right femur	1
left femur	3
right kneecap	0
left kneecap	1
right tibia bone	3
left tibia bone	3
right fibula	3
left fibula	4
right tarsal bone	1
left tarsal bone	3
right metatarsal	2
left metatarsal	2
right bones of toes	0
left bones of toes	1

POINTS FOR DAMAGES TO THE BONE STRUCTURE

0 - no mechanical damages
 1 - single fractures, broken bones
 2 - multiple breaks and fractures, displacements, splinters
 3 - multiple fractures with major displacements, fragmentation or missing pieces of bone
 4 - amputation, crushing, numerous missing pieces, massive damage

DAMAGES TO THE INTERNAL ORGANS	
brain	4
spinal cord	0
mouth	3
esophagus	0
stomach	0
small intestine	2
large intestine	0
liver	3
pancreas	1
thyroid	0
parathyroid	0
pleura	3
genitals and reproductive system	0
nasal cavity	3
throat	0
trachea	0
bronchi	2
lungs	0
spleen	3
heart	3
aorta	3
kidneys and adrenal	3
ureters	3
bladder	0

POINTS FOR DAMAGES TO INTERNAL ORGANS

0 - no damages
 1 - hemorrhage, hematoma, no destruction of the continuity of tissue
 2 - cracks, splits, destruction of the continuity without serious damage to the tissue
 3 - massive damages, tearing, crushing
 4 - massive damages, crushing, tearing with tissue damages

Bone Structure	Body Parts	Internal Organs
4.00	Skull	3.33
1.00	Jaw Region*	
3.00	Neck	0.00
2.00	U. Torso	1.75
1.25	U. Extr.	
2.22	L. Torso	1.17
2.00	L. Extr.	

* Jaw region includes jaw bone and hyoid bone

Seat Number	71
Aircraft Area	1 Left

NUMBER OF DAMAGED AREAS (0 to 72)	54
SUM OF INJURY VALUES (0 to 288)	128
WEIGHTED AVERAGE (0 to 4)	1.78

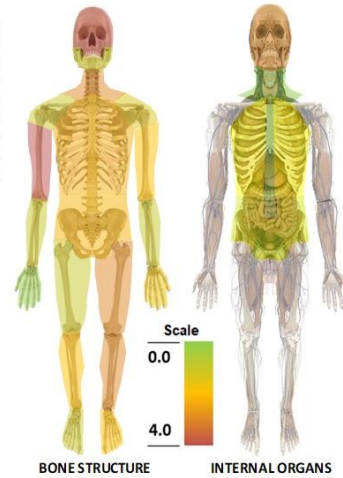


Figure 4.8 Injury report – Passenger #71

4.1.2 Debris Field Evaluation Criteria and Supporting Documentation

4.1.2.1 MAK Report Debris Field Data

MAK report contains a dedicated section called “*Wreckage Information*”, where images of the wreckage site, as well as images of the large fragments are presented. Figure 4.9 illustrates the MAK wreckage plot. The aerial image of the field includes numbers which identify the relevant items documented during the examination of the debris field.



Figure 4.9 MAK report wreckage site [1]

Major debris in the crash site captured by the official MAK report [1] have been previously presented in Figure 1.11 through Figure 1.18. Figure 4.10 gathers together all the large debris images included in the official report [1].



Figure 4.10 MAK large debris [1]

Figure 4.9 wreckage plot contains number labels for all the identified items during the examination of the field. A total of 77 labels conform this documentations, which consist of a description of the item, as well as its distance to the end of the runway. Figure 4.11 and Figure 4.12 collects the labels descriptions for the 79 items identified in the MAK report [1].

item №	Fragments	S longitudinal (m)	Z Lateral (m)				
1	Inner Marker (landing course 259' M) N54° 49,538' E032° 03,612'	1050	0	20	Fragment of left slat №23 drawing. 154.8336.23.100.	698	-53
2	Site of impact №1 on the tree, H=10,8m. N54° 49,521' E32° 03,650'	1100	-35	21	Fragment of left slat, flap carriage, left wing deflector.	694	-51
3	Site of impact №2 on a tree, H=4,1m.	931	-58	22	Fragment of inner flap of the left wing.	674	-73
4	Site of impact №3 on a group of trees.	925	-47	23	Fragment of the left wing in the tree trunk.	660	-64
5	Site of impact №4 on a group of trees.	871	-55	24	Fragment of left wing flap.	642	-44
6	Site of impact №5 on a group of trees.	872	-28	25	Site of impact on a tree.	635	-70
7	Site of impact №6 on a tree, H=4,8m.	853	-33	26	Site of impact on a group of trees.	620	-79
8	Fragments of the left wing in the tree trunk, H=5m. N54° 49,494' E32° 03,422'	856	-61	27	Outer flap deflector of the left wing.	605	-75
9	Fragment of the left aileron, left flap fairing. Fragment of left slat.	845	-42	28	Flap drive fairing of the left wing.	609	-47
9.1	Left outer flap tip.	838	-36	29	Left stabilizer tip.	595	-60
9.2	Left outer flap tip fairing, TM-4, D-10ARU №00900002.	838	-37	30	Fragments of the left wing skin panel.	588	-85
9.3	Left flap track, slat fragment, flap housing.	837	-42	31	Fragment of the primary wing structures.	562	-69
10	Fragment of left wing skin panel.	839	-30	32	Elevator rod, fragment of stabilizer skin panels.	567	-89
11	Spoiler track drive fragment №15483514131 of the left outer wing.	810	-43	33	Fragment of left stabilizer with elevator.	522	-106
12	Fragment of the outer slat tip of the left outer wing.	805	-65	34	Rudder fragment.	543	-94
13	Fragments of left wing skin panels, flap drive gear box fragment.	791	-68	35	Screw jack fairing of the outer flap, fragment of heated stabilizer leading edge.	534	-81
14	Flap drive fragment.	782	-48	36	Site of impact on the ground (trace of the right stabilizer, stabilizer fairing and fin). Fragment of tail light SMI-2KM.	520	-104
15	Collision with power lines and wire tear off.	760	-56	37	Site of impact on the ground (trace of the left wing). Fragment of the left wing panel. Rod №154.83.5711-090-009.	511	-96
16	Fragment of left outer wing with a fragment of slat, left aileron.	745	-40	38	Right stabilizer. At a distance of 3,5m were the fin front spar, RA-56 of the elevator and RA-56 of the rudder.	483	-123
17	Fragment of left wing lower skin panel.	697	-31	40	Fragment of tail fuselage skin panel.	490	-117
18	Site of impact on a tree, H=8,1m.	715	-58	41	Fragment of the Engine №3 cowl.	487	-130
19	Flight control linkage screwdrive with slat fragments.	702	-77	42	Fragments of Engine №3 cowl.	482	-127
				43	Fragment of the passenger cabin decoration (frame 58 to 59).	487	-139
				44	Fragment of Engine №3 pylon. Pylon №154.03.6100.040.009.	474	-138
				45	Flap carriage №154.83.5734.010.	482	-119
				46	Fragment of airframe with fragment of fuel line №104038.	470	-113
				47	Fragment of fin spar, flap carriage. Carriage №154.83.5734.020.	481	-112
				48	Fragment of the right outer wing upper skin panel with ID-3 probe.	463	-110
				49	Fragment of fin front spar.	475	-106

Figure 4.11 MAK identified fragments – 1 through 49 [1]

Figure 4.13 presents the main debris field area, where the majority of the aircraft debris were located at. MAK report [1] does not record the date when the attached field image was taken. Major aircraft fragments can be identified image, such as left horizontal stabilizer (38), right horizontal stabilizer (38), vertical stabilizer (54), fuselage tail cone (64), tight outer-wing (69), right wing root (75) and left wing root (74)



50	Slat screw jack №154.83.5732.020. with gear box.	471	-122	72	Fragments of lower middle fuselage with primary structures from frame 24 to frame 38.	381	-133
51	KURS MP-70 control panel.	470	-128		Fragments of lower middle fuselage with primary structures from frame 38 to frame 42.		
52	Fragment of fuselage skin.	469	-120	73	Two spare wheels KT-141E assembly.	374	-141
53	Tail fuselage (starboard) with emergency exit door. Oxygen bottle 1-2-2-210.	468	-125	74	Left part of the middle wing with left main gear assembly and inner flap.	362	-142
54	Fin with fragment of fairing. Stabilizer control mechanism MUS-3PTV.	472	-140	75	Right middle wing with right main landing gear assembly with fragment of inner flap.	380	-153
55	Engine №3 D-30KU-154 2 series №59219012414.	467	-134	76	Fragment of middle wing leading edge, cooling turbine 3318. Air conditioning system units.	368	-160
56	Fragment of lower wing skin panel with aileron spoiler, RP-59 actuator.	460	-119	77	Trash container, spare wheel KT-183.	348	-151
57	Fragment of lower skin of the right outer wing. flap leading edge, outer flap.	451	-114				
58	Engine №3 air inlet, heat exchanger.	439	-120				
59	Fragment of slat with track and screw jack.	447	-125				
60	Aileron rods №08-09-010-011, 085-095-85-095.	451	-128				
62	Fragment of middle fuselage from frame 40 to frame 64. Rear baggage compartment, wing leading edge, storage battery 20HKBH25Y3.	454	-137				
63	Engine №1 air inlet, passenger cabin emergency exit.	451	-149				
64	Tail part of the fuselage from frame 65 to frame 83, Engine №2 D30KU-154 2 series №59249012426. Engine №1 D30KU-154 2 series №59319012423.	436	-137				
65	Fragment of the primary structures of the front spar of the middle wing.	427	-117				
66	Engine №2 cowling. Fragments of passenger seats in the radius of 6m.	412	-139				
67	The pilot control panel PU-46 (ABSU-154) with a plug (from spare parts set). Center panel with speed indicator.	411	-141				
68	Fragment of central fuselage skin panel, front toilet. Service galley door.	402	-147				
69	Right wing, outer flap, screw jack fairing EPV-SPM, aileron.	390	-158				
70	Fragment of the nose, nose landing gear, shutter with the tail number 101. Cockpit appliances, units, cockpit accessory compartments.	397	-144				
71	Fragment of lower middle fuselage with primary structures from frame 16 to frame 24.	389	-134				

Figure 4.12 MAK identified fragments – 50 through 71 [1]



Figure 4.13 MAK report main debris field image [1]

4.1.2.2 PSC Data Debris Field Data

- PSC collected extensive data from several sources that documented the events in the day of the crash and in the following days. This data includes a large amount of images of the debris and their location in the debris field.
- The accident site has been divided in three major areas to facilitate the debris analysis task:
 - A. Bodin Birch Debris Region: surroundings area to the Bodin birch tree impacted by the left wing, according to MAK [1].
 - B. Pre-Ground Impact Debris Region: area following the Bodin birch region and prior to the ground marks.
 - C. Post-Ground Impact Debris Region: area following the ground marks, where most of the large fragments were located.

Figure 4.14 presents the separation of the three debris regions on a satellite image of the Smolensk Airport surroundings on April 10th, 2010. The satellite image contains a 10 by 10 m section grid to facilitate the calculation of relative distances.

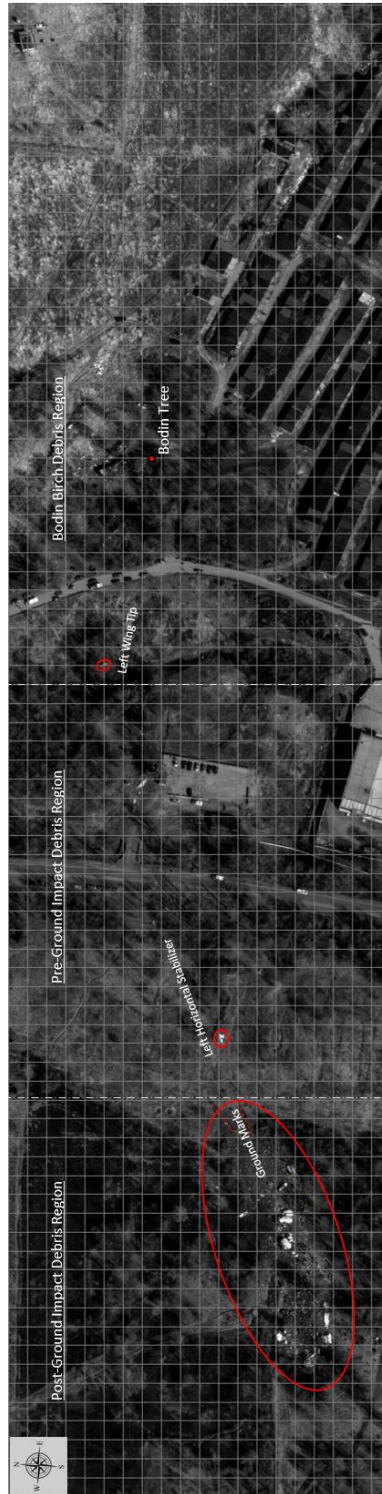


Figure 4.14 PSC satellite image [6]

A. Bodin Birch Debris Region

The Bodin birch debris region has fragments of the left wing, which is associated by MAK report [1] to the impact with the tree. Figure 4.15 presents the satellite image of the Bodin birch debris region on the 10th of April of 2010, indicating the location of the Bodin tree and left wing tip fragment. The grid overlaid on Figure 4.15 divides the image on areas of 10x10 meters. Figure 4.16 shows the large debris located in this region, which corresponds to the left wing tip.

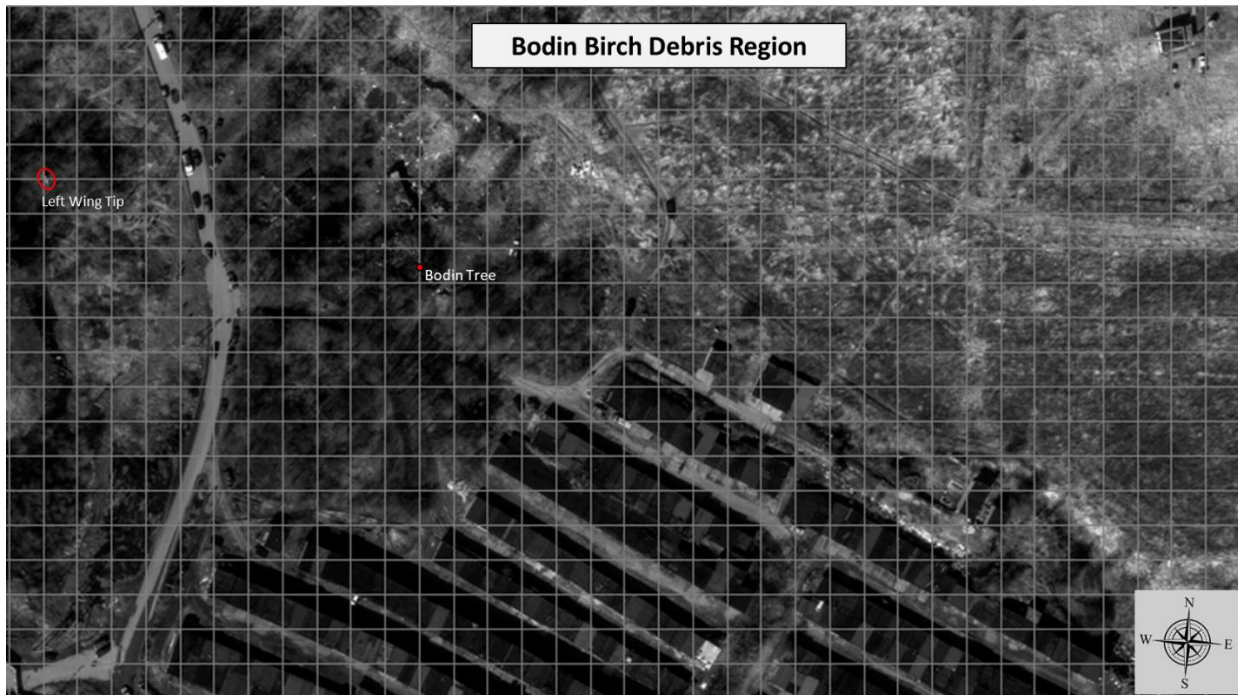


Figure 4.15 Bodin birch debris region [6]



Figure 4.16 PSC large debris images – left wing tip [6]

B. Pre-Ground Impact Debris Region

Figure 4.17 presents the satellite image of the pre-ground impact debris region on the 10th of April of 2010, specifying the location of the left horizontal stabilizer fragment. The grid overlaid on Figure 4.17 divides the image on areas of 10 x10 meters. Figure 4.18 shows the large debris located in this region, which corresponds to the left horizontal stabilizer.

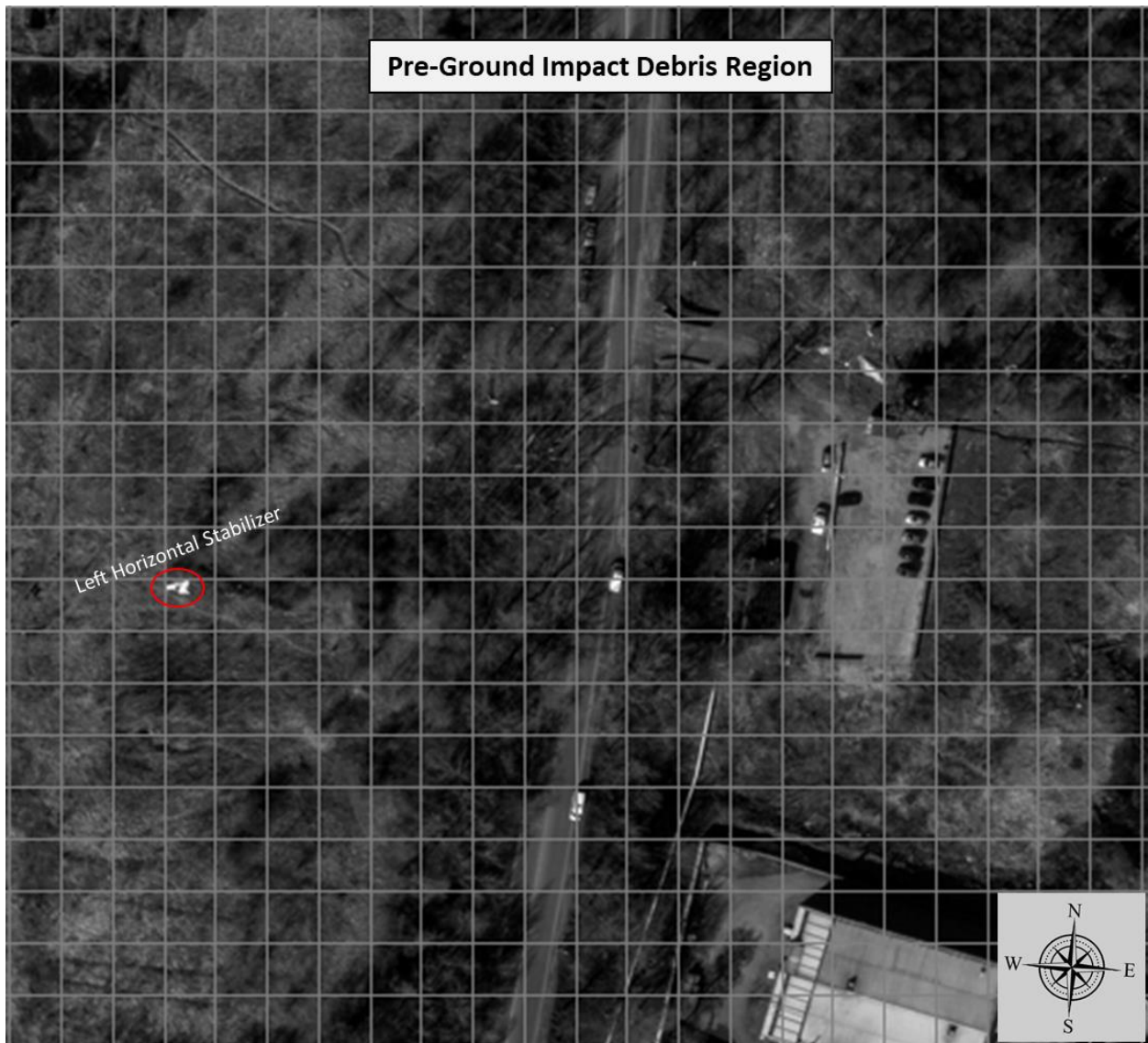


Figure 4.17 Pre-ground impact debris region [6]



Figure 4.18 PSC large debris images – left horizontal stabilizer [6]

C. Post-Ground Impact Debris Region

Figure 4.19 presents the satellite image of the post-ground impact debris region on the 10th of April of 2010, specifying the location of the large debris identified in this area. The grid overlaid on Figure 4.19 divides the image on areas of 10x10 meters. Figure 4.21 through Figure 4.25 show the large debris documented in this region, which corresponds to the aircraft fuselage body fragments, engines, right wing, tail section and the majority of the left wing structure.

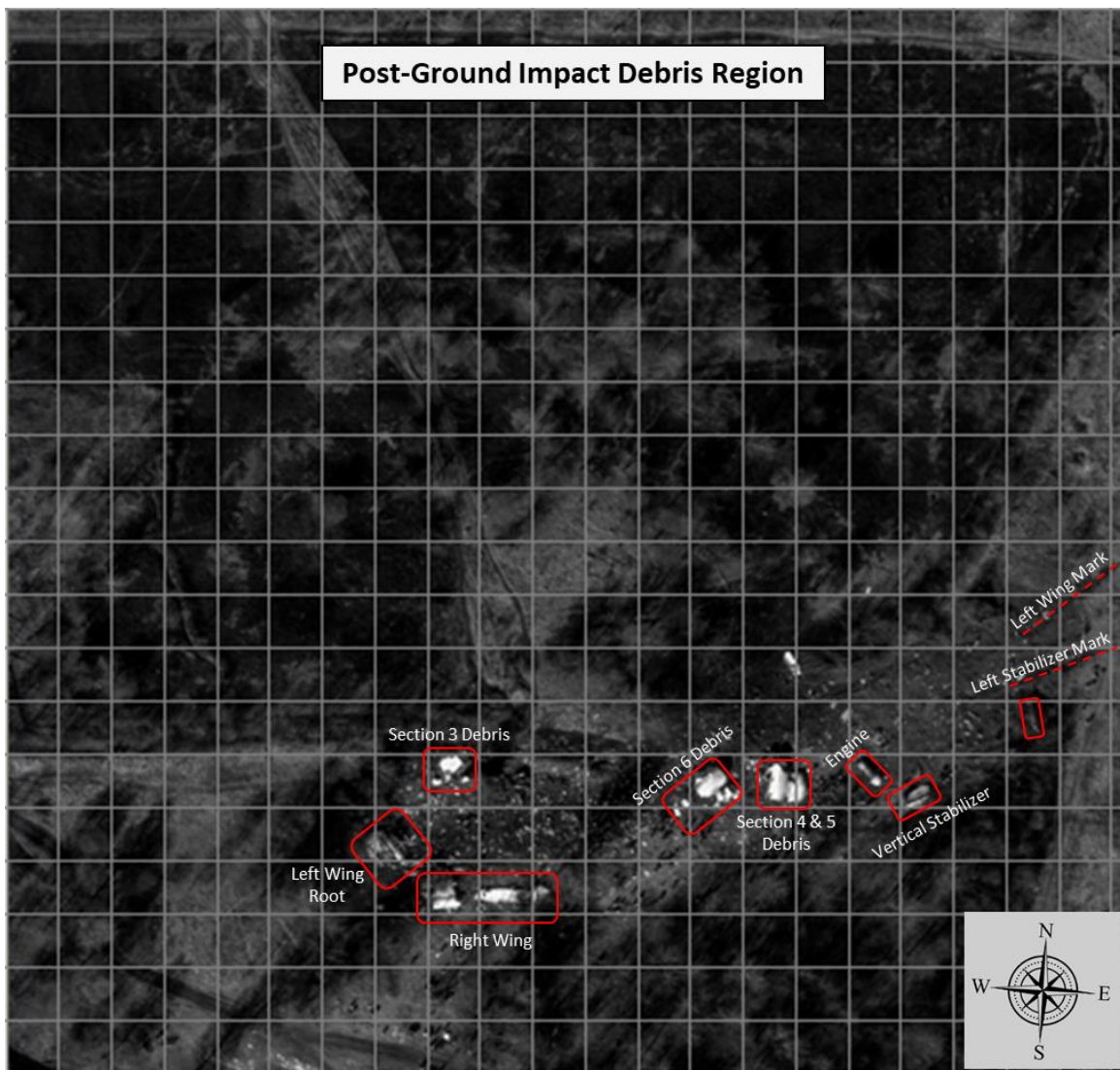


Figure 4.19 Post-ground impact debris region [6]

Figure 4.20 illustrated the ground marks located in the boundary between Figure 4.17 and Figure 4.19, where the pre-ground impact debris region ends and the post-ground impact debris region begins. These marks are associated to the stabilizer and the wing contact with the ground according to the accident reconstruction description provided by the MAK report [1].



Figure 4.20 PSC ground marks images [6]

Figure 4.21 through Figure 4.25 show the large debris documented in this region, which comprise of to the aircraft fuselage fragments, engines, right wing, tail and the majority of the left wing structure.



Figure 4.21 PSC large debris images – Section 1-2-3 [6]



Figure 4.22 PSC large debris images – Section 5-6 [6]



Figure 4.23 PSC large debris images – Stabilizers [6]



Figure 4.24 PSC large debris images – Left wing [6]



Figure 4.25 PSC large debris images – Right wing [6]

Figure 4.26 corresponds to the fragmentation sketch prepared by PSC based on all the fragments of the aircraft identified in the crash site. All size of fragments, small and large have been included in this drawing. The fracture lines indicate the areas the sustained high stresses during the crash, leading to their failure.

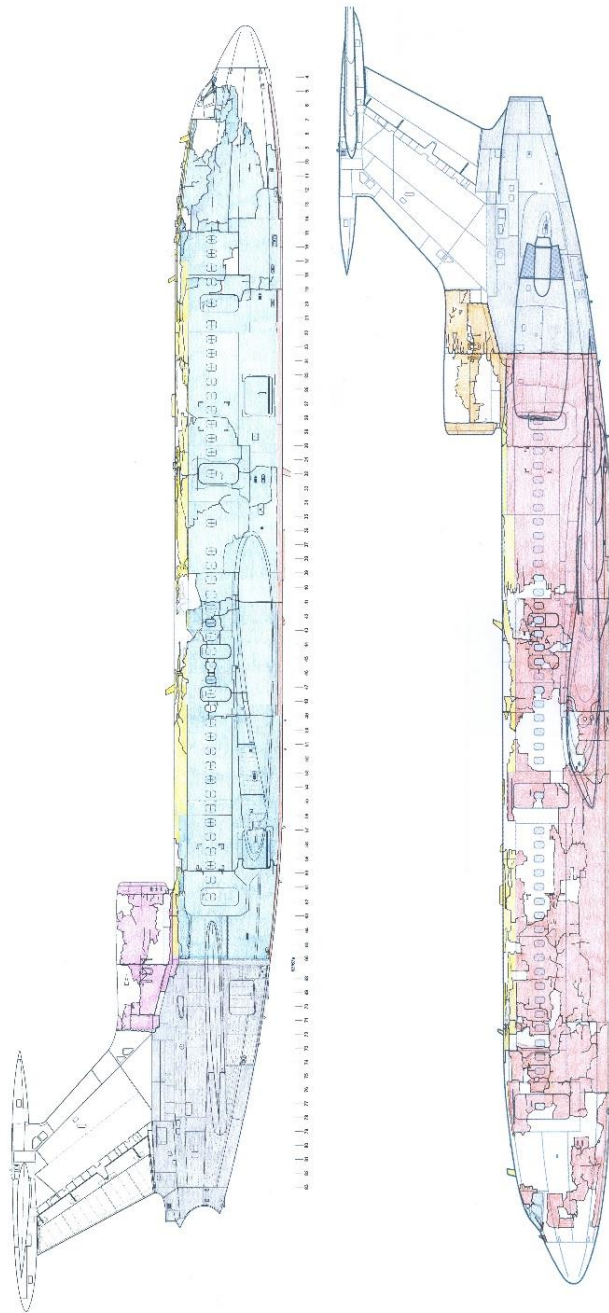


Figure 4.26 PSC aircraft debris fragmentation sketch [25]

4.1.2.3 Debris Field Analysis: Discrepancies with MAK Report

During the comparison of data collected by the available sources (MAK and PSC), some discrepancies were identified between the MAK documentation and the additional images of the crash site provided by PSC. This section summarizes some of the discrepancies documented by NIAR when comparing MAK report [1] against PSC images [6].

Figure 4.27 shows the description of MAK fragment #57, which was recorded as a lower skin panel of the right wing. The location of this skin panel was determined in the North area of the crash site.

56	Fragment of lower wing skin panel with aileron spoiler, RP-59 actuator.	460	-119
57	Fragment of lower skin of the <u>right</u> outer wing, flap leading edge, outer flap.	451	-114
58	Engine №3 air inlet, heat exchanger.	439	-120

Figure 4.27 MAK debris documentation table – Fragment #57 [1]

Figure 4.28 crosses the data available on the wing lower skin panel with the actual image of the Tu-154M n. 101 during his flying life. The comparison between the white and red marks on the skin panel found at the debris field and the actual aircraft indicate that the lower skin panel corresponds to the left wing. The identification of the correct wing side can be done by following the orientation of the red and white squares through the wingspan. This fact also agrees with the distribution of the aircraft debris along the crash site. Most of the left outer-wing fragments were located in the Northeast area of the crash site. On the contrary, the right wing root and right outer wing was located in the South-West area of the crash site.

Other discrepancies identified between the official MAK report [1] and PSC images correspond to differences in fragments locations at the crash site. The satellite image provided by PSC (gray scale image) belongs to the 10th of April of 2010. This image presents the status of the debris field hours after the crash. MAK report wreckage section [1] did not include any indications of the date of the provided wreckage image. Figure 4.29 overlays the Northeast wreckage area the MAK image and the PSC satellite image.

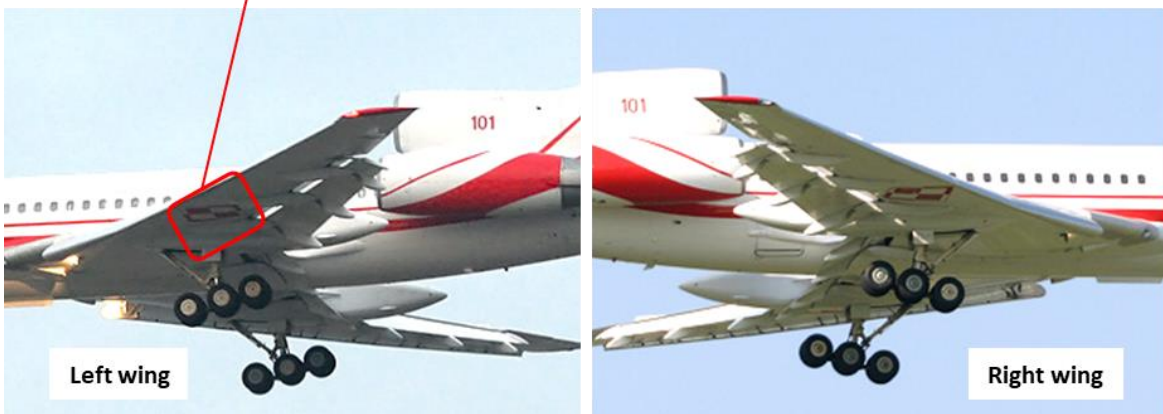
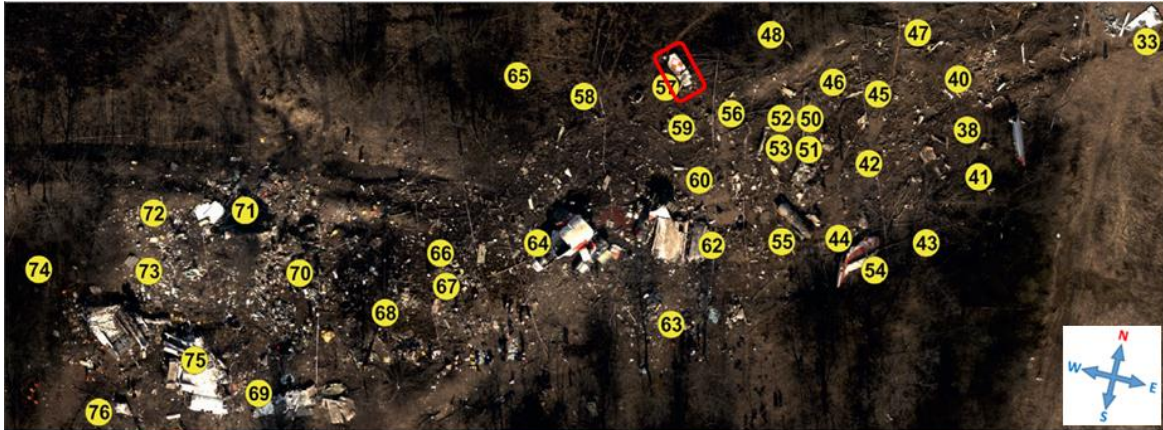
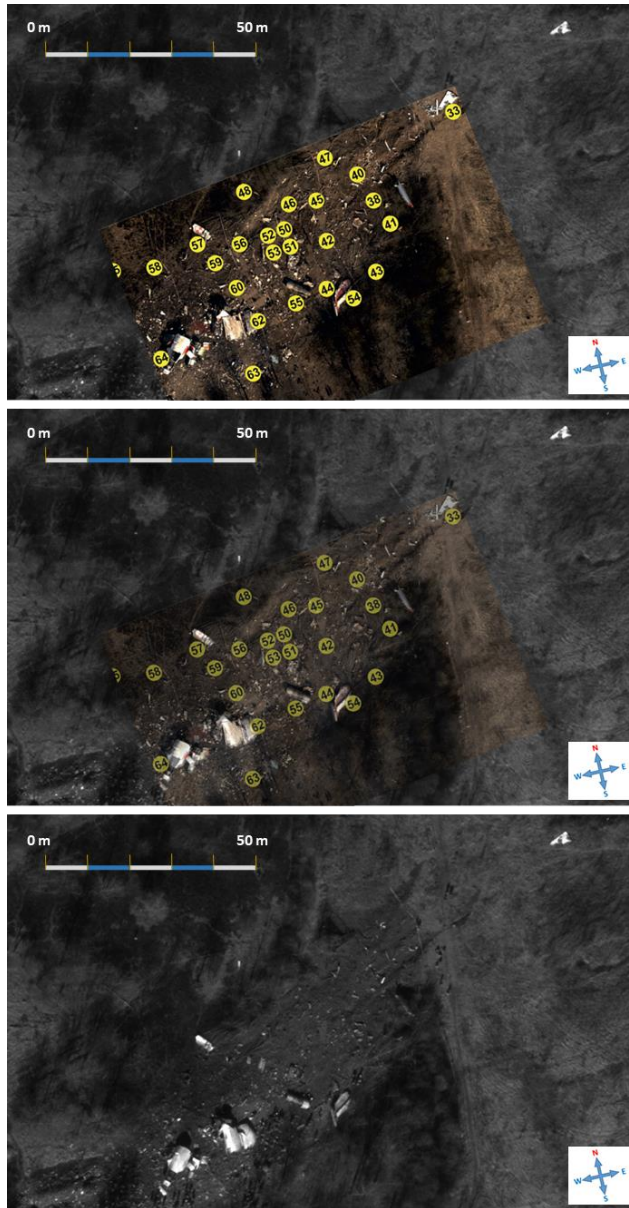


Figure 4.28 Left outer-wing lower skin panel



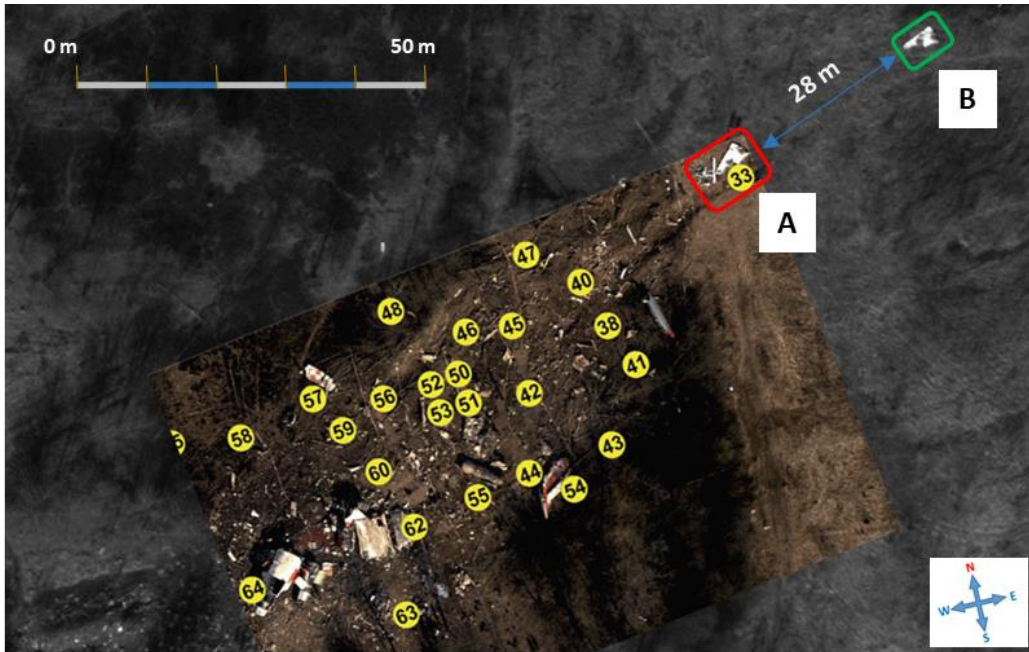
MAK transparency 0%

MAK transparency 50%

MAK transparency 100%

Figure 4.29 Northeast debris field images overlay. MAK [1] (color) and PSC [6] (gray scale)

Upon overlaying both images, the location of the left stabilizer had a difference of 28 meters approximately. Figure 4.30 presents the distance discrepancy between both images and attaches the images collected by PSC of the location of the left stabilizer prior and after being moved.



Grayscale image: Satellite April 10th

Color image: MAK report

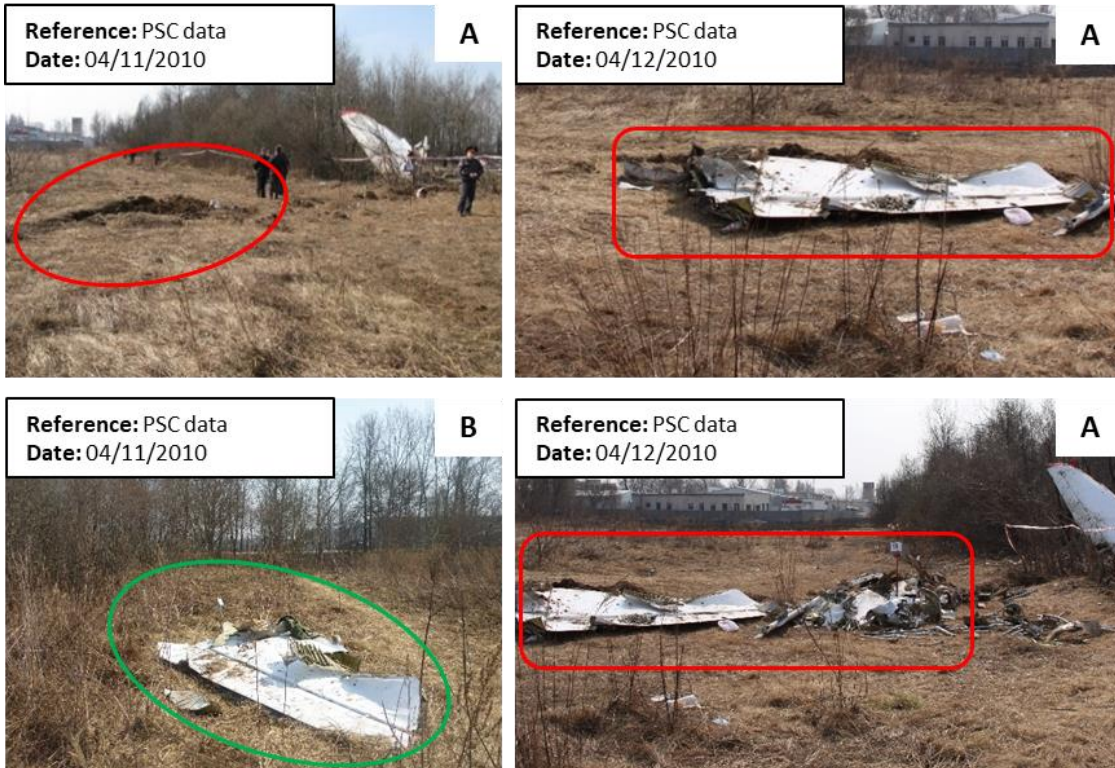


Figure 4.30 Left stabilizer debris alteration

Figure 4.31 overlays the South-West wreckage area the MAK image and the PSC satellite image. Orientation of the right wing fragments does not match when comparing both images. These debris seem to be rotated from its original position presented in the satellite image (gray scale image).

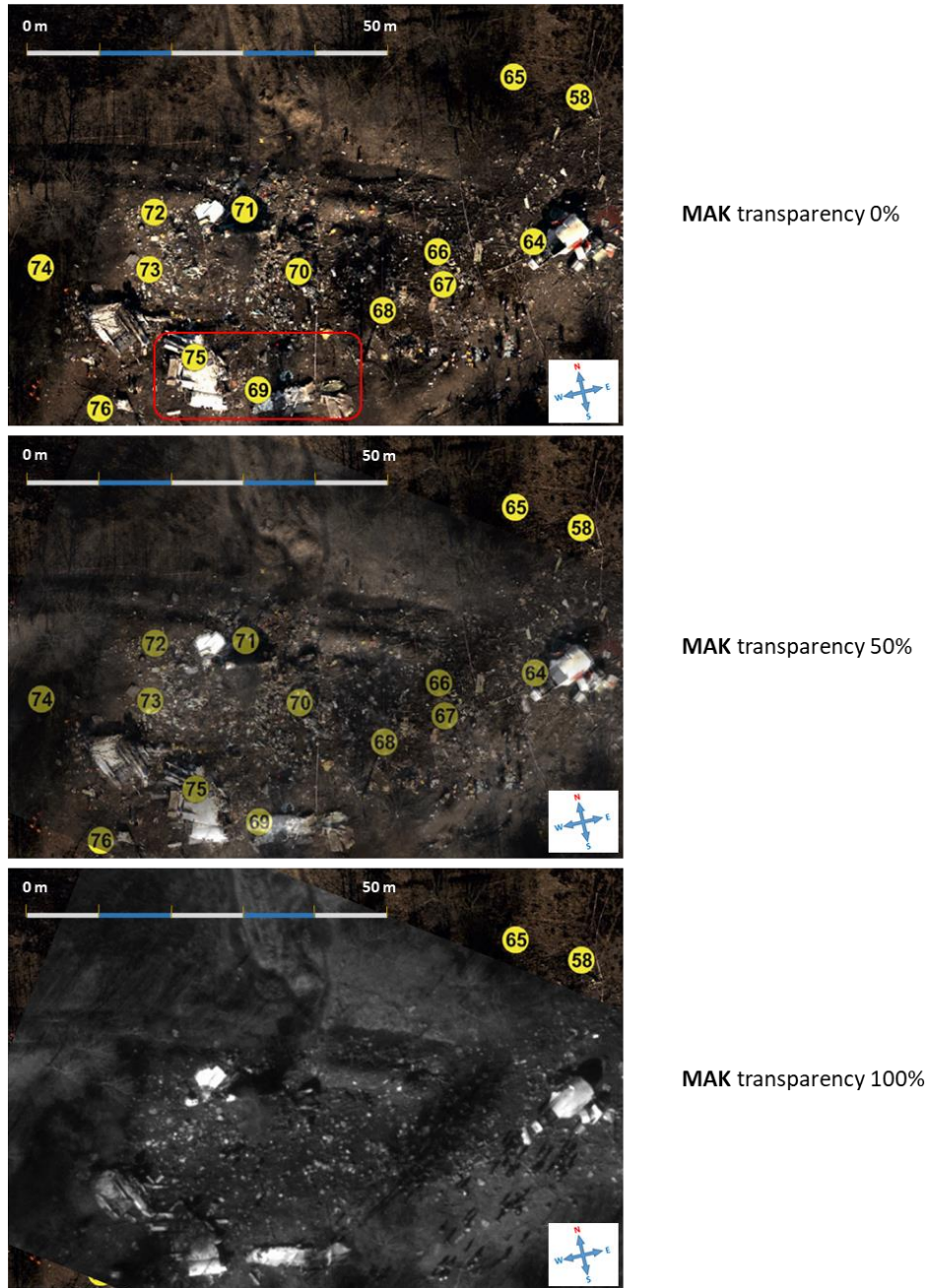


Figure 4.31 Southwest debris field images overlay. MAK [1] (color) and PSC [6] (gray scale)

4.2 Ground Collision Reconstruction

This section discusses the results from the accident reconstruction numerical analysis. Global aircraft kinematics are presented in section 4.2.1. Ground marks analysis and comparison to MAK report are presented in section 4.2.2.

4.2.1 Overall Aircraft Kinematics and Damage Evaluation

The remaining outboard portion of left wing, left horizontal stabilizer, and section 1 are the initial parts that came in contact with the ground. Due to the ground impact, the remaining outboard portion of the left wing separated from the center wing section. The left wing impact caused section 4 and the right wing to yaw clockwise (looking from directly above the aircraft and ground), while the ground impact ripped open the ceiling of sections 3 and 4. At the same time, the inertia of the forward fuselage caused sections 1, 2, and a portion of 3 to yaw counterclockwise (looking from directly above the aircraft and ground). The vertical stabilizer impact with the ground caused section 6 to separate from section 5 and rotate against its direction of travel. The vertical stabilizer remained attached to section 6 throughout the simulation. However, the horizontal stabilizer separated from the vertical stabilizer during ground impact. Both engines also separated from section 6 as they came into contact with the ground. A sequence of these aforementioned events are presented in Figure 4.32 through Figure 4.40. An image of the overall damage in the model at time = 1035 ms, as shown in Figure 4.47.

As shown in Figure 4.47 and Figure 4.48 the aircraft fuselage breaks into four major sections, forward and aft of the wing box, and forward of the pressure bulkhead. This type of fuselage fragmentation is typical of emergency landing conditions. The fuselage tends to fracture in the areas where there is a significant change in structural stiffness (Bulkheads, and Wing Box).

A comparison with the fragmentation sketches provided by the PSC [25] is provided in Figure 4.49 and Figure 4.50. Large opening in the middle sections (Sections 3, 4 and 5) of the fuselage are noticeable in both the numerical model and the debris sketch. However, the forward fuselage sections (Sections 1 and 2) do not have less level of fragmentation compared to the debris sketches (this differences in damage on section 1 and 2 are due to the lack of information regarding the tree location, type, and size in the accident site). Significant stress concentration bend lines in areas of section 5 and the vertical stabilizers are observed in Figure 4.49 through Figure 4.53. It is important to note that, for this accident reconstruction analysis, trees were not modeled in the impact site, since data pertaining their location, size, type, etc. was not available. The contact with these trees and shrubs could result in a different kinematic path and damage of the structure (specially for Section 1 and 2) after the initial 385 ms of the accident reconstruction (Between 0 to 385 ms the accident site was free of large trees). The entire survivable volume was compromised during the first 385 ms which resulted in fatal injuries to the aircraft occupants. More details on the crash kinematics can be found in the videos contained in the final presentation package submitted with this report.

Image: Tu 154 - 165 ms - Top View (165 ms)



Time: 165 ms

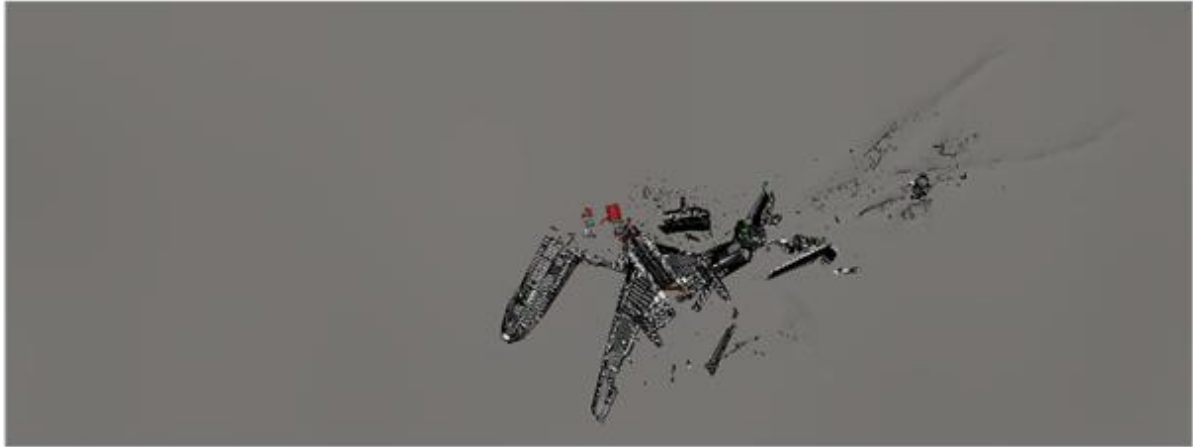
Image: Tu 154 - 335 ms - Top View (335 ms)



Time: 335 ms

Figure 4.32 Tu154 numerical model kinematics – Top view (time: 165 ms and 335 ms)

042964 - 16.204 - 1035.000 - 1035.0000000000000



Time: 845 ms

042964 - 16.204 - 1035.000 - 1035.0000000000000



Time: 1035 ms

Figure 4.34 Tu154 numerical model kinematics – Top view (time: 845 ms and 1035 ms)

tu154_165.ms | 165.ms | 165.ms | 165.ms | 165.ms | 165.ms



Time: 165 ms

tu154_335.ms | 335.ms | 335.ms | 335.ms | 335.ms | 335.ms



Time: 335 ms

Figure 4.35 Tu154 numerical model kinematics – Bottom view (time: 165 ms and 335 ms)

04804 - Tu 154 - 5143 302 - 1000 6.00000000 00



Time: 505 ms

04804 - Tu 154 - 5143 326 - 1000 6.00000000 00



Time: 675 ms

Figure 4.36 Tu154 numerical model kinematics – Bottom view (time: 505 ms and 675 ms)

048264 1 Tu 154 1 5143 579 1296.8400000000000



Time: 845 ms

048264 1 Tu 154 1 5143 580 1296.8400000000000



Time: 1035 ms

Figure 4.37 Tu154 numerical model kinematics – Bottom view (time: 845 ms and 1035 ms)

0123456789 : Tu 154 : 51A1E 04 : TIME 3.340599221E 01



Time: 165 ms

0123456789 : Tu 154 : 51A1E 04 : TIME 3.340599221E 01



Time: 335 ms

Figure 4.38 Tu154 numerical model kinematics – Right side view (time: 165 ms and 335 ms)

0123456789101112131415161718192021222324252627282930313233343536373839404142434445464748495051525354555657585960616263646566676869707172737475767778798081828384858687888990919293949596979899100



Time: 505 ms

0123456789101112131415161718192021222324252627282930313233343536373839404142434445464748495051525354555657585960616263646566676869707172737475767778798081828384858687888990919293949596979899100



Time: 675 ms

Figure 4.39 Tu154 numerical model kinematics – Right side view (time: 505 ms and 675 ms)

003.jpg : tu 154 : STATE 178 ,LINE 6,403095961 01



Time: 845 ms

003.jpg : tu 154 : STATE 205 ,LINE 2,034095961 00



Time: 1035 ms

Figure 4.40 Tu154 numerical model kinematics – Right side view (time: 845 ms and 1035 ms)

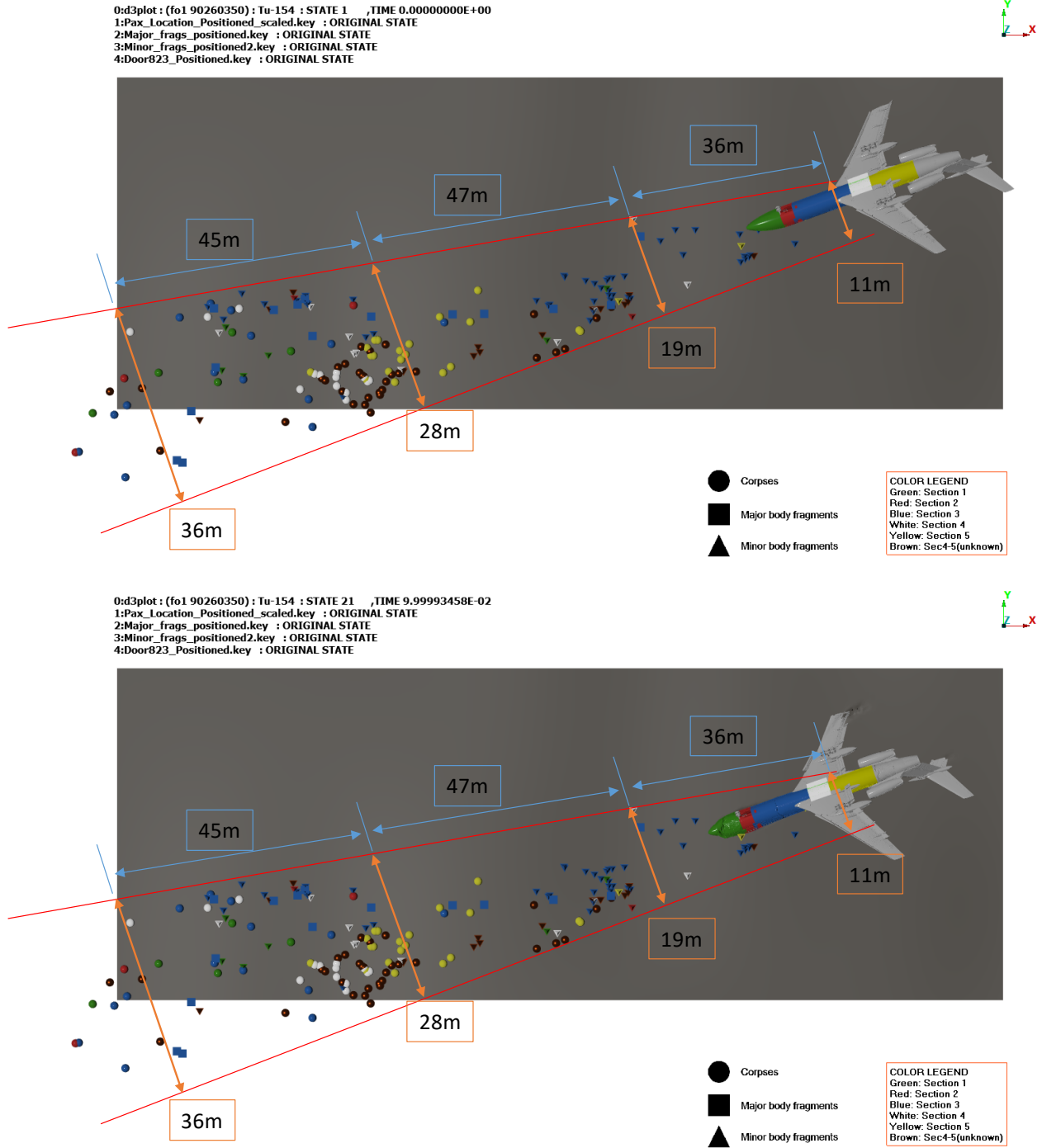


Figure 4.41 Tu154 numerical model kinematics – top view overlaid with corpses and body fragments (time: 0 ms and 100 ms)

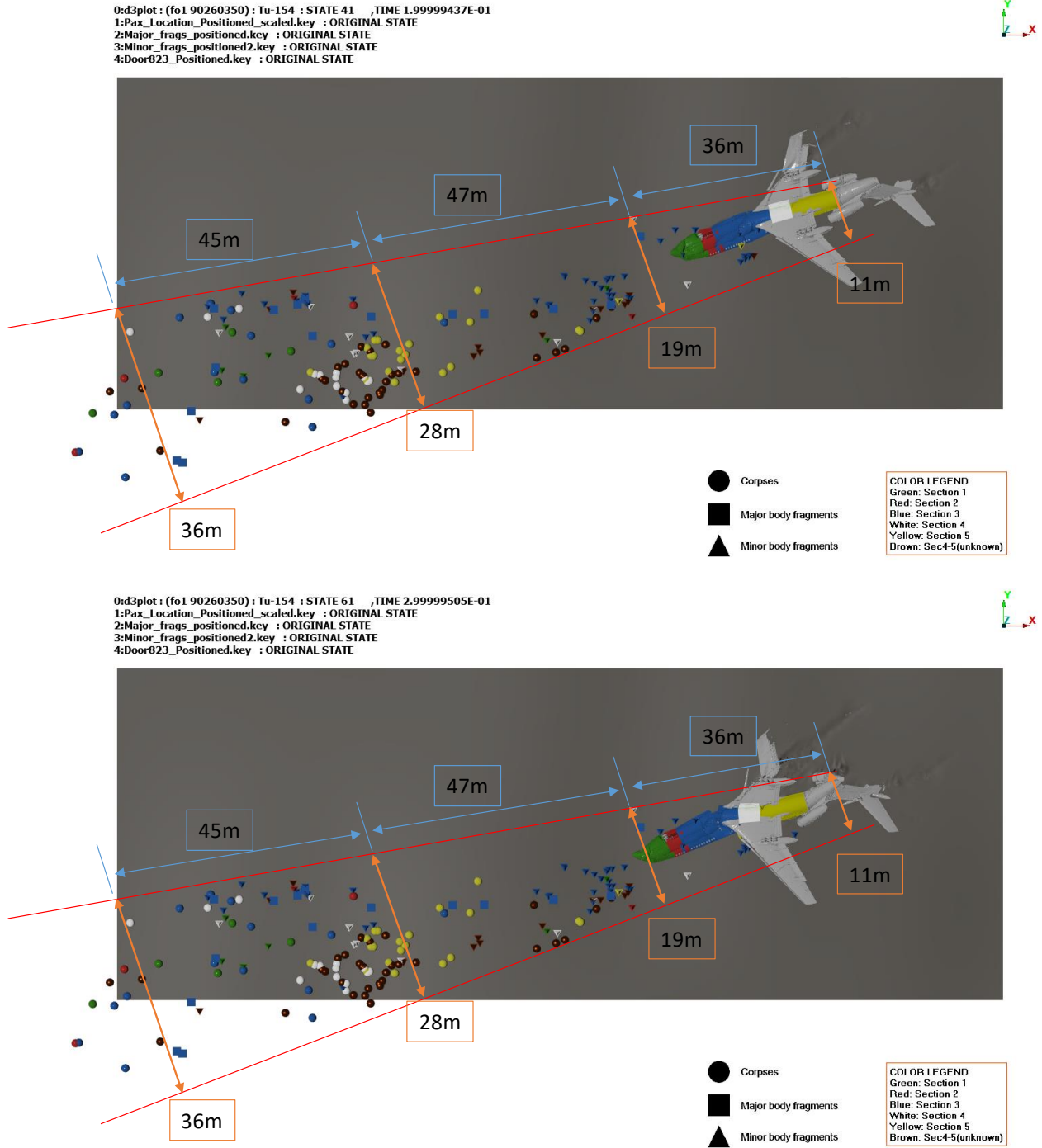


Figure 4.42 Tu154 numerical model kinematics – top view overlaid with corpses and body fragments (time: 200 ms and 300 ms)

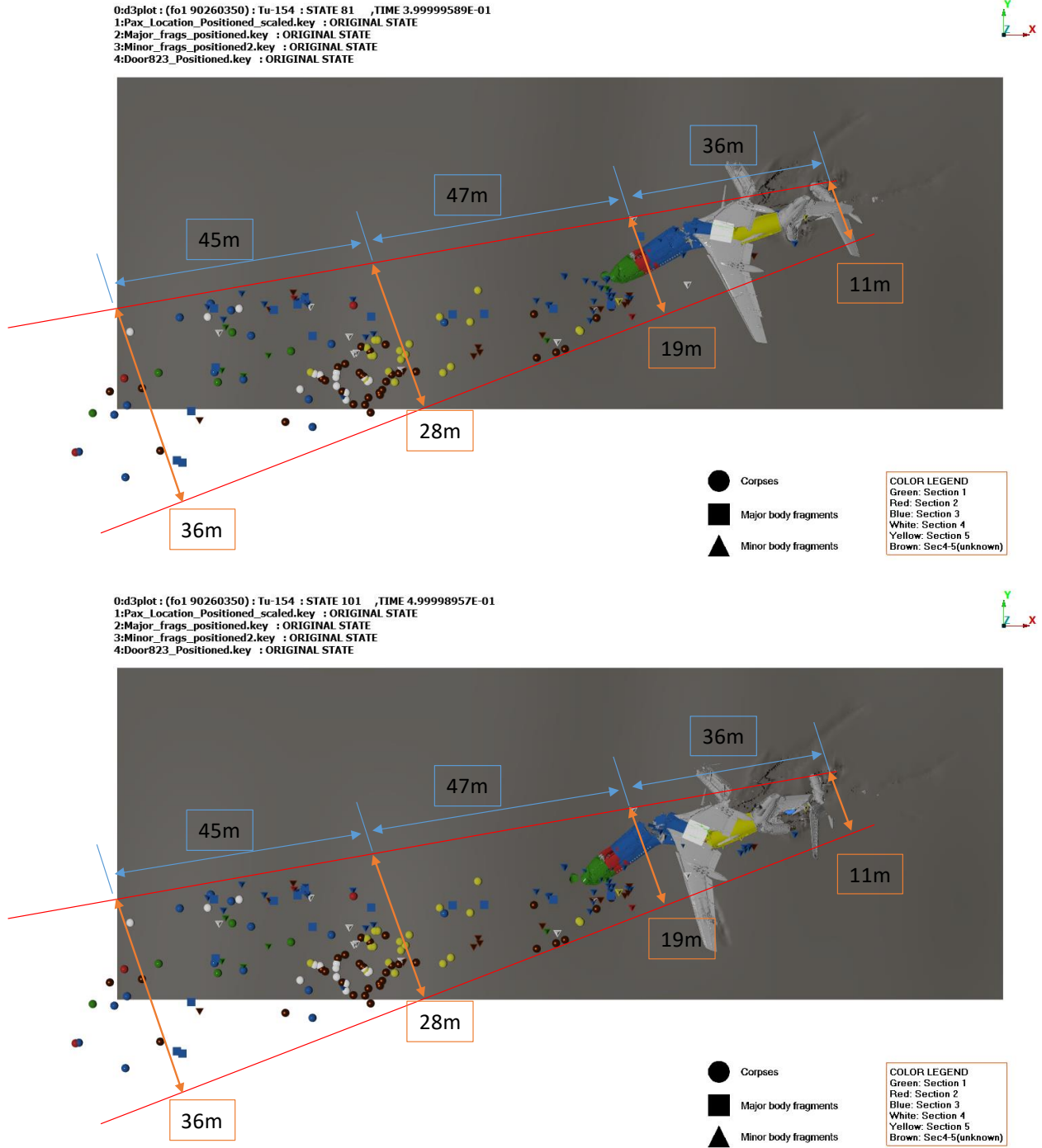
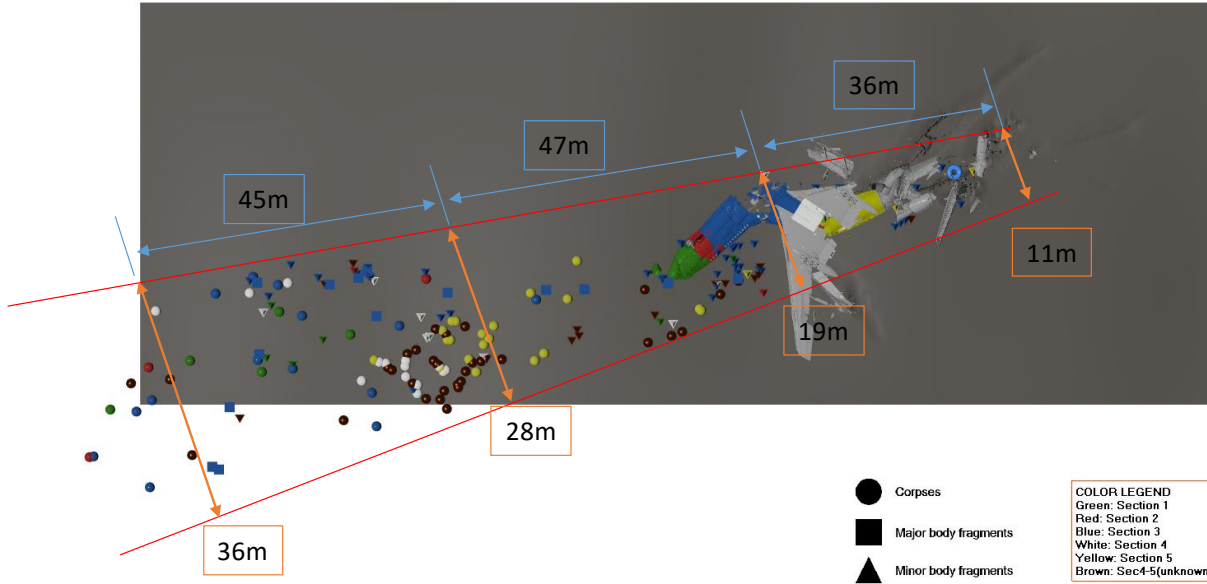


Figure 4.43 Tu154 numerical model kinematics – top view overlaid with corpses and body fragments (time: 400 ms and 500 ms)

0:d3plot : (fo1 90260350) : Tu-154 : STATE 121 ,TIME 5.99999011E-01
 1:Pax_Location_Positioned_scaled.key : ORIGINAL STATE
 2:Major_frags_positioned2.key : ORIGINAL STATE
 3:Minor_frags_positioned2.key : ORIGINAL STATE
 4:Door823_Positioned.key : ORIGINAL STATE



0:d3plot : (fo1 90260350) : Tu-154 : STATE 141 ,TIME 6.99999094E-01
 1:Pax_Location_Positioned_scaled.key : ORIGINAL STATE
 2:Major_frags_positioned2.key : ORIGINAL STATE
 3:Minor_frags_positioned2.key : ORIGINAL STATE
 4:Door823_Positioned.key : ORIGINAL STATE

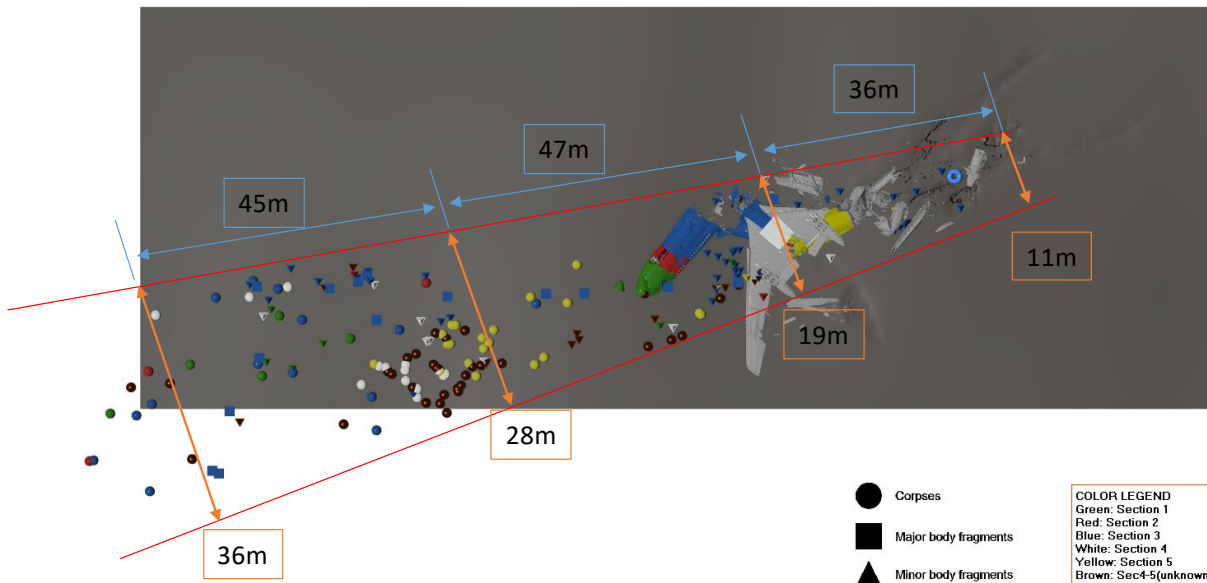
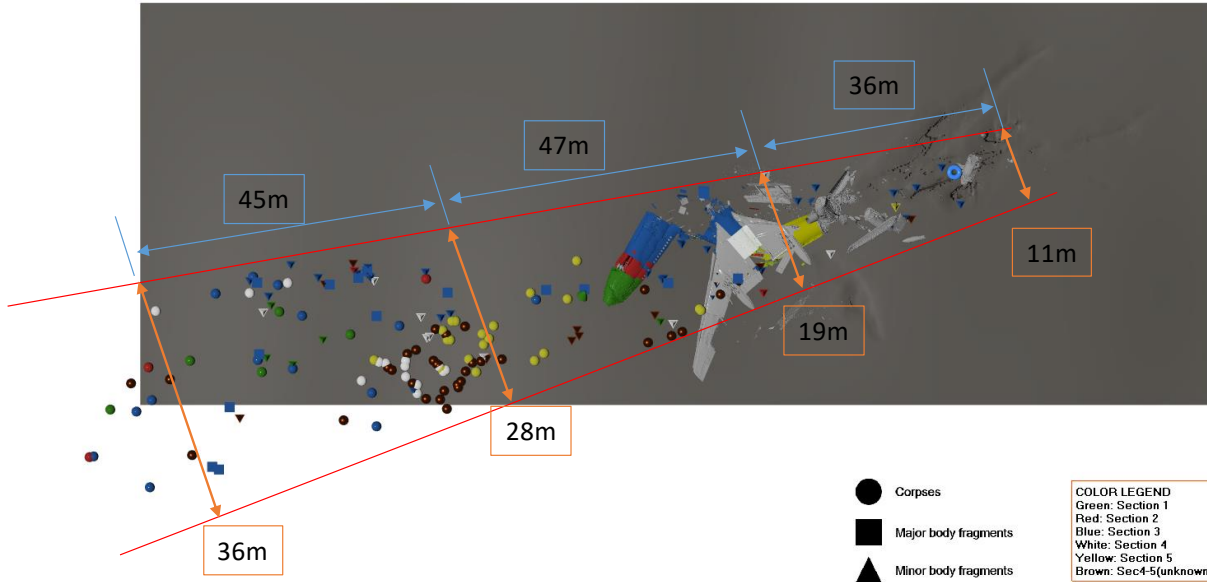


Figure 4.44 Tu154 numerical model kinematics – top view overlaid with corpses and body fragments (time: 600 ms and 700 ms)

0:d3plot : (fo1 90260350) : Tu-154 : STATE 161 ,TIME 7.99998760E-01
 1:Pax_Location_Positioned_scaled.key : ORIGINAL STATE
 2:Major_frags_positioned2.key : ORIGINAL STATE
 3:Minor_frags_positioned2.key : ORIGINAL STATE
 4:Door823_Positioned.key : ORIGINAL STATE



0:d3plot : (fo1 90260350) : Tu-154 : STATE 181 ,TIME 8.99999082E-01
 1:Pax_Location_Positioned_scaled.key : ORIGINAL STATE
 2:Major_frags_positioned2.key : ORIGINAL STATE
 3:Minor_frags_positioned2.key : ORIGINAL STATE
 4:Door823_Positioned.key : ORIGINAL STATE

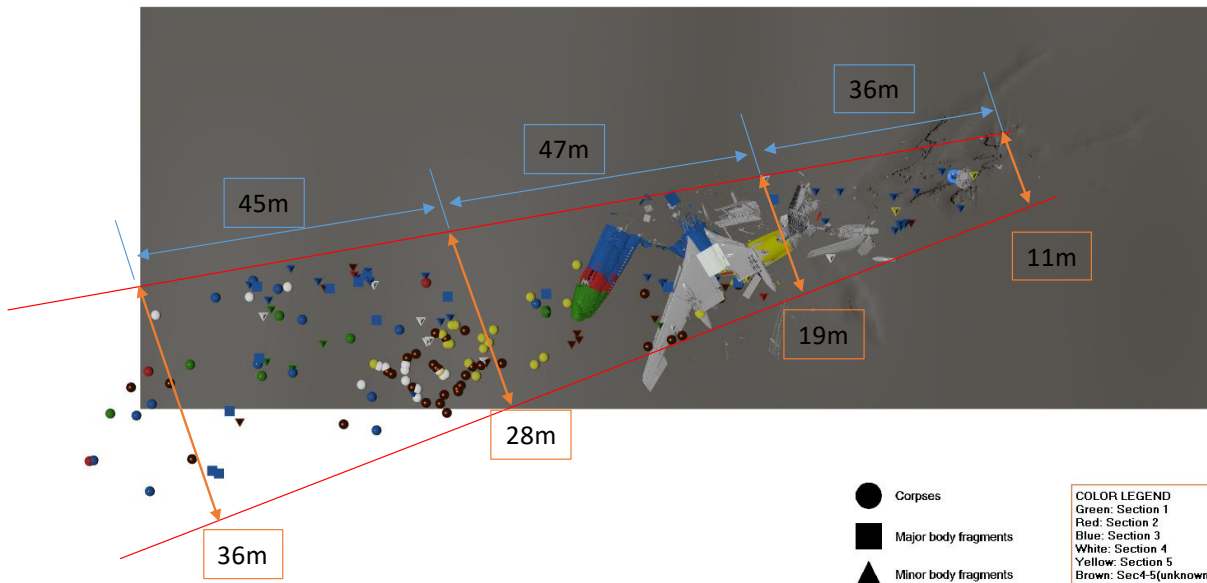


Figure 4.45 Tu154 numerical model kinematics – top view overlaid with corpses and body fragments (time: 800 ms and 900 ms)

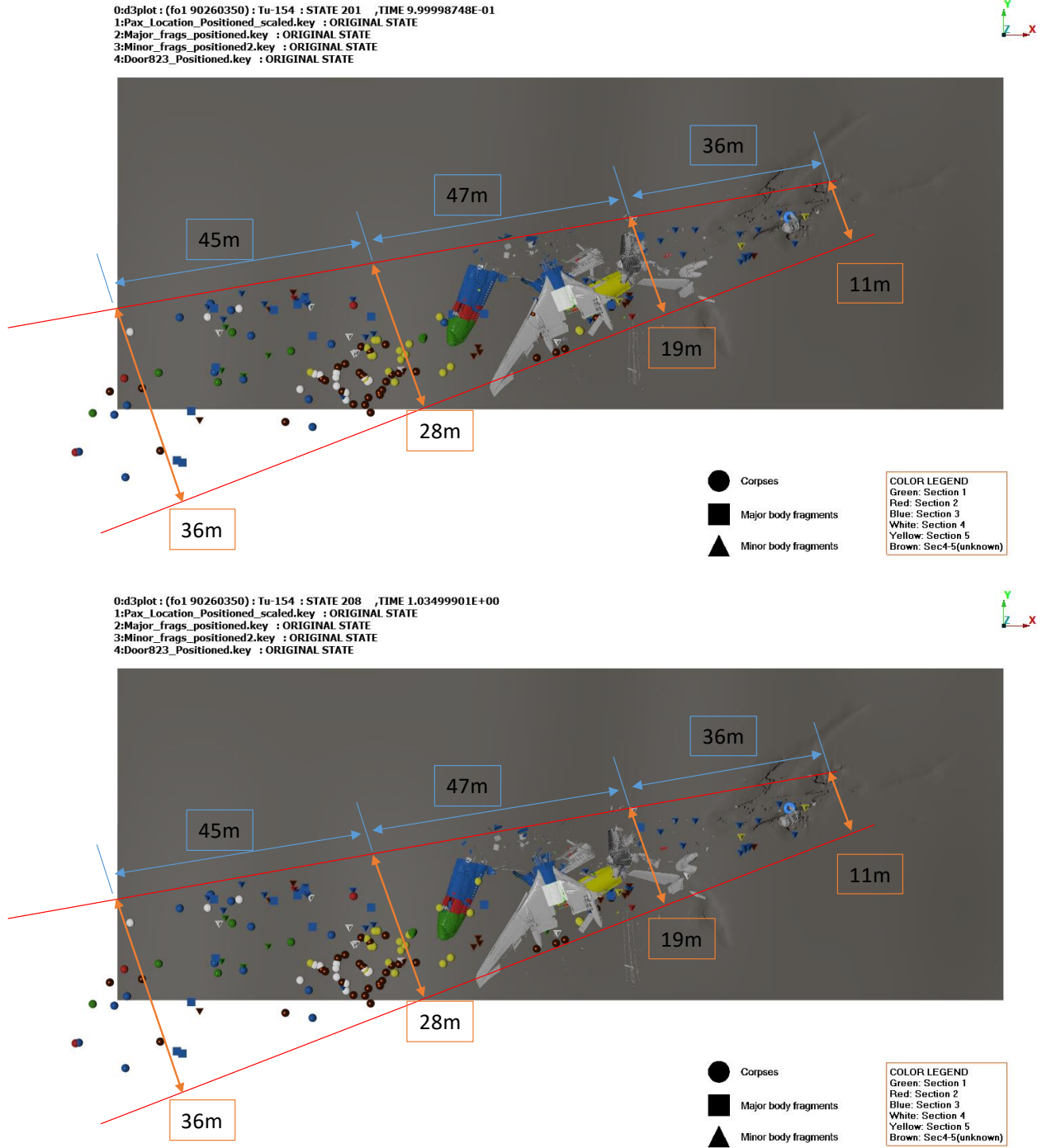


Figure 4.46 Tu154 numerical model kinematics – top view overlaid with corpses and body fragments (time: 1000 ms and 1035 ms)

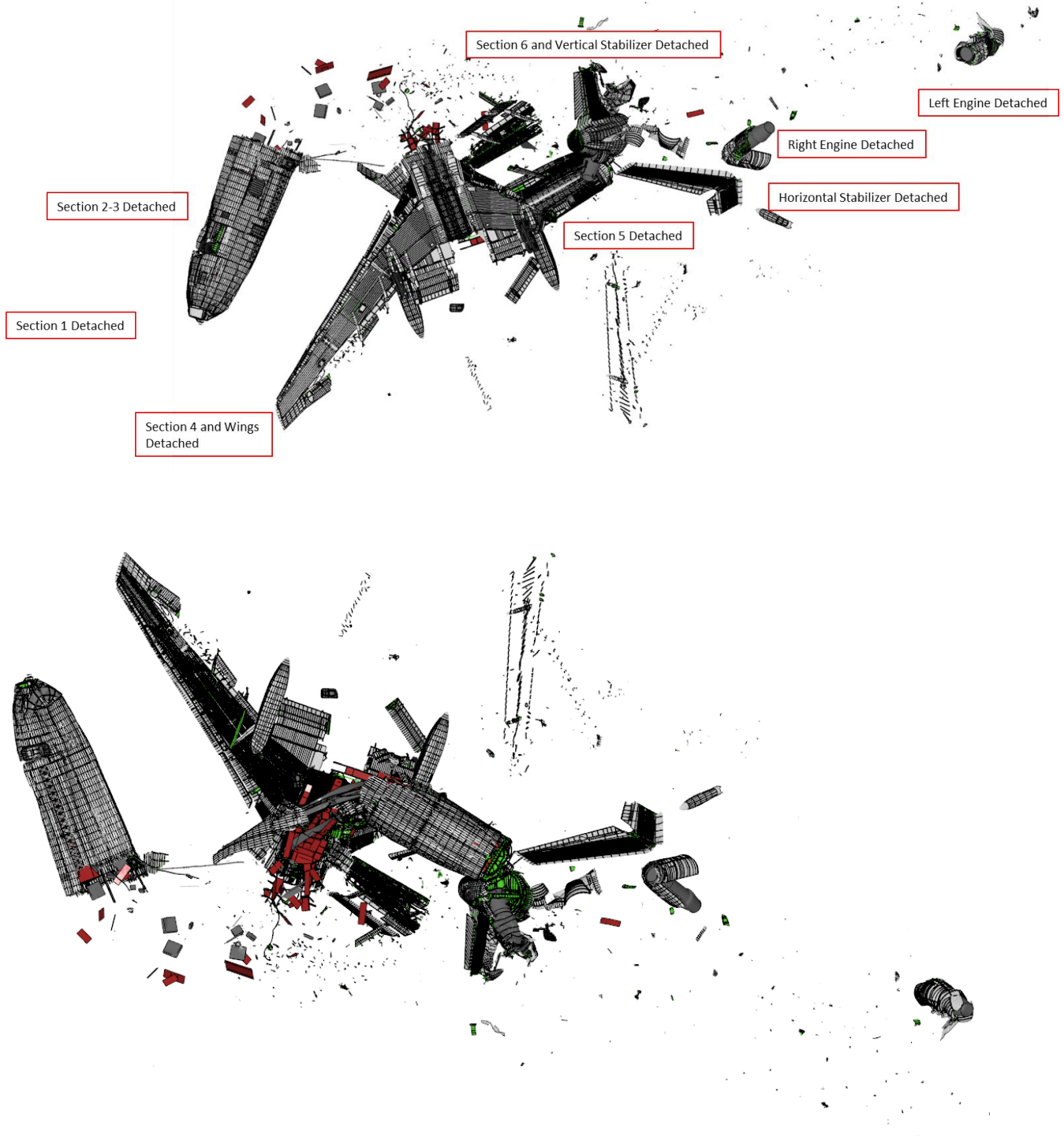


Figure 4.47 Tu154 numerical model damage at $t = 1035$ ms – Top view (top) and bottom view (bottom)

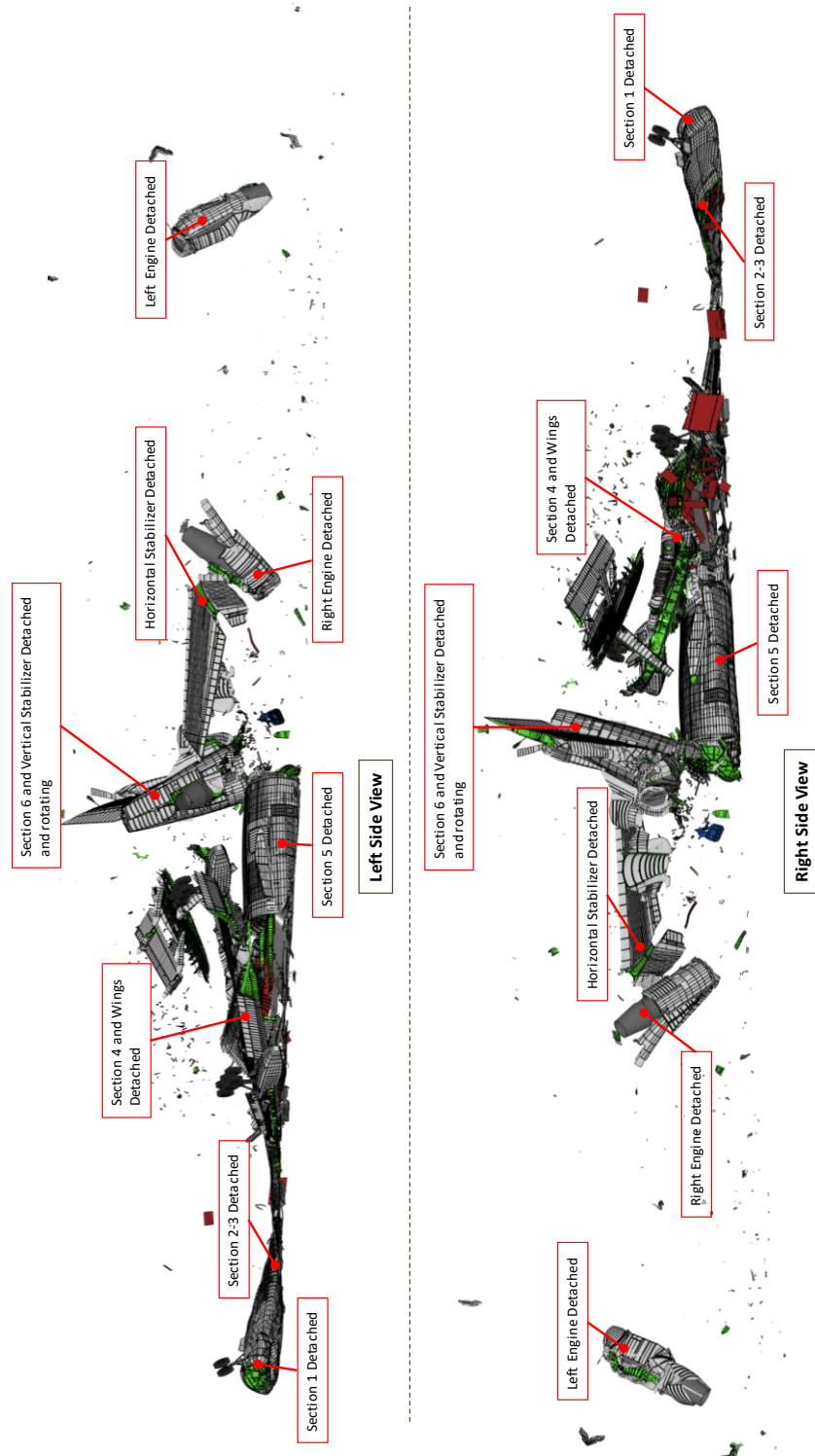


Figure 4.48 Tu154 numerical model damage at $t = 1035$ ms – Left side view (left) and right side view (right)

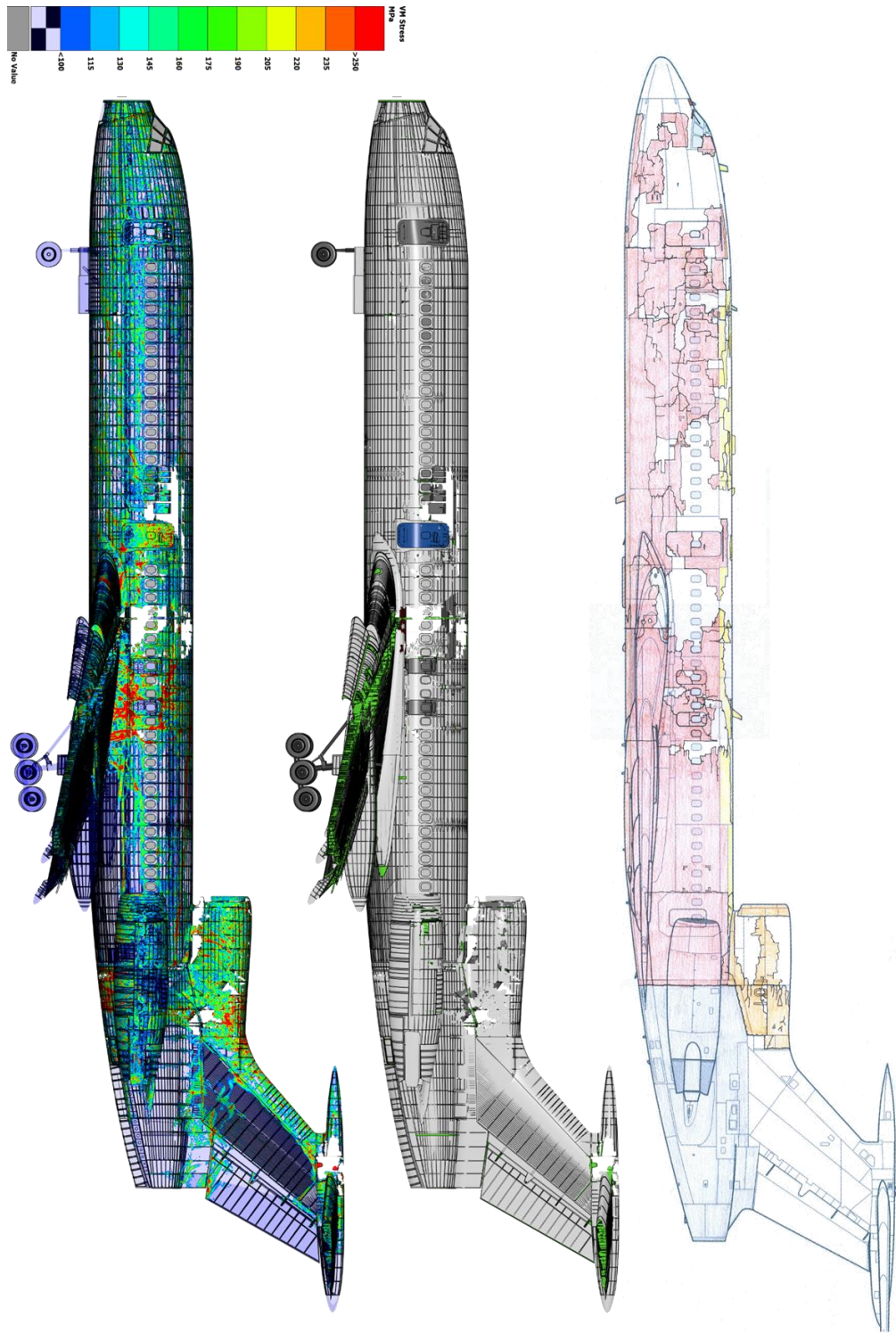


Figure 4.49 Left side Tu154 numerical model damage at $t = 1035$ ms – Comparison with PSC debris sketch [25]

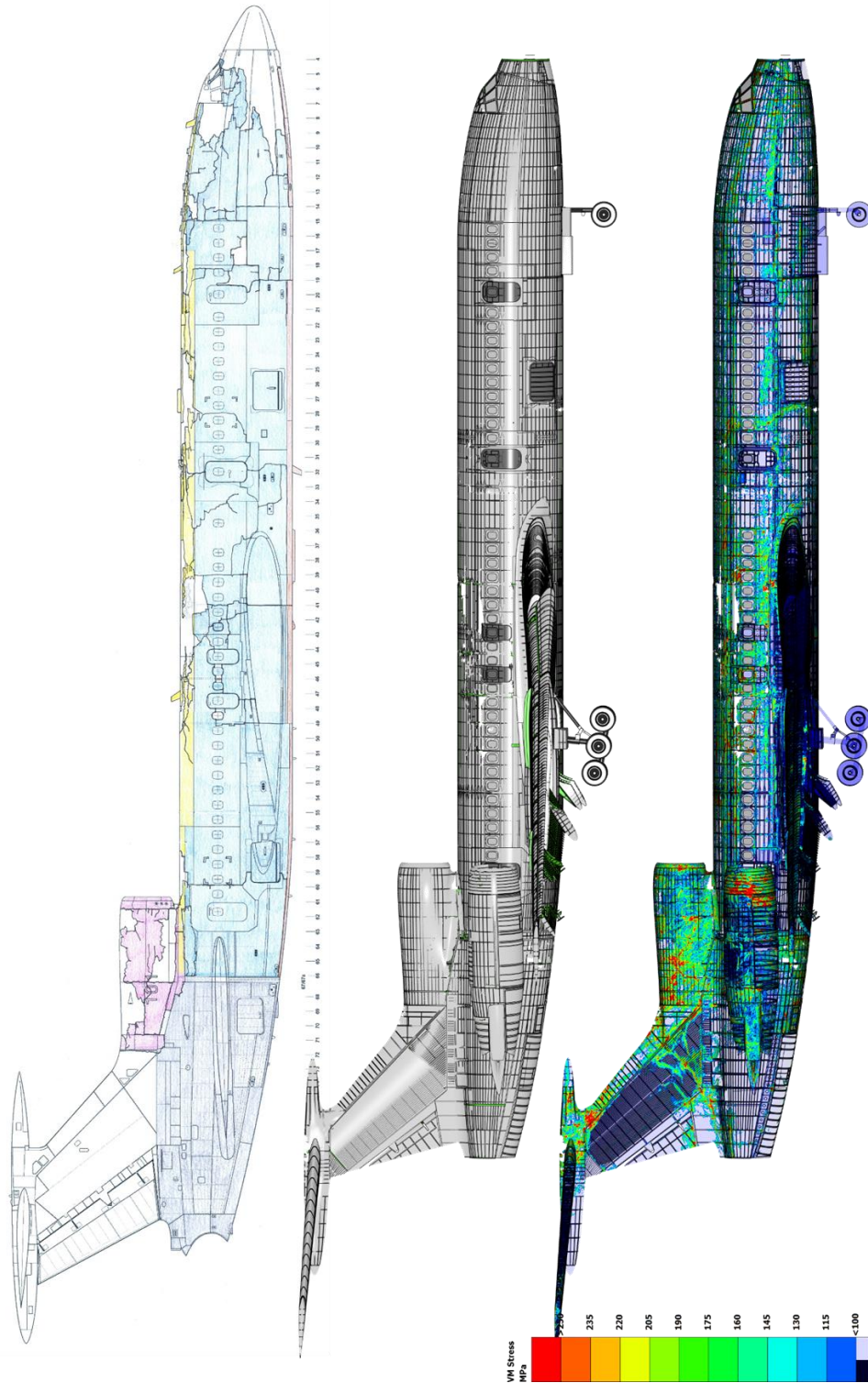
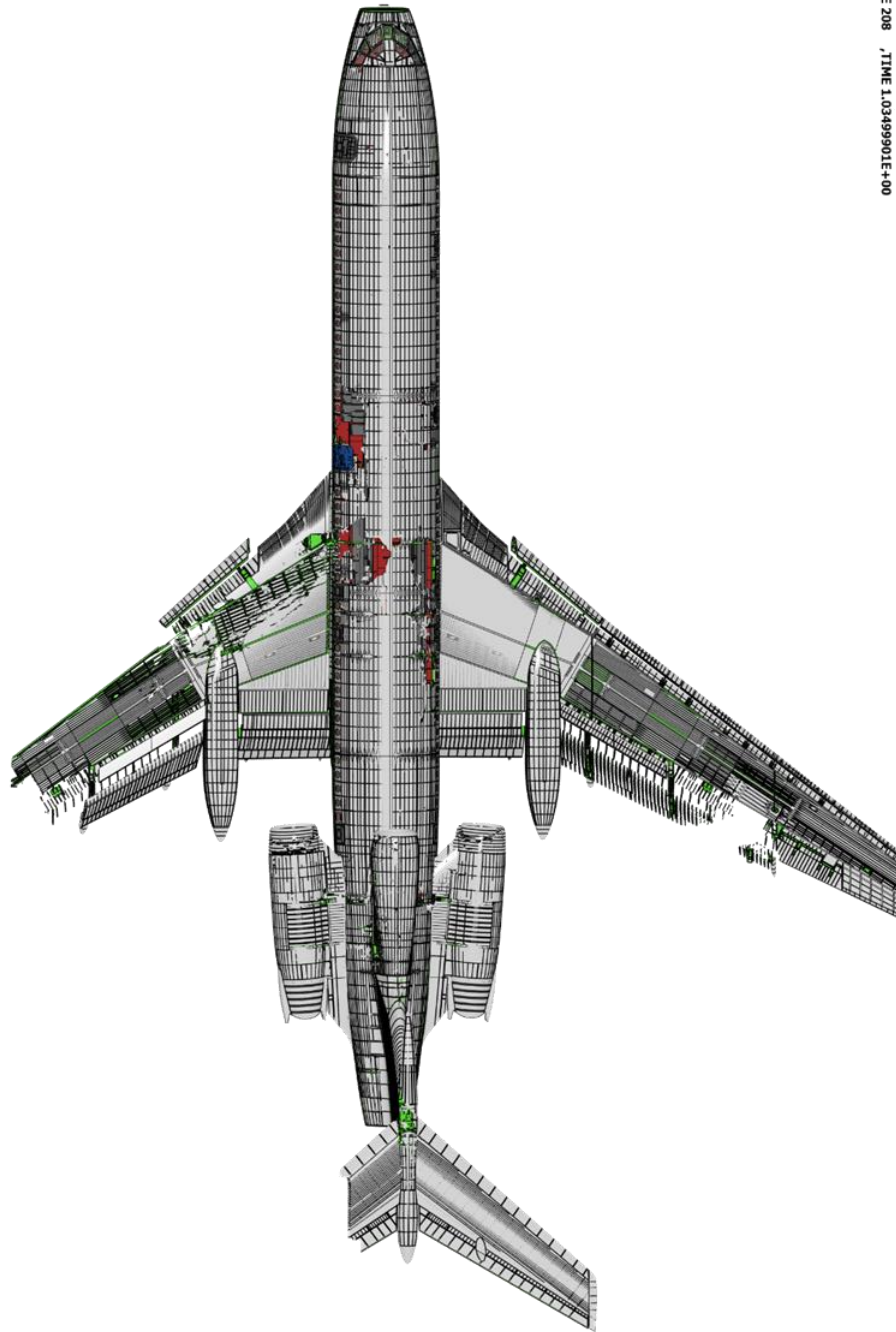


Figure 4.50 Right side Tu154 numerical model damage at $t = 1035$ ms – Comparison with PSC debris sketch [25]



0:\d3plot : Tu-154 : STATE 208 .TIME 1.03499901E+00

Figure 4.51 Top side Tu154 numerical model damage at $t = 1035$ ms

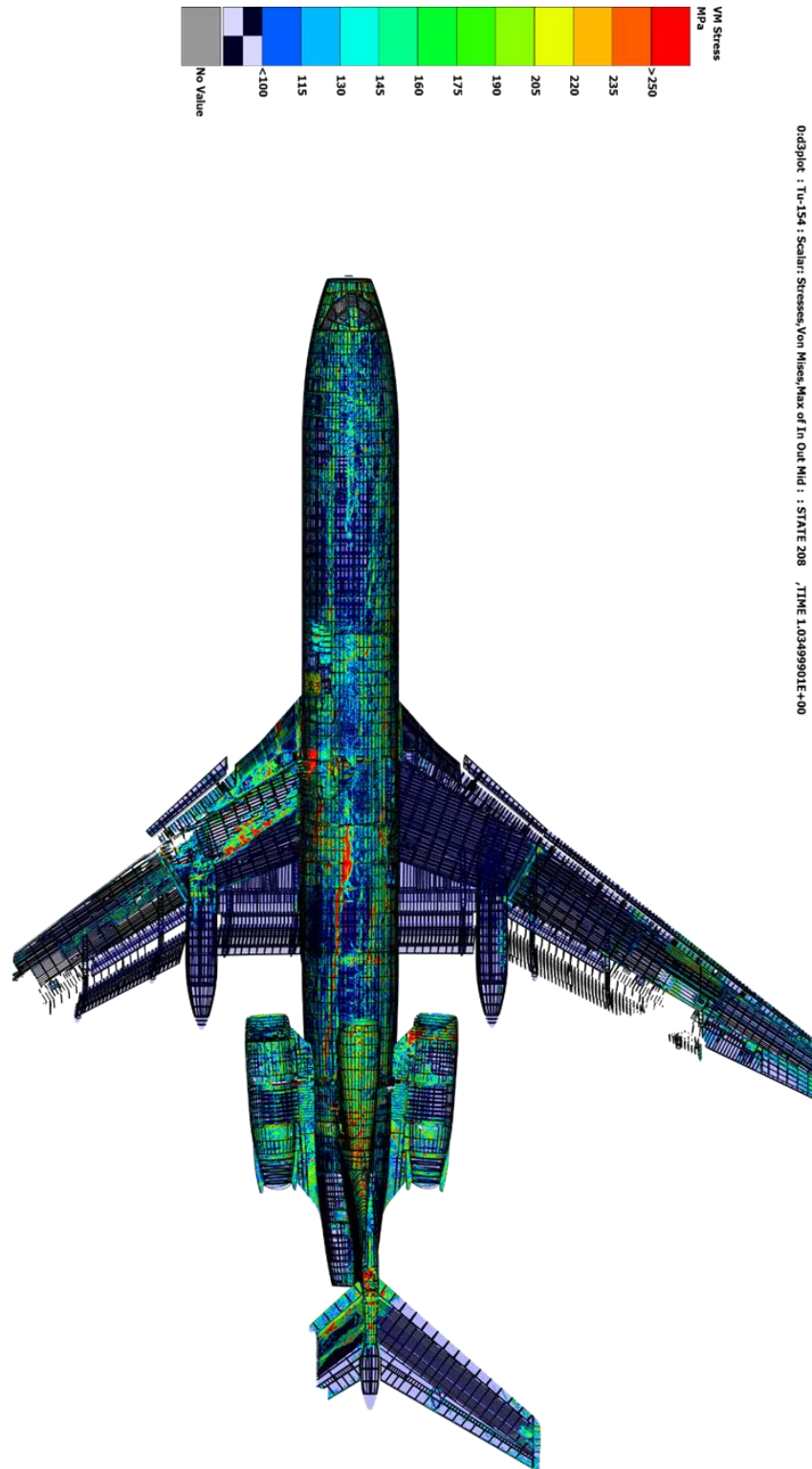


Figure 4.52 Top side Tu154 numerical model damage (Von-Mises Stress) at t = 1035 ms

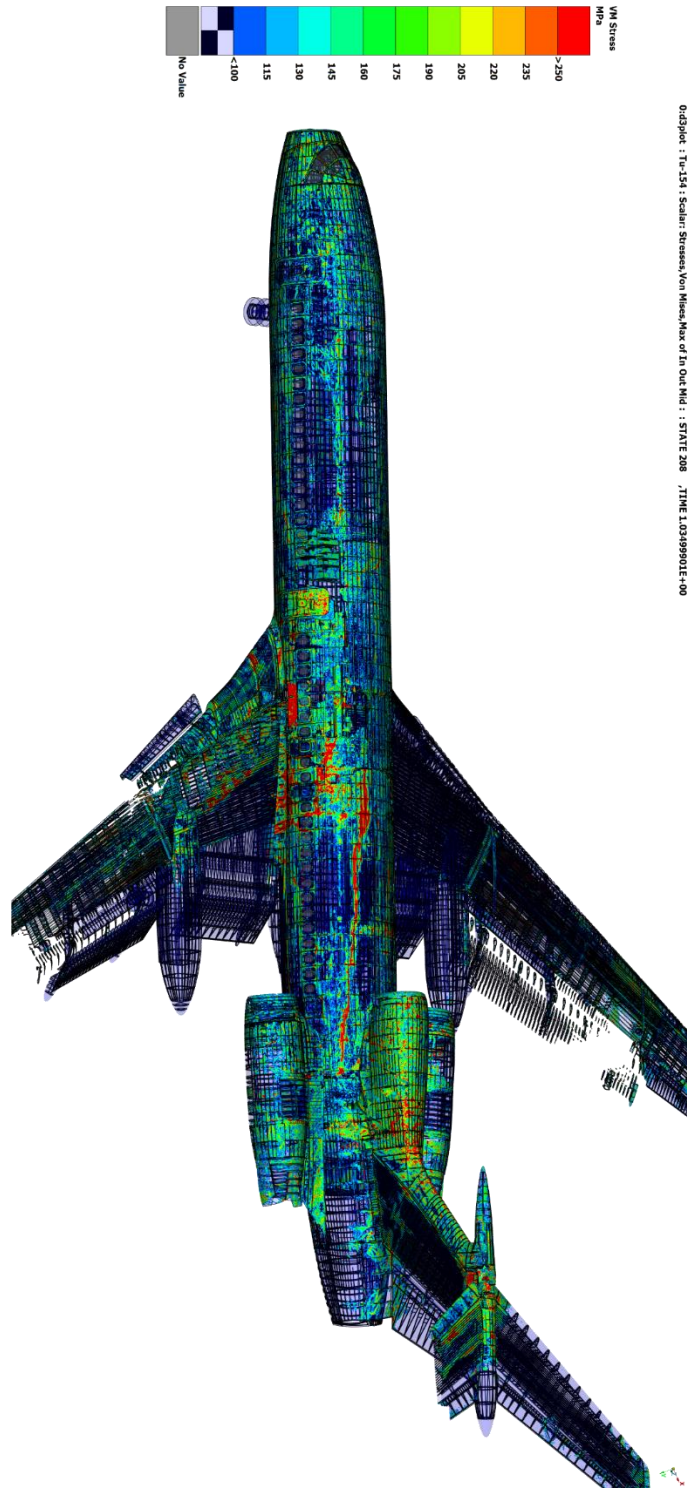


Figure 4.53 Tu154 numerical model damage (Von-Mises Stress) at $t = 1035$ ms

4.2.2 Ground Marks Analysis – Comparison with MAK Report

The MAK report states “initial ground impact has a furrow made by the stabilizer and fin leading edges up to with fragments of the SI-2U light of the SMI-2KM lighting set as 0.5 m deep and 22 m long as well as a furrow made by the left wing up to 0.4 m deep and 22 m long with fragments of the left wing panel and rod N 154.83.5711-090-009” [1]. An image of the accident site furrows is shown in Figure 4.54.

The numerical analysis produced a stabilizer furrow approximately 21.5 m long and 0.46 m deep, as shown in Figure 4.56. On the other hand, the left wing furrow in the numerical analysis is approximately 23.1 m long and 1.03 m deep, as shown in Figure 4.57. The ground marks measurements are tabulated in Table 4.5. It is important to highlight that these values are dependent on mesh density of the soil elements. The soil in the numerical model was modeled with 0.2 m x 0.2 m x 0.33 m solid elements due to computational efficiency constraints. Therefore, the resolution of the measured furrow depth will vary if a different element density is used in the soil model.

Table 4.5 Ground mark analysis results

	Length in accident site	Length in numerical analysis	Depth in accident site	Depth in numerical analysis
Left wing furrow	22 m	23.1 m	0.4 m	1.03 m
Stabilizer furrow	22 m	21.5 m	0.5 m	0.46 m



Figure 4.54 Stabilizer (left) and left wing (right) furrows in the accident site

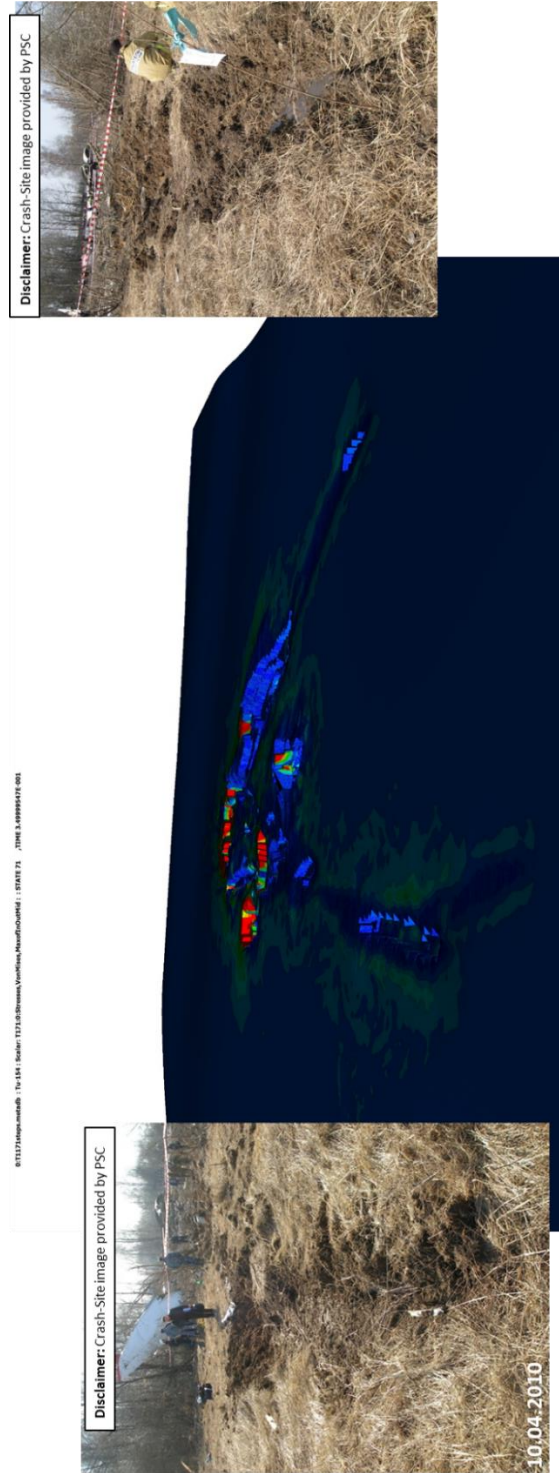


Figure 4.55 Stabilizer (left) and left wing (right) furrows in the accident site and the numerical model

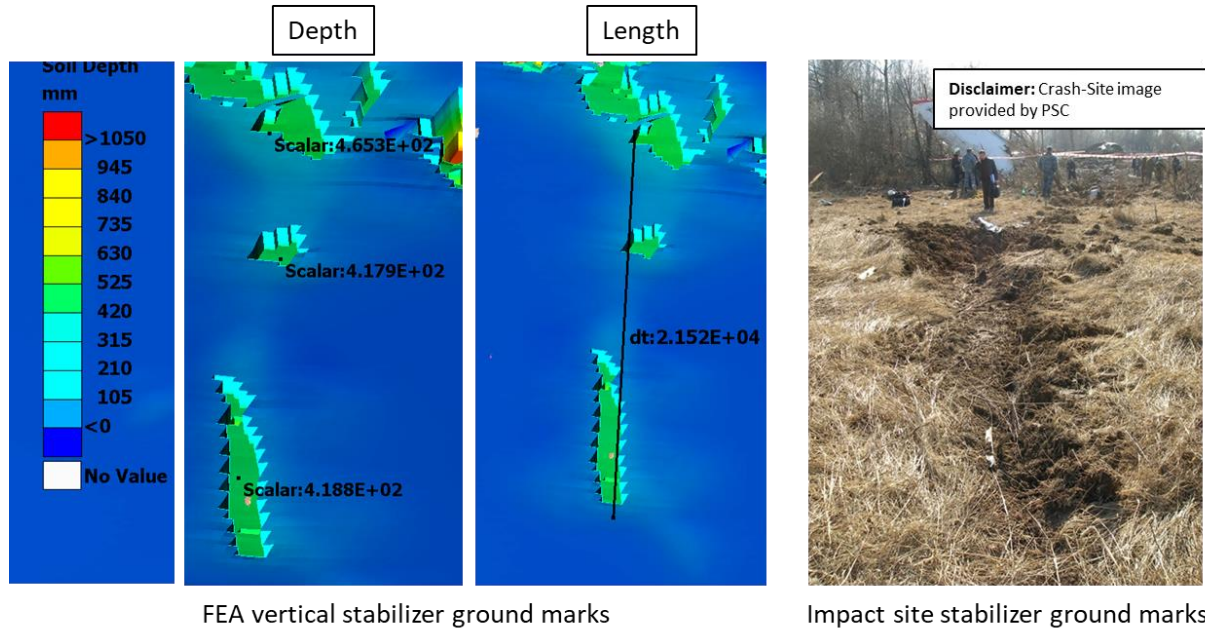


Figure 4.56 Comparison of the stabilizer furrow in the numerical model and the accident site

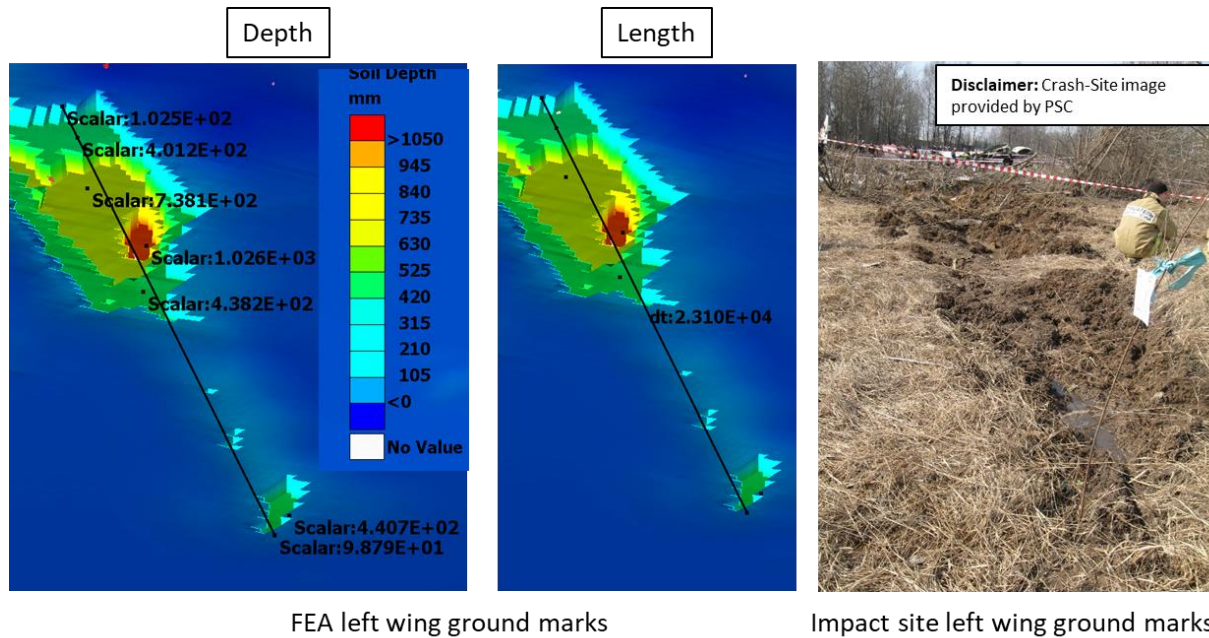


Figure 4.57 Comparison of the left wing furrow in the numerical model and the accident site

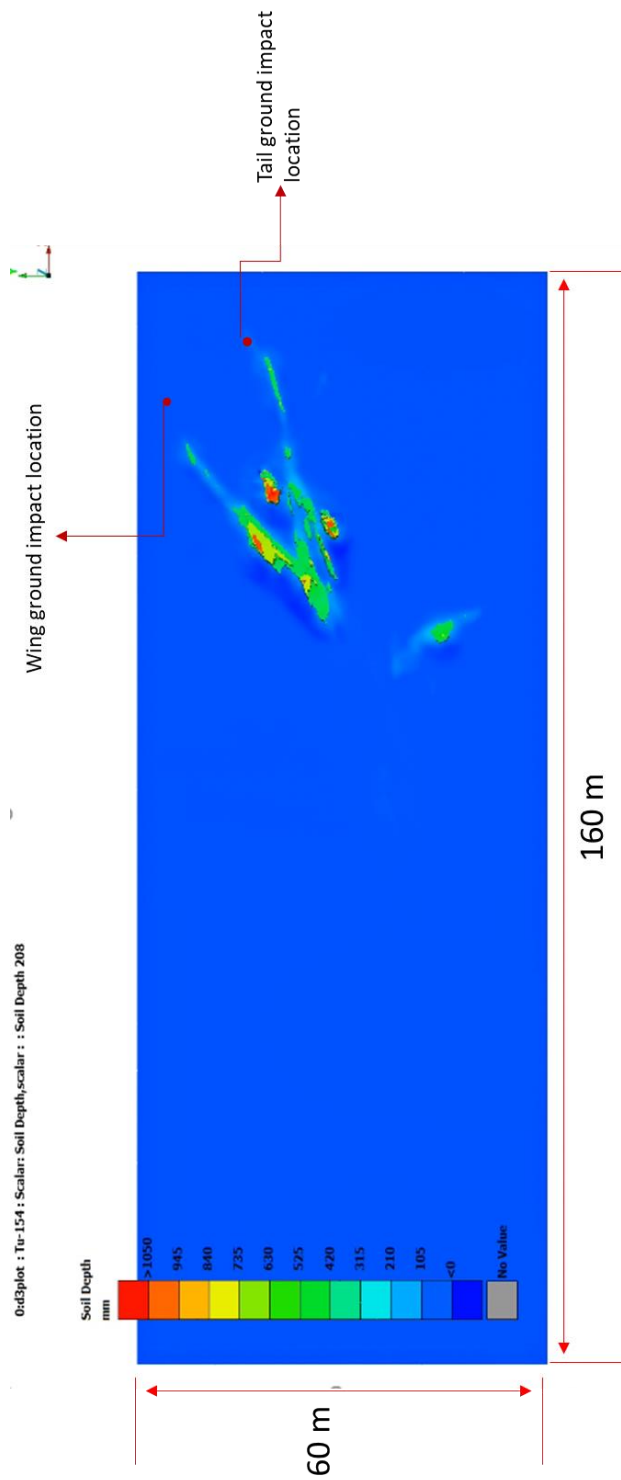


Figure 4.58 Depth of the ground marks in the numerical model

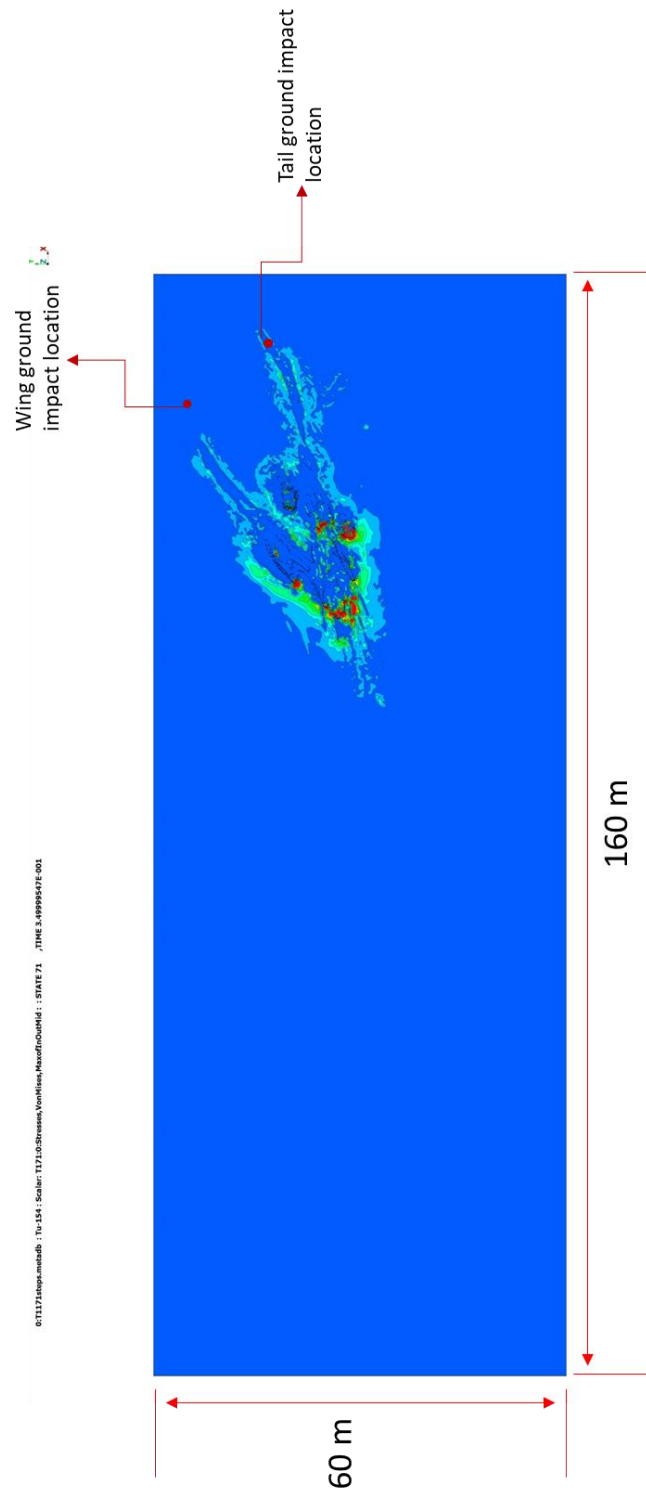


Figure 4.59 Von Mises stress of the ground marks in the numerical model – Time = 350 ms

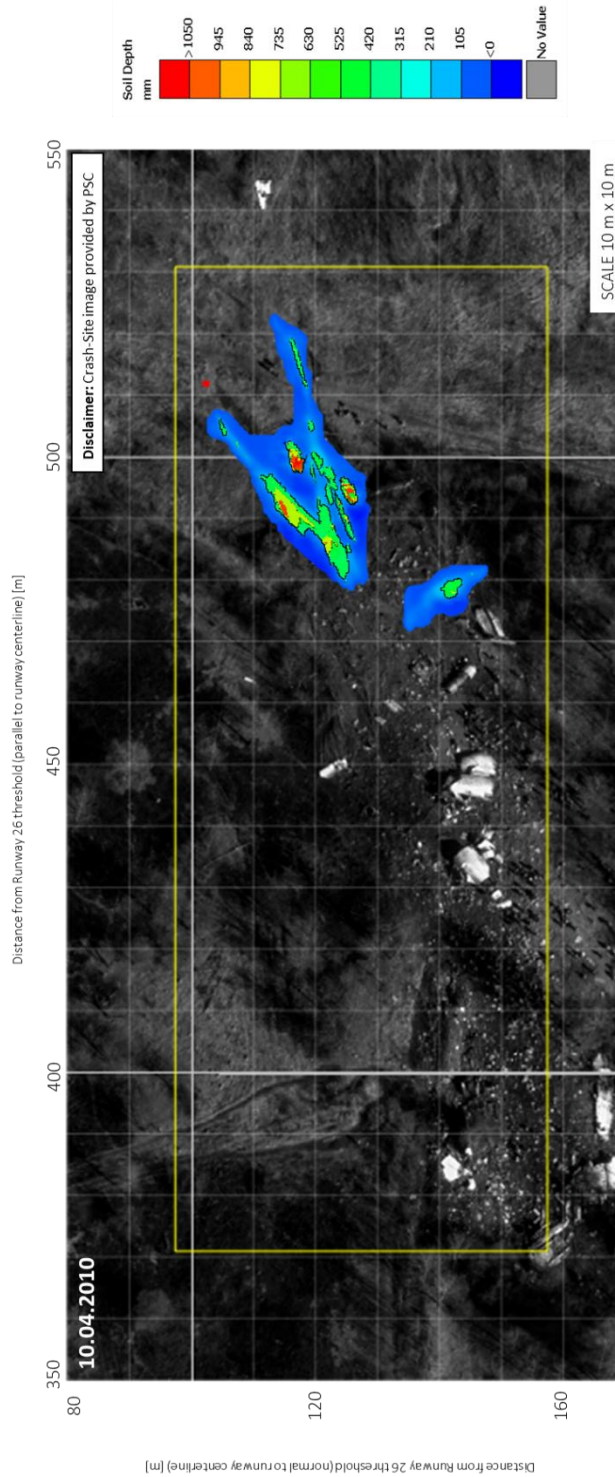


Figure 4.60 Overlay of the depth of the ground marks in the numerical model – Time = 350 ms

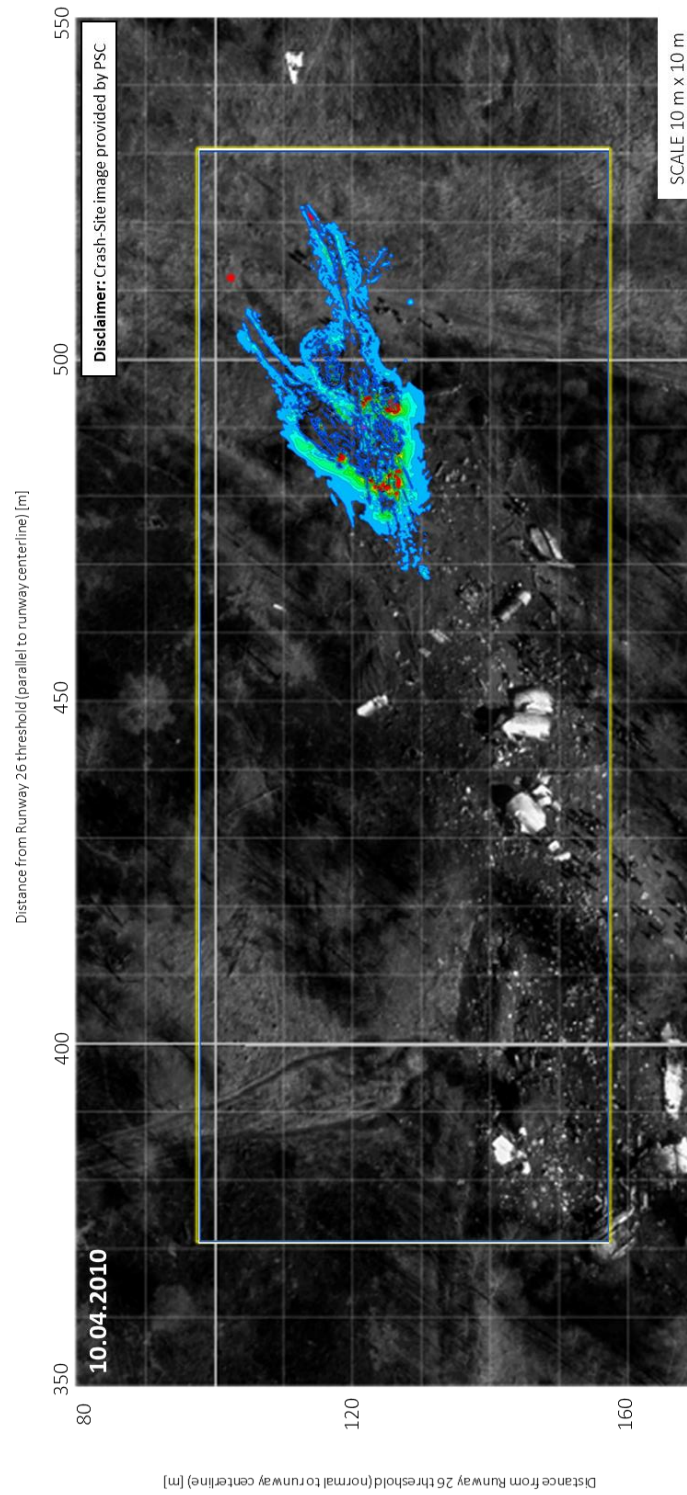


Figure 4.61 Overlay of the Von Mises stress ground marks in the numerical model – Time = 350 ms

4.3 Door 823 Analysis

Door 823 was highlighted as a critical point of analysis for the crash due to the way it was embedded in the soil. The kinematics of the door in the simulation are analyzed in detail to understand the feasibility for this to occur. Note that the simulation has limitations in this regard, as the soil was modeled with coarse elements (up to 0.2 m by 0.2 m by 0.33 m element length).

The initial impact of the door 823 with the soil and the respective door 823 location in the debris field are highlighted in Figure 4.62. The door impacts about 2.4 m away from the actual location. In the simulation, door 823 separates from the fuselage within 180 ms due to ground impact and as shown in Figure 4.63. The location of the door at various times during the simulation is shown in the door kinematics presented in Figure 4.64. At 180 ms, the door is 4.3 m away from the actual location in debris field. Although the door is released at this point, the door does not get embedded into the soil due to large soil elements (0.2 m by 0.2 m by 0.33 m) as shown in Figure 4.65. The damage of the door at 180 ms is compared to the door 823 from debris field in Figure 4.65. The simulation model shows similar damage to the door around the door window area.

Further analysis on door 823 is presented in Figure 4.66. The kinematics and total velocity plot on Figure 4.66 indicates that when the door impacts the ground its total velocity drops from 70 m/s to 31 m/s (from 160ms to 180ms). In the same time frame, the fuselage velocity drops from 75 m/s to 66 m/s. As a result, the fuselage would ride over the door exerting inertial loads on the door. In order to estimate the load exerted on the door the following is considered:

- The mass of the remaining aircraft (excluding section 1,2 and 3) – 61,574 Kg
- Change in Z velocity of the aircraft (from 180 to 200 ms based on Figure 4.66) – 1 m/s
- Estimated change in kinetic energy ($1/2 * m * v^2$) – 30,787 J
- The distance travelled by fuselage (from 180 to 200 ms based on Figure 4.66) – 0.1 m
- Force estimate ($F = E/d$) – 307,870 N – 69,209 lbs

Based on the analysis performed in the door study [30] and shown in Figure 4.67, it required an average of 25,000 lbs to push the door into the soil once the soil was penetrated. From the analysis performed, the estimated force exerted by the aircraft is 69,209 lbs which exceeds the 25,000 lbs required. This indicates that it could be possible for the door to be driven into the ground due to the inertia loads and the interior cabinets transmitting high forces. A very detailed soil model would be required to have a more detailed analysis; however, the simulation shows that it is feasible for the door 823 to be embedded in the soil.

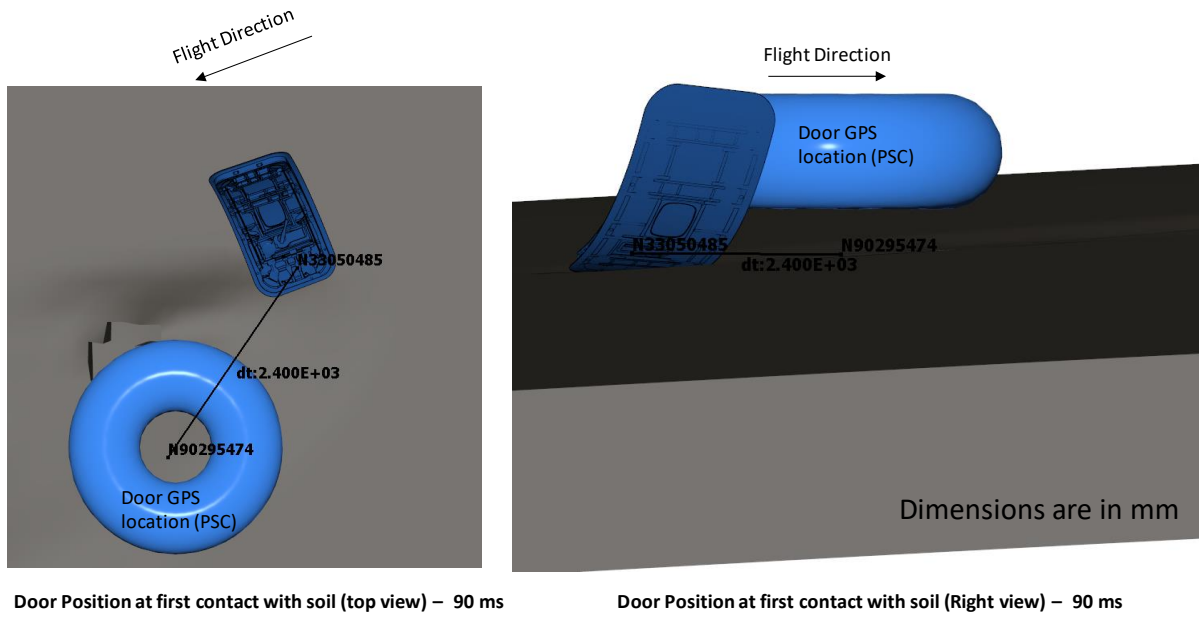


Figure 4.62 Section 3 (Simulation Time: 90 ms) – Door 823 initial impact versus door debris GPS location

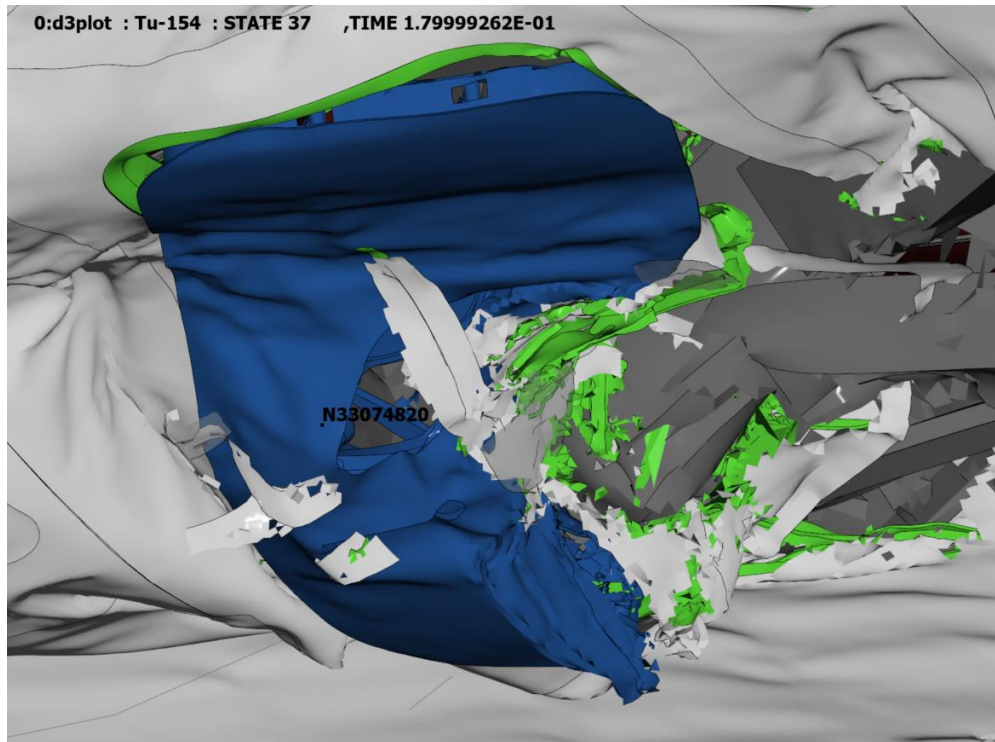


Figure 4.63 Section 3 (Simulation Time: 180 ms) – Door 823 release

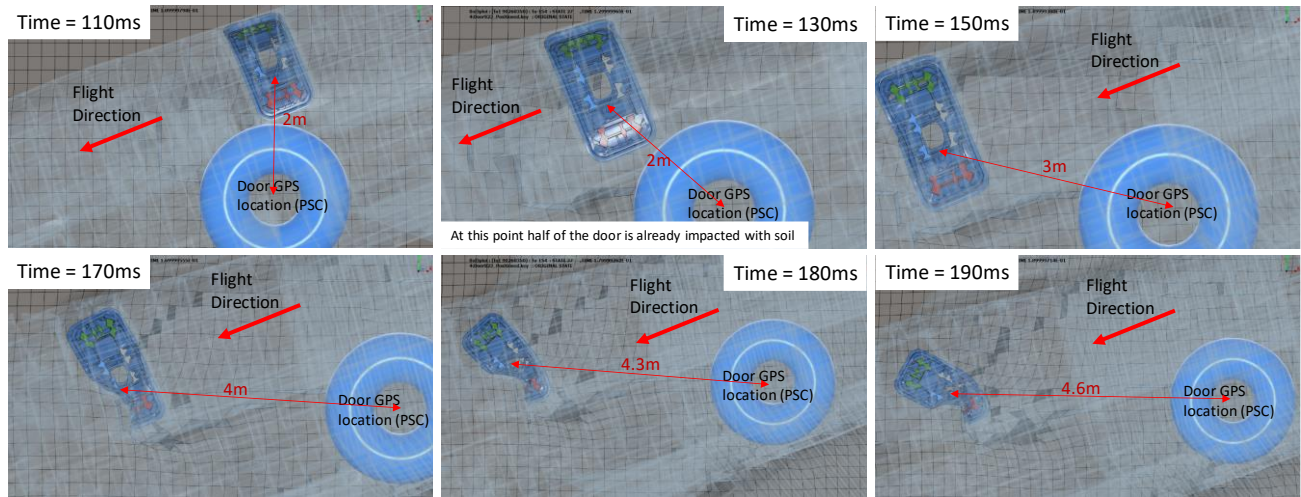


Figure 4.64 Section 3 door 823 top view kinematics overlaid with door debris GPS location

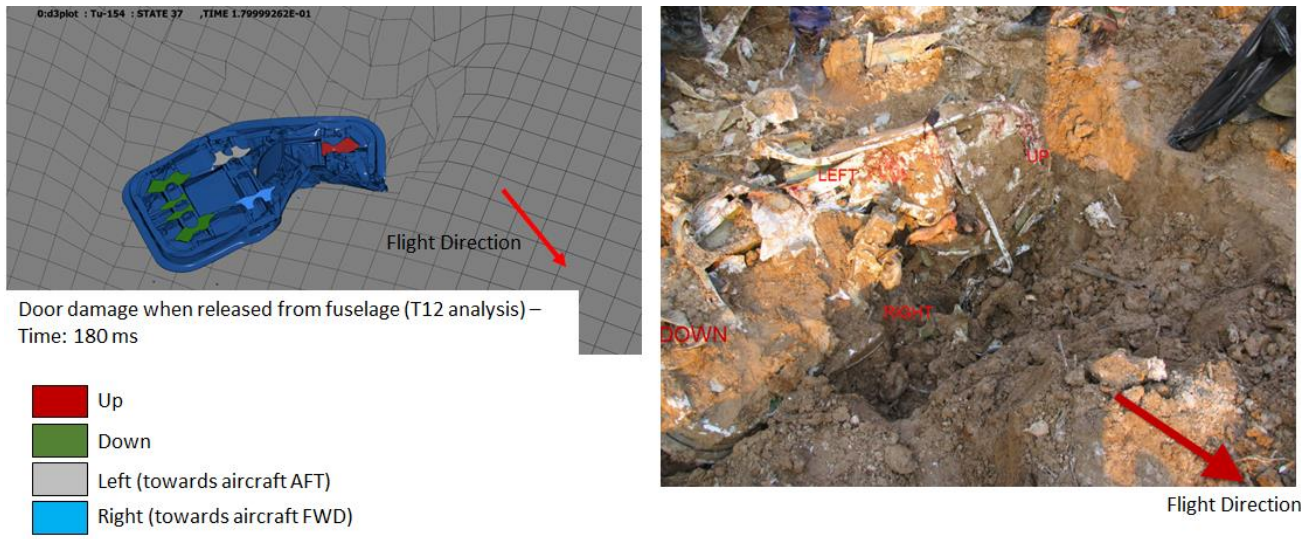


Figure 4.65 Section 3 door 823 (Simulation Time: 180ms) compared to door debris image by PSC [6]

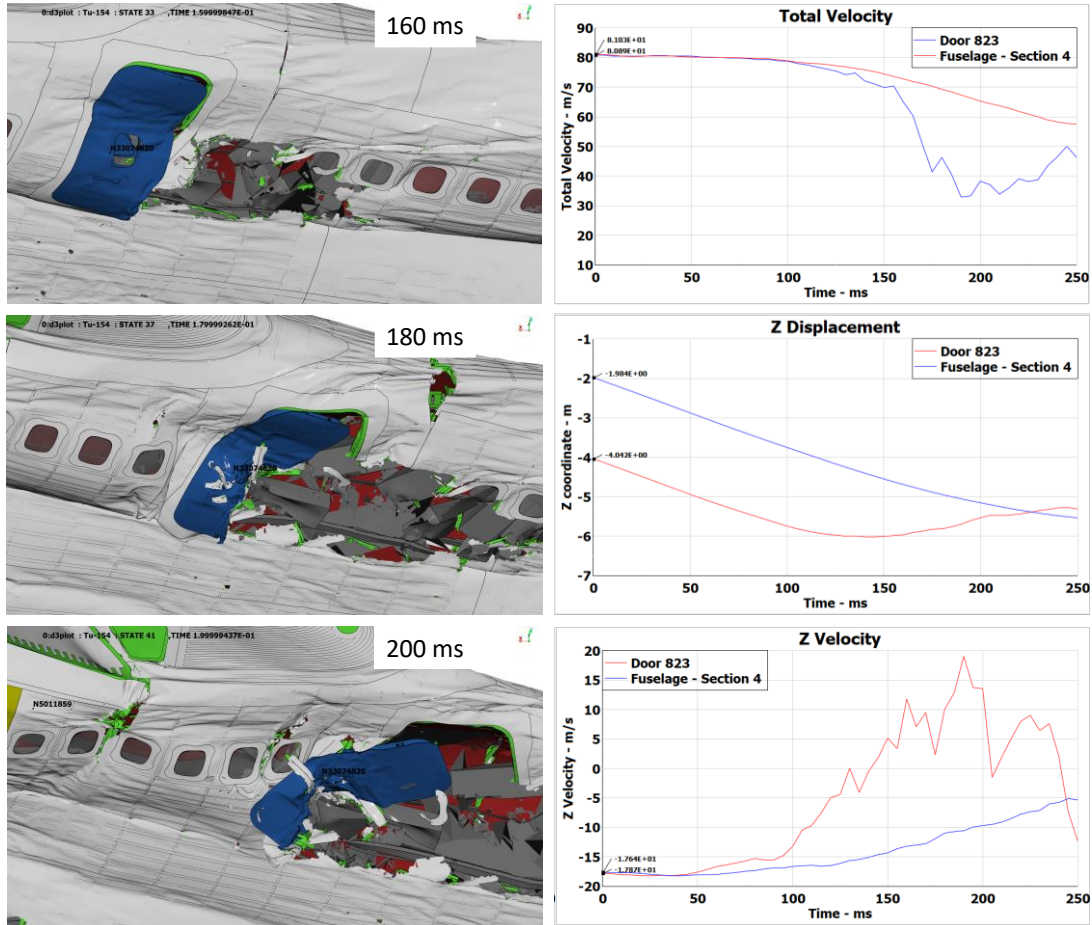


Figure 4.66 Section 3 door 823 kinematics (time: 160 – 200 ms) and total velocity and Z displacement and velocity of door 823 and fuselage section 4

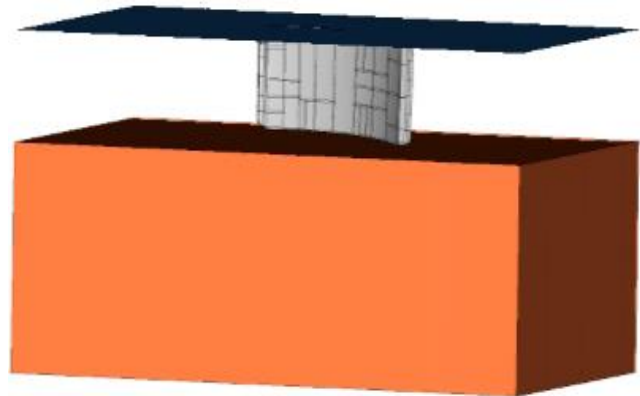
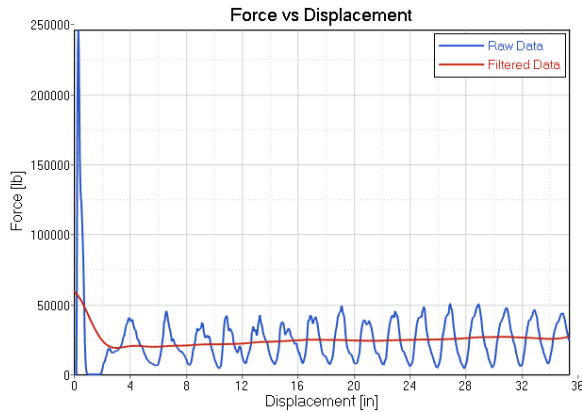


Figure 4.67 Case C1 – pushing door into soil [30]

4.4 Survivability evaluation summary

In sections 4.4.3 through 4.4.10 of the annex IV report, each aircraft section was analyzed and evaluated against the survivability criteria and debris field evaluation explained in section 4.1.1 and section 4.1.2 respectively. A summary of the findings for each section is tabulated in Table 4.6 through Table 4.10. The survivable volume for each aircraft section at 300 ms is shown in Figure 4.68

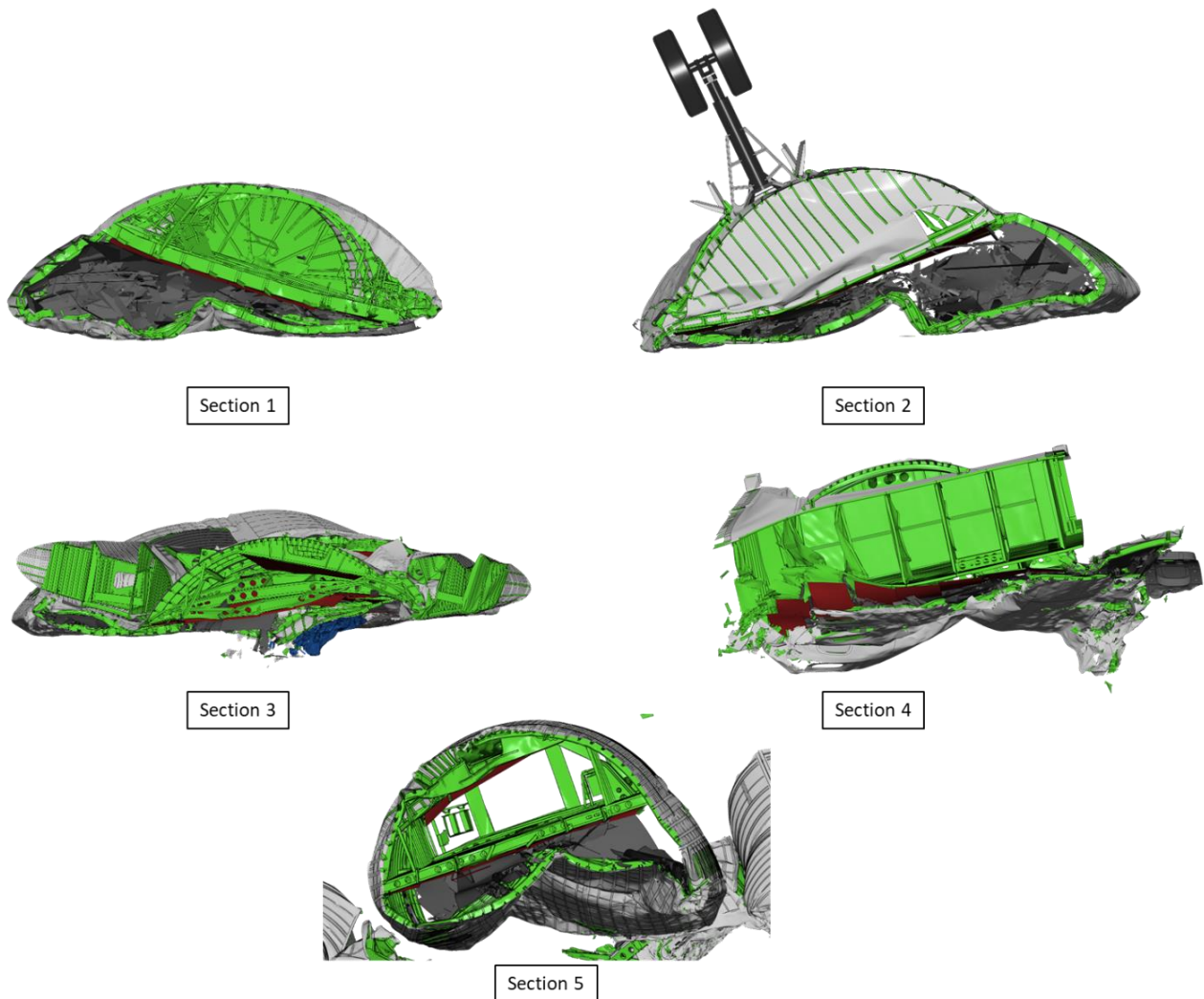


Figure 4.68 Aircraft sections survivable volume cross sections at 300 ms



Table 4.6 Section 1 survivability analysis summary

Criteria	Analysis Result
Maintain Survivable Volume	Survivable Volume Compromised within 95 ms after initial ground impact
Maintain Survivable Deceleration Loads to Occupants	Peak resultant floor accelerations in section 1 range from 150 g's to 230 g's.
Retention Items of Mass	Due to a combination of high acceleration levels and compromise of the survivable space there is no retention of items of mass. These acceleration loads will result in structural failures of the seats.
Maintain Egress Paths	No egress paths post impact, Survivable Volume is compromised within 95 ms after initial ground impacts
Passenger Fragments	Agreement up to 1035 ms except for a minor fragment. The path and orientation of Section 1 in the analytical model indicates that the passenger fragment distribution from the crash, for section 1, is plausible. It should be noted that additional secondary impacts with trees might influence the final position of fragments and corpses in the debris field.

Table 4.7 Section 2 survivability analysis summary

Criteria	Analysis Result
Maintain Survivable Volume	Survivable Volume Compromised by 115 ms after initial ground impact
Maintain Survivable Deceleration Loads to Occupants	Peak resultant floor accelerations in section 2 range from 63 to 168 g's.
Retention Items of Mass	Due to a combination of high acceleration levels and compromise of the survivable space there is no retention of items of mass. These acceleration loads will result in structural failures of the seats.
Maintain Egress Paths	No egress paths post impact, Survivable Volume is Compromised by 115 ms after initial ground impacts
Passenger Fragments	Agreement up to 1035 ms except for a minor fragment. The path and orientation of Section 2 in the analytical model indicates that the passenger fragment distribution from the crash, for section 2, is plausible. It should be noted that additional secondary impacts with trees might influence the final position of fragments and corpses in the debris field.



Table 4.8 Section 3 survivability analysis summary

Criteria	Analysis Result
Maintain Survivable Volume	Survivable Volume Compromised by 190 ms after initial ground impact
Maintain Survivable Deceleration Loads to Occupants	Peak resultant floor accelerations in section 3 range from 54 to 386 g's.
Retention Items of Mass	Due to a combination of high acceleration levels and compromise of the survivable space there is no retention of items of mass. These acceleration loads will result in structural failures of the seats.
Maintain Egress Paths	No egress paths post impact, Survivable Volume is Compromised by 190 ms after initial ground impacts
Passenger Fragments	The path and orientation of Section 3 in the analytical model indicates that the passenger fragment distribution from the crash, for section 3, is plausible

Table 4.9 Section 4 survivability analysis summary

Criteria	Analysis Result
Maintain Survivable Volume	Survivable Volume Compromised by 275 ms after initial ground impact
Maintain Survivable Deceleration Loads to Occupants	Peak resultant floor accelerations in section 4 range from 33 to 240 g's.
Retention Items of Mass	Due to a combination of high acceleration levels and compromise of the survivable space there is no retention of items of mass. These acceleration loads will result in structural failures of the seats.
Maintain Egress Paths	No egress paths post impact, Survivable Volume is Compromised by 275 ms after initial ground impacts
Passenger Fragments	The path and orientation of Section 4 in the analytical model indicates that the passenger fragment distribution from the crash, for section 4, is plausible



Table 4.10 Section 5 survivability analysis summary

Criteria	Analysis Result
Maintain Survivable Volume	Survivable Volume Compromised by 360 ms after initial ground impact
Maintain Survivable Deceleration Loads to Occupants	Peak resultant floor accelerations in section 5 range from 43 to 219 g's.
Retention Items of Mass	Due to a combination of high acceleration levels and compromise of the survivable space there is no retention of items of mass. These acceleration loads will result in structural failures of the seats.
Maintain Egress Paths	No egress paths post impact, Survivable Volume is Compromised by 360 ms after initial ground impacts
Passenger Fragments	The path and orientation of Section 5 in the analytical model indicates that the passenger fragment distribution from the crash, for section 5, is plausible

4.5 Conclusion of the ground collision reconstruction

The objectives of the accident reconstruction of the Tu154M crash at Smolensk, Russia, on April 10th, 2010, are listed below:

- 1) Evaluate the overall structural damage of the Tu154 numerical model and compare it to the observed damage in the actual accident as reported in the MAK report [1].
- 2) Determine the survivability criteria of the Tu154M accident using numerical analysis and compare the findings to the known injuries of each passenger.

The following damage was observed from the accident reconstruction simulation:

- For the initial 400 ms of the ground impact sequence, the damage observed to the Tu154M fuselage numerical model captures the overall failure mechanisms expected for this type of impact condition, i.e. collapse of the fuselage internal volume and fractures of the fuselage at the wing box and pressure bulkhead locations.
 - The simulation model was able to capture the length and depth of the ground marks introduced by the contact with the left wing and stabilizer.
 - The numerical model shows lesser fragmentation damage in the forward fuselage (sections 1 and 2), while it was highly fragmented in the actual accident. As alluded previously, the trees, shrubs, and other obstacles in the terrain were not modeled due to lack of information, and may introduce greater fragmentation in the numerical model (see Figure 4.70 and Figure 4.71).
 - Door 823 does not get embedded in the soil in the simulation due to larger soil elements (0.2 m by 0.2 m by 0.33 m). The kinematics and analysis of door 823 show that the aircraft inertial loads can push the door into the soil once it is separated from the fuselage (see section 4.3).
 - As the forward fuselage created a path for the rest of the aircraft, the rear section of the fuselage (section 5 and 6) sustained less severe fragmentation with clear defined fracture lines. There are major openings in the middle of the fuselage as shown in Figure 4.70 (Tu-154M fuselage sections 3 and 4). These openings are also present in the actual accident, albeit larger in size (see Figure 4.70 and Figure 4.71).
 - Other discrepancies in the numerical model include the vertical and horizontal stabilizers. The horizontal stabilizer separated from the vertical stabilizer, while the vertical stabilizer primarily remained attached to section 6. The response of section 6 and the vertical stabilizer can be attributed to several reasons, which include simplifications in geometry and connections due to the lack of detailed information, and assumptions in material properties of the linked/connected parts.
-

Figure 4.72 depicts a comparison of the overall passenger injury assessments of the actual accident [7] and the fuselage cabin floor deceleration peaks observed in the numerical analysis. The forward fuselage (sections 1, 2, and 3) exhibited higher peak deceleration loads as it takes the brunt of the initial ground impact. The rear fuselage (sections 4 and 5) exhibited lower peak deceleration loads. Nonetheless, deceleration peak values (33 to 300 g's) are well beyond survivable limits. A similar pattern emerges in the injury level assessments. Passengers sitting in the forward fuselage (sections 1, 2 and 3) exhibit a greater number of severe injuries compared to those sitting in the rear fuselage (sections 4 and 5).

The cabin floor deceleration loads observed in the numerical model alone would result in seat and/or seat track failures before the survivable volume of each section is compromised as shown in Figure 4.69. This creates a situation in which the passengers would be able to flail inside the cabin (unrestrained), which leads to additional injuries as they come into contact with the fuselage structure, large items of mass, other occupants, and the terrain (including trees).

When an aircraft crashes on level terrain without any major obstacles (trees, buildings, abrupt terrain changes, etc.), the majority of fatal injuries occur during the time that it takes to reduce the initial vertical impact velocity to zero (in this case, within the first 300 ms, the vertical velocity is reduced from 17 m/s to 0 m/s). This abrupt change of vertical velocity in conjunction with the compromised survivable volume during the first 300 ms, are a major cause of the fatal injuries sustained by the aircraft occupants.

Three hundred milliseconds after the initial impact, section 1 moves through areas of the debris field that were identified to contain trees. For this subject accident reconstruction analysis, trees were not modeled at the impact site, since data pertaining to their location, size, type, etc. was not available. The contact with these trees and shrubs can result in a different kinematic path and damage to the structure after 300 ms. However, the survivable limits of the accident, as discussed in the results section of this report, have been exceeded prior to 300 ms after initial ground impact. Therefore, any impact with trees will only increase the amount of fragmentation in the forward fuselage cabin structure and, correspondingly, create more occupant body fragmentation.

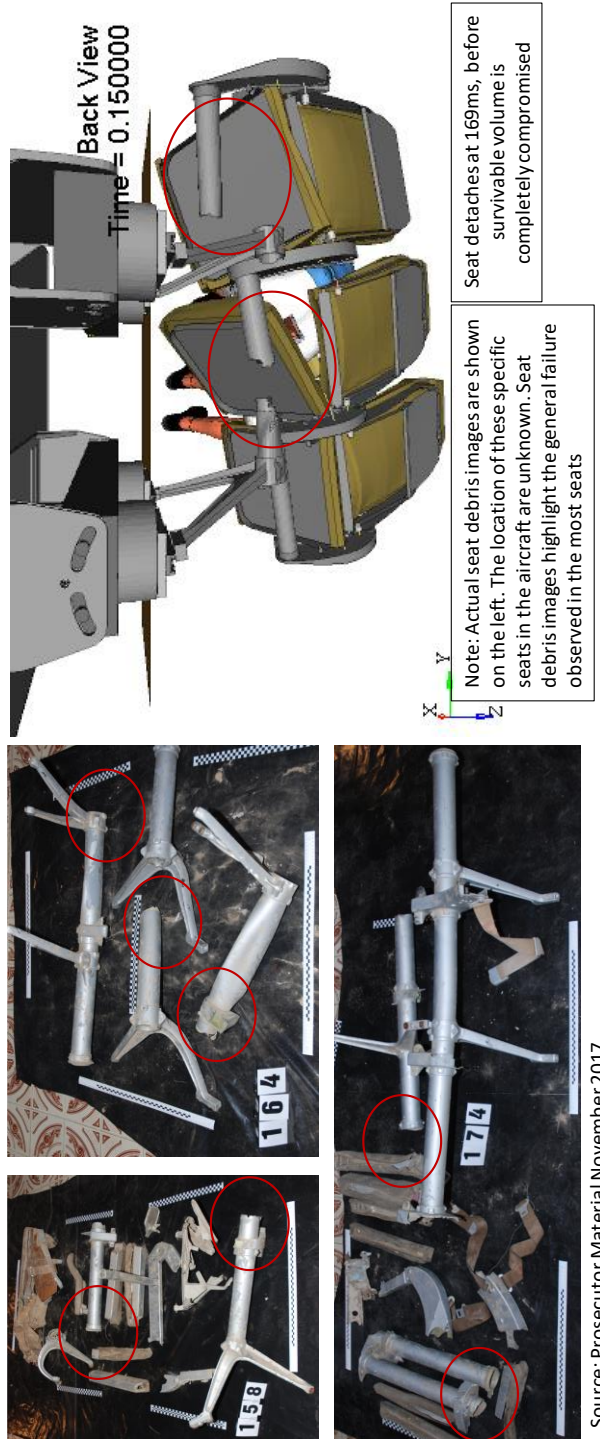


Figure 4.69 Seat analysis results with row 10 right outboard accelerations compared to various seat debris images provided by the PSC [6]

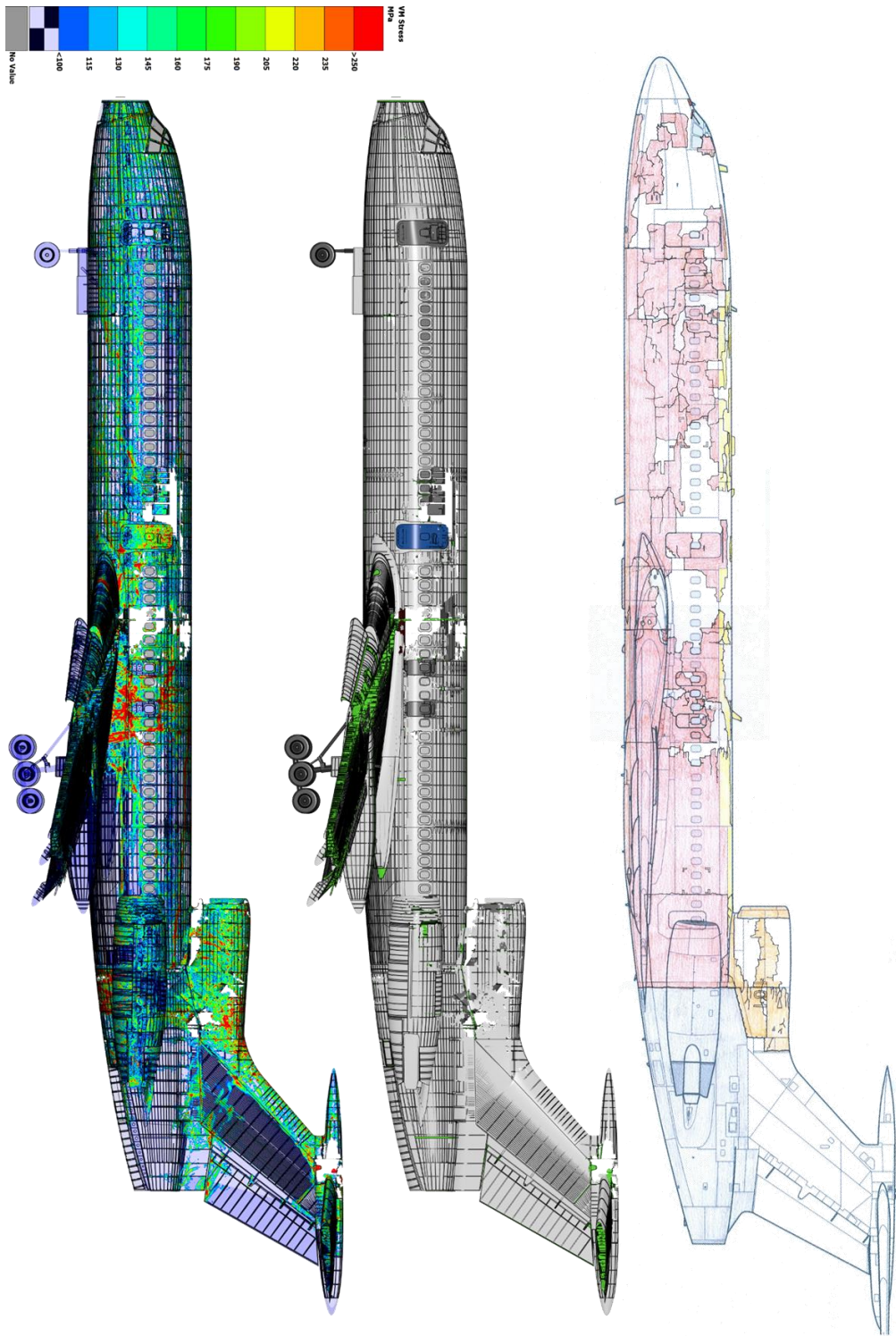


Figure 4.70 Left side Tu154 numerical model damage at $t = 1035$ ms – Comparison with PSC debris sketch [25]

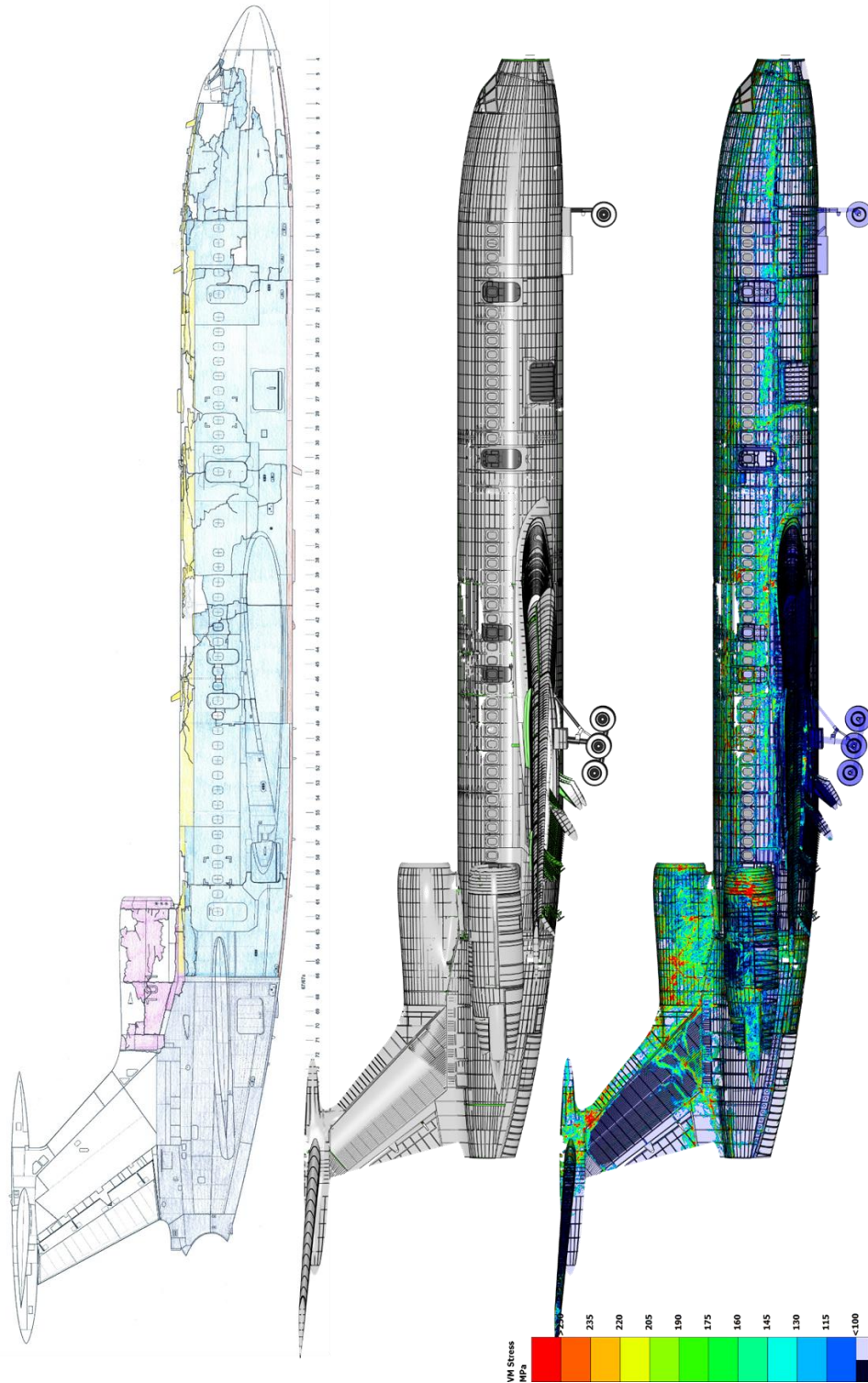


Figure 4.71 Right side Tu154 numerical model damage at $t = 1035$ ms – Comparison with PSC debris sketch [25]

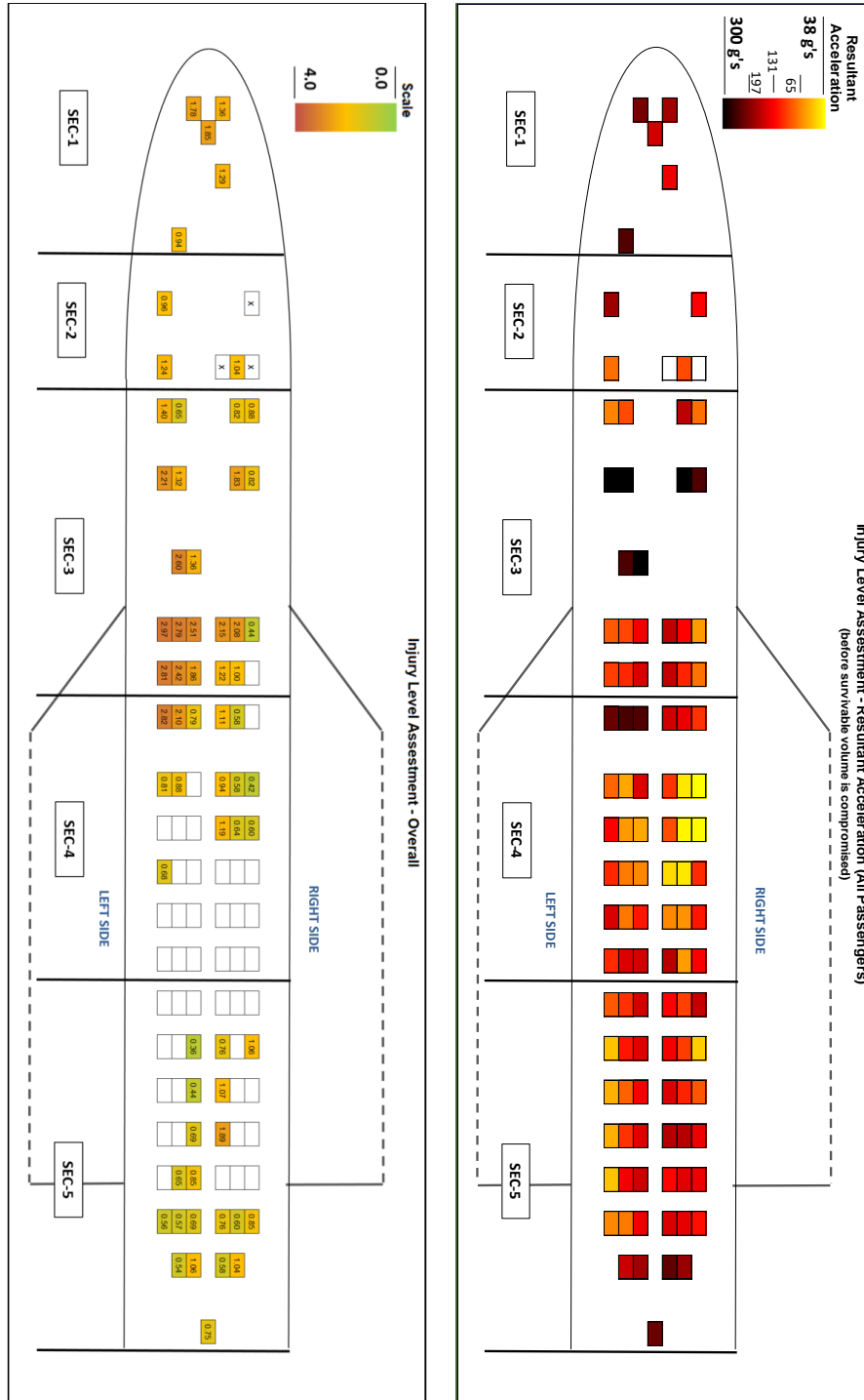


Figure 4.72 Overall passenger injury assessment [7] (left) and floor peak resultant accelerations (right)

5 References

- [1] MAK Report, Morozow A.N. (Investigator in Charge), Interstate Aviation Committee, “Final Report on the investigation of air accident of Tu154M, tail number 101 of Republic of Poland”, Moscow, June 2011, pp 1-184.
 - [2] Aircraft Accident and Incident Investigation, Annex 13, International Civil Aviation Organization, 9th Edition, November 2001.
 - [3] Definitions, 49 CFR § 830.2, accessed December 15, 2020.
 - [4] Data from PSC, Prosecutor office documentation, Data Received: February 2018
 - [5] KBWLLP Report, Miller J. (Chairman), committee for investigation of state aviation accidents, “Final report on investigation of air incident No 192/2010/11 of a Tu-154M aircraft No 101 which occurred on 10th of April 2010 near Smolensk North airfield”, Warsaw, June 2011, pp 1–328
 - [6] Data from PSC, Prosecutor office documentation, Debris Images. Data Received: February 2018
 - [7] PSC updated documents with passengers’ injury data updated, Email attachment: “*PASSENGERS ver. 4.0_12_03_2020.xlsm*” and “*Comment for PASSENGERS file.docx*”, March 13th , 2020
 - [8] Tupolev TU-154M Accident Statistics, Aviation Safety Network Database. Accessed at <http://aviation-safety.net/database/types/Tupolev-154/database>
 - [9] Biechtir, W.P., Rzhovsky, W.M. and Tsipenko, W.G., “Practical aerodynamics of Tu-154M aircraft (in Russian)”, Air Transport, 1997, Moscow
 - [10] Annex II Report TU-154M 101 Accident Reconstruction - Trajectory Analysis, NIAR Report POL-002.
 - [11] “Materials Sent in Response to Requests for Legal Assistance from the District Military Prosecutor in Warsaw,” Investigative Committee of the Russian Federation. Volume N9 1. 04/10/2010, 08/05/2010, 11/18/2011.
 - [12] "TAWS Data Extraction for NTSB Identification: ENG10SA025, Original". Universal Avionics Systems Corporation, June 28, 2010.
 - [13] "FMS Data Extraction for NTSB Identification: ENG10SA025, Original". Universal Avionics Systems Corporation, June 25, 2010.
-



- [14] KBWLLP Report, “Annex 4 (2011) to final report on investigation of air incident No 192/2010/11 of a Tu-154M aircraft No 101 which occurred on 10th of April 2010 near Smolensk North airfield”, Warsaw, June 2011.
 - [15] Data from PSC, Accident site Landmarks – Heights, Positions, and Images. Data Received: January 2020.
 - [16] Flight Data from PSC, Document uploaded to NIAR FTP Server: “*MLP-corrected-MSRP-UTC-Relative Time-pure.xlsx*”, November 30, 2019
 - [17] PSC Response document with Tree geometry information, Email attachment: 2019_11_01_Wing_Tree_Impact_Information_Request.docx and wing_tree.docx, November 7th, 2019.
 - [18] Biechtir, W.P., Rzhevsky, W.M. and Tsipenko, W.G., “Practical aerodynamics of Tu-154M aircraft (in Russian)”, Air Transport, 1997, Moscow.
 - [19] Data from PSC, Prosecutor Material November 2017, Data Received: February 2018 Poland Visit
 - [20] Data from PSC, Prosecutor office visit to Smolensk, Debris Images, Left Wing, Data Received: February 2018
 - [21] Data from PSC, Odłamki white w pień brzozy 2019.11.06, Data Received: November 6th 2019
 - [22] “Materials Sent in Response to Requests for Legal Assistance from the District Military Prosecutor in Warsaw,” Investigative Committee of the Russian Federation. Volume N9 1. 04/10/2010, 08/05/2010, 11/18/2011.
 - [23] Ding, M. and Binienda, W., “Simulations of Trajectory of Separated Objects after Impact”, ASCE Earth and Space Conference 2018, April 9-12, 2018
 - [24] LS-DYNA Keyword User’s Manual – I accessed at http://lstc.com/pdf/ls-dyna_971_manual_k.pdf, June 2019.
 - [25] Data from PSC, Aircraft fragmentation documentation, E-mail attachment from Dr. Binienda, Friday, April 3, 2020, 8:48 AM
 - [26] Shanahan, D. F. "Basic principles of crashworthiness." Pathological Aspects and Associate Biodynamics in Aircraft Accident Investigation. October 2004.
 - [27] Hyde, A. S., Crash injuries: how and why they happen. A primer for anyone who cares about people in cars. 1992
-



- [28] Hurley, Todd R., and Jill M. Vandenburg. "Small airplane crashworthiness design guide." AGATE Report Reference No. AGATE-WP3: 4-034043, 2002.
 - [29] "Emergency landing dynamic conditions". Code of Federal Regulations, title 14: 25.562 . https://www.ecfr.gov/cgi-bin/text-idx?node=pt14.1.25&rgn=div5#se14.1.25_1562
 - [30] Olivares, G., "*Polish Government Tupolev TU-154M Flight PLF101 - Door Impact Analysis*", NIAR, August 25th, 2017.
 - [31] Annex I Report TU154M 101 Accident Reconstruction – Reverse Engineering Process, CAD, FEA, and CFD Models, NIAR Report POL-001.
 - [32] Annex III Report TU-154M 101 Accident Reconstruction – Bodin Birch Tree Impact Reconstruction, NIAR Report POL-003.
 - [33] Annex IV Report TU-154M 101 Accident Reconstruction – Ground Collision, NIAR Report POL-004.
-